Synthesis of Carbon Nanomaterials by Thermal Chemical Vapor Deposition Method

（熱化学気相成長法によるカーボンナノ材料の合成）

2014

Bao Jianfeng

包　建峰

Graduate School of Engineering

Nagoya Institute of Technology

Contents

Chapter 1

Introduction

1.1. General Introduction

Carbon is basic chemical element for all known life forms and the 4th most abundant element in the universe after hydrogen, helium, and oxygen being present in the sun, stars, meteors, comets, and in the atmosphere of most planets. It is a known element by human for over 6000 years. Carbon is the 15th most abundant element in the earth's crust. In combination with oxygen to form carbon dioxide is dissolved in the air and in the water bodies, mainly in the ocean (Figure 1.1) [1.1].

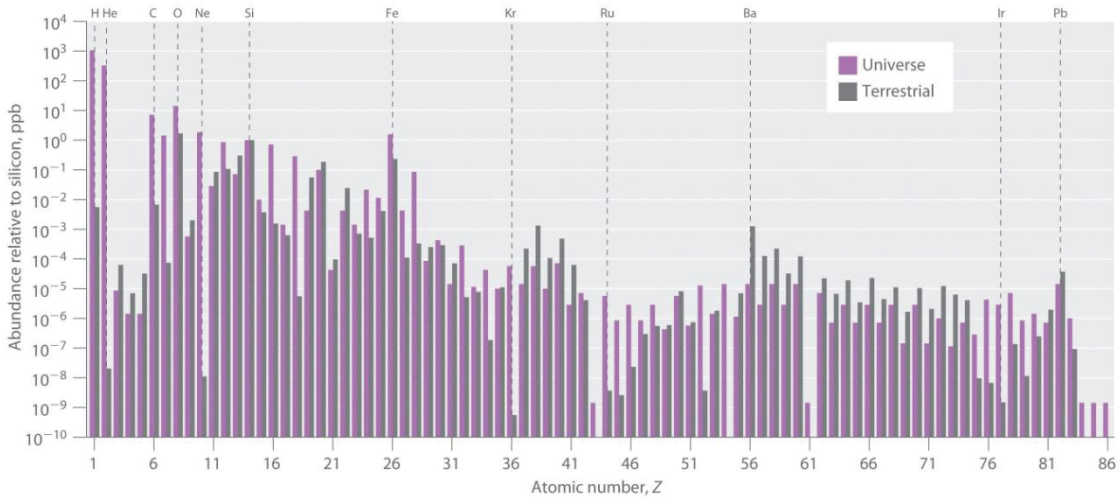

Figure 1.1 the relative abundances of the elements in the universe and on earth [1.1].

The diversity in bonding makes carbon the most important element in variety of disciplines. The catenation property, i.e. the ability to form large stable frameworks of

interconnecting bonds with different hybridization allows carbon to form distinct solid state allotropes with diverse structures and properties ranging from sp^3 hybridized diamond to sp^2 hybridized graphite. Mixed states are also possible and form the basis of amorphous carbon, diamond-like carbon, and nanocrystalline diamond (Figure 1.2) [1.2].

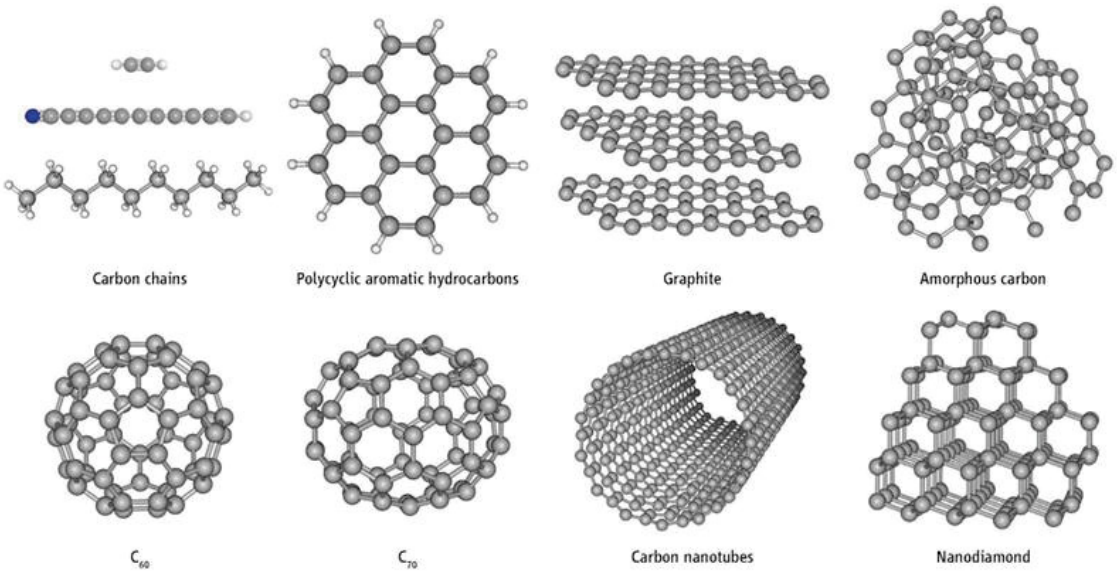

Figure 1.2 allotropes of carbon [1.2].

Diamond is a metastable from of carbon that possesses a three-dimensional cubic lattice with a lattice constant of 0.357 nm and C-C band length of 0.154 nm. In contrast, graphite is the most thermodynamically stable form of carbon at room temperature and consists of a layered two dimensional structure where each layer possesses a hexagonal honeycomb structure of sp^2 bonded carbon atoms with a C-C bond length of 0.142 nm. These single atom thick layers interact via non-covalent van

der Waals forces with an interlaying spacing of 0.335 nm. The weak interlayer bonding in graphite implies that single graphene layers can be exfoliated via mechanical or chemical methods. Graphene is often viewed as the two-dimensional building block of other sp^2 hybridized carbon nanomaterials in that it can be conceptually rolled or distorted to form zero-dimensional fullerenes, one-dimensional carbon nanotubes or carbon nanofibers.

Twenty-first century, the merging need for high speed electronics and renewable clean energy has motivated researchers to discover, develop, and assemble new classes of nanomaterials in unconventional device architecture. Among these materials, carbon nanomaterials have a unique place in nanoscience owing to their exceptional electrical, thermal, chemical and mechanical properties and have found application in areas diverse as composite materials, energy storage and conversion, sensors, drug delivery, field emission devices and nanoscale electronic components. Consequently, significant recent effort has been devoted to the mass production of structurally homogenous, high purity, and low cost [1.3].

1.2. Carbon Nanofibers

Carbon nanofibers (CNFs) are solid or hollow structures with graphene layers arranged as stacked cones, cups or plates (Figure 1.3) [1.4]. CNFs have diameters varying from a few to hundreds of nanometers and lengths ranging from less than a micron to millimeters [1.3]. Materials in a form of fibers are of great practical and scientific importance. The combination of high specific area, flexibility, and high mechanical strength allow nanofibers to be used in our daily life as well as in fabricating tough composites for vehicles and aerospace. CNFs could be fabricated by

the right combination of electro-spinning of organic polymers and thermal solution by using electrostatic forces. Electro-spun based nanofibers exhibited noticeable properties, such as nanosized diameter, high surface area and thin web morphology, which make them applicable to the fabrication of high performance nanocomposites, tissue scaffolds and energy storage devices [1.3, 1.5].

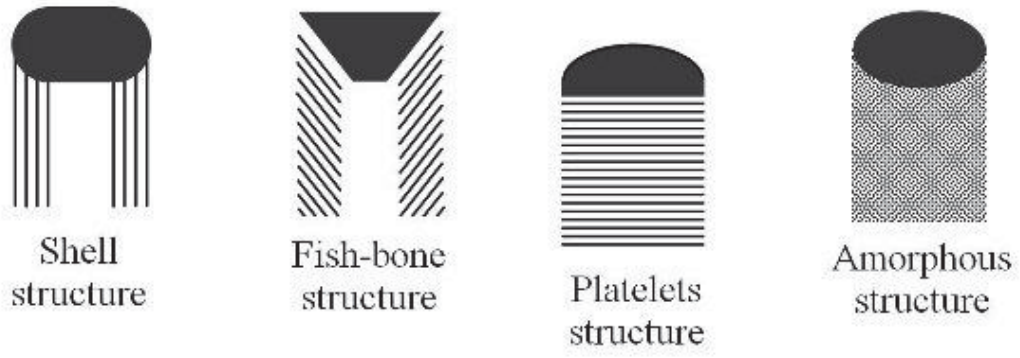

Figure 1.3 schematic cross sectional illustration of CNFs [1.4].

Among the various synthesis methods for CNFs, a catalytic chemical vapor deposition (CCVD) method has been considered as a promising method for large-scale production because this method has been shown to be more controllable and cost efficient than the arc discharge or laser ablation methods[1.6]. In general, CCVD methods for growth of CNFs, carbon feedstock were passing the reaction chamber over nano-sized catalyst metal at high temperature, which is very similar to the growth condition of carbon nanotubes. However, their geometry is different from concentric carbon nanotubes containing an entire hollow core, because they can be visualized as regularly stacked truncated conical or planar layers along the filament length [1.4].

Generally, metal catalysts, typically iron-group elements (Fe, Co, Ni) and their

alloys, are indispensable for the growth of CNFs by CVD methods. However the unavoidable metal species remaining in the products would result in obvious disadvantages for both intrinsic property characterization (e.g., chemical, electronic and magnetic properties, thermal stability, and toxicity) and application exploration (e.g., catalyst supports, biology, and medicine) of CNFs and CNTs. Detriment effects of these metal particles to carbon nanomaterials based electronic devices are also of concern because metal catalyst residues are incompatible with silicon semiconductor technology. Despite sustained efforts, it has been until now an intractable problem to remove metal catalysts completely from carbon nanomaterials without introducing defects and contaminations.

Recent experimental and theoretical studies show that hydrocarbon-molecule decomposition and graphite formation abilities are not essential and lead to a new interpretation of the role of catalyst particle in CNFs and CNTs growth: only a pore structures or nanoscale curvature would be necessary to grow CNFs and CNTs if carbon atoms are supplied to the nanocurvature [1.7, 1.8]. From a view point of process simplification and product purification, catalyst-free synthesis is attractive.

1.3. Carbon Nanotubes

Carbon nanotubes (CNTs) are hollow cylinders made of seamlessly rolled graphene perfectively. Structure well-ordered CNTs were discovered and their structures were well characterized by Iijima in 1991 [1.9]. CNTs composed of one sheet of graphene are called single walled carbon nanotubes (SWNTs), and those made of more than two sheets, multiwall carbon nanotubes (MWNTs).

There are numerous ways of rolling a sheet of the sheet of the honeycomb

pattern into a seamless cylinder, which gives rise to vast range of diameter and various helical structures. The way the graphene sheet is wrapped is represented by a vector $C_h = na_1 + ma_2$. The integers n and m ($0 \leq |m| \leq n$) denote the number of unit vector (a_1, a_2) along two directions in the honeycomb crystal lattice of graphene. T denotes the tube axis, and a_1, a_2 are unit vectors (Figure 1.4). The structure of CNTs can be characterized by chiral indices n and m. CNTs with n = m and m = 0, called armchair type and zigzag type, respectively. CNTs with other chiral indices ($n \neq m \neq 0$) have helical structures and are called chiral type. In Figure 1.5 (a-c), structure models of armchair, zigzag, and chiral type CNTs, respectively, are shown.

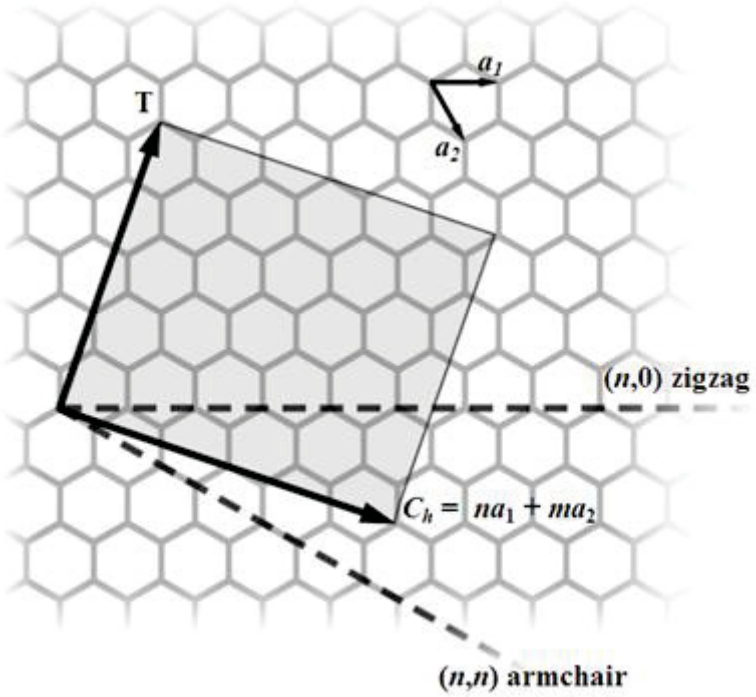

Figure 1.4 the unrolled sheet of honeycomb lattice of graphene. C_h is an example of a chiral vector. T denotes the tube axis, and a_1, a_2 are the unit vectors [1. 10].

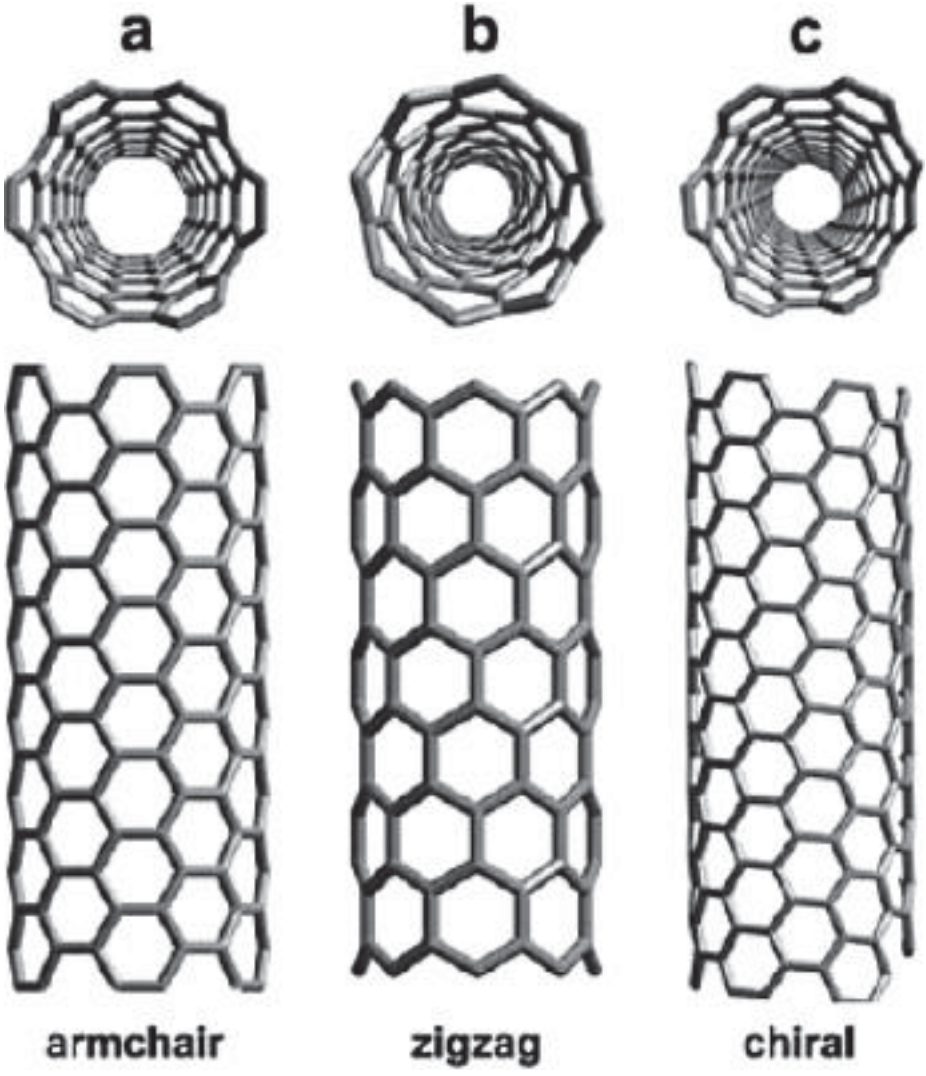

Figure 1.5 structure models of CNTs exhibiting different chiralities (a) armchair-, (b) zigzag-, (c) chiral-type [1.11].

Arc discharge, laser vaporization, and chemical vapor deposition (CVD) methods have been actively investigated for the synthesis of CNTs. In 1991, Iijima reported the first observation of MWNTs in carbon soot produced by arc discharge. The first syntheses of SWNTs were also achieved by using arc discharge methods. By using the laser ablation method, high quality SWNTs having narrow diameter distributions

have been obtained. In 1996, gram-scale synthesis of SWNTs was achieved using laser ablation [1.12]. Both arc discharge and laser ablation methods involve the condensation of carbon atoms generated from evaporation of solid carbon sources. The temperatures required in these methods of 3000 °C - 4000 °C are close to the melting temperature of graphite.

CVD is one of the more promising methods to realize large-scale synthesis of CNTs [1.13, 1.14]. The general CNTs growth mechanism in CVD is the dissociation of the carbon source catalyzed by a transition metal, and dissolution and saturation of carbon atoms in the metal nanoparticles. The precipitation of carbon from the saturated metal particle leads to the formation of tubular carbon solids. Catalysts are heated to 600-1200 in a furnace, and after reaching the reaction temperature, the carbon source such as hydrocarbon and alcohol vapor is introduced into the reactor chamber for a specific period of time. CNTs grown over the catalyst are collected after cooling the system to room temperature. The key parameters in the synthesis of CNTs are the carbon source, the catalyst used and the growth temperature.

CNTs show a variety of electronic behavior from metallic to semiconducting, depending on their composition, chirality, etc. However, it is still a big challenge to control precisely these parameters during the process of CNTs. the deliberate introduction of defects and impurities into the CNTs could offer a possible route to change and tune its electronic properties. Heteroatoms (boron, nitrogen, phosphorous) [1.15-1.17] doping into graphitic carbon lattice effect various properties of sp2 carbon material. The advantage of such nanotubes is that their electronic properties are primarily determined by composition and are thus relatively easy to control. Among these heteroatoms boron and nitrogen atoms are the most effective dopant. Recent

research in that field reveals that incorporated nitrogen atom in carbon nanostructure can enhance the mechanical, electrical properties and increase the energy storage capacity [1.17].

1.4. Graphene

Graphene, a planar monolayer sheet of sp^2-hybridized carbons arranged on a two-dimensional hexagonal lattice, has become one of the most exciting topics of research in the recent years. It is distinctly different from carbon nanotubes and fullerenes, exhibiting unique properties which have fascinated the scientific community. Graphene can be considered as the parental compound for the carbon allotropes of other dimensionalities (Figure 1.6) [1.18-1.20]. Typically important properties of graphene are fractional quantum Hall effect at room temperature, an am-bipolar electric field effect along with ballistic conduction of charge carriers, tunable band gap and high elasticity. Although graphene is expected to be perfectly flat, ripples occur because of thermal fluctuations. Ideally graphene is a single-layer carbon atoms thick of materials but graphene samples with two or more layers are being investigated with equal interest. One can definite three different types of graphene: mono-layer graphene, bi-layer graphene and few layer graphene (number of layers < 10). Graphene has been characterized by a variety of microscopic and other physical techniques including atomic force microscopy, transmission electron microscopy, scanning tunneling microscopy and Raman spectroscopy.

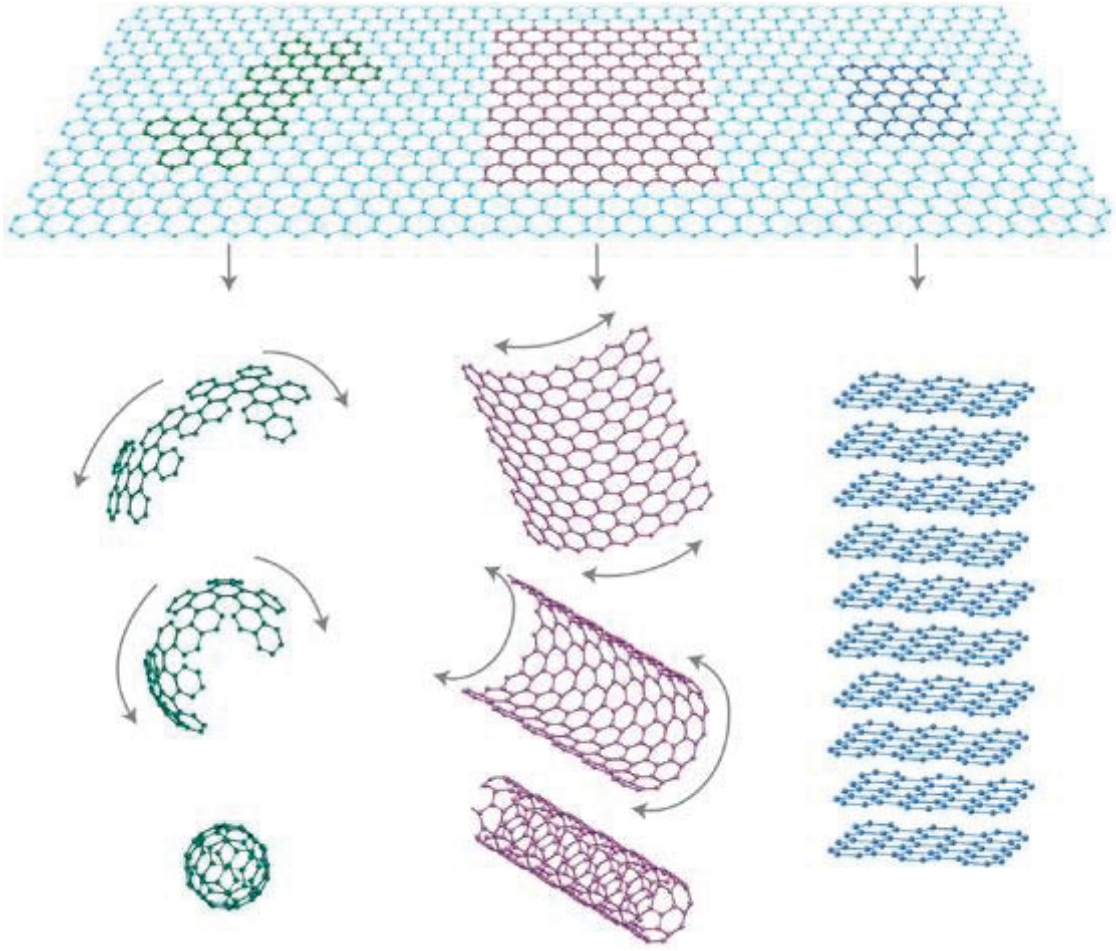

Figure 1.6 graphene is a 2D building material for carbon materials of all other dimensionalities. It can be wrapped up into 0D buckyballs, rolled into 1D CNTs or stacked into 3D graphite [1.19].

A plenty of graphene preparation methods have been reported, *e.g*. mechanical exfoliation, epitaxial growth on SiC single crystal [1.21], chemical vapor deposition (CVD) growth on transition metals Cu [1.22], Ni [1.123], Co [1.24], Fe [1.25], and other metallic single crystal substrates like Ir (111) [1.26], Rh (111) [1.27], and Ru (0001) [1.28]. Normally CVD processes employ gaseous hydrocarbon as carbon precursors. Nevertheless, it was recently report by Srivastava *et al.* [1.29] that centimeter size, uniform, and continuous single- and few-layer graphene was

synthesized on polycrystalline Cu substrates using liquid precursor (hexane). Sun *et al.* [1.23] reported that high quality graphene can be converted from a solid carbon source (poly methyl methacrylate (PMMA)). The use of soft polymer as carbon source not only increases the experimental safety, but also makes it possible to coat graphene only on desired area of the substrate. Following that, various polymer, such as polystyrene spheres (PS), poly acrylonitrile (PAN), and camphor have been used to synthesize graphene successfully [1.30, 1.31].

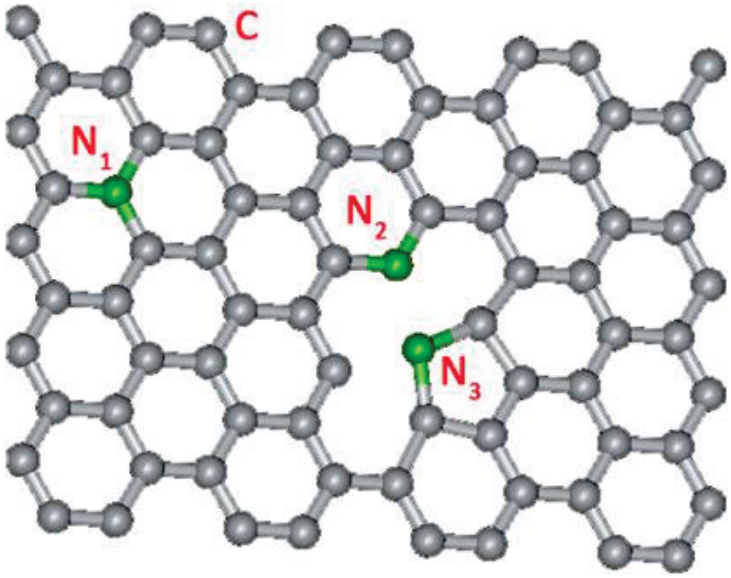

Figure 1.7 molecular models showing the types of nitrogen doping in a graphene sheet, in which the gray and green atoms denote carbon (C) and nitrogen (N), respectively. The sites N1, N2, and N3 represent substitutional graphitic nitrogen, pyridine-like nitrogen, and pyrrole-like nitrogen, respectively [1.35].

Recently, many research efforts are directed toward the elaboration of methods that allow inducing and fine-tuning of a band gap of graphene. The promising approach for tuning and controlling the electronic properties of graphene is doping with

heteroatoms [1.32-1.34], similar to that elaborated for the silicon-based technology. Thus, doping with boron or nitrogen atoms allows graphene transformation into p-type or n-type semiconductor respectively, accompanied by opening of a band gap. For nitrogen-doped graphene, there are usually three kinds of ways of introducing nitrogen atoms within the hexagonal lattice, and these are substitutional graphite-like nitrogen (N1), pyridine-like nitrogen (N2) and pyrrole-like nitrogen (N3) as shown in Figure 1.7 [1.35]. The ability to tune the electron-hole doping in graphene opens perspectives for developing tunable electronic devices through external control of the electron-phonon coupling. Another issue is that n-type or p-type graphene is also a promising candidate for applications in electrochemical biosensing, lithium battery, and fuel cells.

1.5. Purpose and Organization of Dissertation

As was mentioned above, due to their unique structural and properties, carbon nanomaterials have attracted much attention in materials science and nanoelectronicas technology. Synthesis of carbon nanomaterials with simple, low-cost and high purity is a one of the fundamental research to understand growth mechanism and intrinsic properties. Among the various synthesis methods, thermal CVD method was considered to be a simple and cost effective method for the industrial synthesis. The chief purpose of this thesis is to synthesize catalyst-free CNFs, nitrogen-doped CNTs and Nitrogen-doped graphene from a single liquid precursor by simple thermal CVD method.

In this chapter, the structure, synthesis method, and general properties of CNFs, CNTs, and graphene are introduced, their historical backgrounds, and purpose of this thesis are described. The present thesis consists of five parts. In chapter 2, the

catalyst-free synthesis of CNFs by ultrasonic spray pyrolysis of alcohol was reported. The reaction temperature, substrates, and alcohol type dependence on CNFs are studied. In chapter 3, the nitrogen-doped CNTs were synthesized directly on the metal (Ni and Fe) substrates by thermal CVD of monoethanolamine were reported. The reaction temperature and substrates dependence on nitrogen-doped CNTs are studied. In chapter 4, the nitrogen-doped graphene were synthesized on Polycrystalline Ni substrates by thermal CVD of monoethanolamine were reported. The growth temperature, deposition time, and nitrogen doping level dependence on nitrogen-doped graphene were studied. In the last chapter, summary of the present work and suggestion for future work have been discussed.

References

[1.1] Bruce A. Averill (2012), Principles of General chemistry (v. 1.0), section 20.6, http://2012books.lardbucket.org/books/principles-of-general-chemistry-v1.0/s24-06-the-origin-of-the-elements.html/ (accessed 2013-12-13).

[1.2] P. E. Bernard and H. Foing, Science 329, (2010) 1159.

[1.3] A. V. Melechko, V. I. Merkulov *et al*., J. Appl. Phys. 97, (2005) 041301.

[1.4] Shinsuke Mori and Masaaki Suzuki (2010), Nanotechnology and Nanomaterials, chapter 15 (accessed 2013-12-16).

[1.5] Y. A. Kim, T. Hayashi, M. Endo, M. S. Dresselhaus (2011), Springer Handbook of Nanomaterials, Part 7 (accessed 2013-12-16).

[1.6] M. Endo, Y. A. Kim, T. Hayashi, T. Yanagisawa *et al*., Carbon 41, (2003) 1941.

[1.7] S. Mori and M. Suzuki, Appl. Phys. Express 2, (2009) 015003.

[1.8] J. H. Lin, C. S. Chen *et al*., Carbon 46, (2008) 1619.

[1.9] S, Iijima, Nature 354, (1991) 56.

[1.10] Wikipedia (2013), http://en.wikipedia.org/wiki/Carbon_nanotube/ (accessed 2013-12-13).

[1.11] M. Scarselli, P. Castrucci and M. De. Crescenzi, J. Phys.: Condens. Matter 24, (2012) 313202.

[1.12] A. Thess, R. Lee et al., Science 273, (1996) 483.

[1.13] K. Mukhopadhyay, A. Koshio, N. Tanaka and H. Shinohara, Jpn. J. Appl. Phys. 37, (1998) L1257.

[1.14] A. Okamoto, T. Kawakubo, T. Hiraoka, T. Okazaki, T. Sugai and H, Shinohara, Mol. Cryst. Liq. Cryst. 387, (2002) 317.

[1.15] M. Terrones, N. Grobert and H. Terrones, Carbon 40, (2002) 1665.

[1.16] J. Liu, S. Webster and D. L. Carroll, J. Phys. Chem. B 109, (2005) 15769.

[1.17] M. Terrones, P. M. Ajayan and F. Bsnhsrt *et al*., Appl. Phys. A 74, (2002) 355.

[1.18] Novoselov. K. S, Geim. A. K, Morozov. S. V, Jiang. D, Zhang. Y, Dubonos, S. V, Grigorieva. I. V and Firsov. A. A, Science 306, (2004) 666.

[1.19] Geim. A. K and Novoselov. K. S, Nat. Mater 6, (2007) 183.

[1.20] Stoller. M. D, Park. S, Zhu. Y, An. J and Ruff. R. S, Nano Lett. 8, (2008) 3498.

[1.21] C. Berger, Z. Song, X. Li, X. Wu, N. Brown, C. Naud, D. Mayou, T. Li, J. Hass, A. N. Marchenkov, E. H. Conrad, P. N. First and W. A. de Heer, Science 324, (2009) 1312.

[1.22] X. Li, W. Cai, L. Colombo and R. S. Ruoff, Nano Lett. 9, (2009) 4268.

[1.23] Z. Sun, Z. Yan, J. Yao, E. Beitler, Y. Zhu and J. M. Tour, Nature 468, (2010) 549.

[1.24] A. Varykhalov and O. Rader, Phys. Rev. Lett. 80, (2009) 035437.

[1.25] Y. Z. Xue, B. Wu, Y. L. Guo, L. P. Huang, L. Jiang, J. Y. Chen, D. C. Geng, Y. Q. Liu, W. P. Hu and G. Yu, Nano Res. 4, (2011) 1208.

[1.26] S. H. Phark, J. Borme, A. L. Vanegas, M. Cobetta, D. Sander and J. Kirschner, Phys. Rev. B 86, (2012) 045442.

[1.27] E. N. Voloshina, Y. S. Dedkov, S. Torbrugge, A. Thissen and M. Fonin, Appl. Phys. Lett. 100, (2012) 241606.

[1.28] G. Li, H. T. Zhou, L. D. Pan, Y. Zhang, J. H. Mao, Q. Zou, H. M. Guo, Y. L. Wang, S. X. Du and H. J. Gao, Appl. Phys. Lett. 100, (2012) 013304.

[1.29] Srivastava. A, Galande. C, Ci. L, Song. L, Rai. C, Chem Mater 22, (2010) 3457.

[1.30] S. J. Byun, H. Lim, G. Y. Shin, T. H. Han, S. H. Oh, J. H. Ahn, H. C. Choi and T. W. Lee, J. Phys. Chem. Lett. 2, (2011) 493.

[1.31] F. Liu and Y. Zhang, Carbon 48, (2010) 2394.

[1.32] Wang. Y, Shao. Y, Maston. D. W and Li. U, ACS Nano 4, (2010) 1790.

[1.33] Hanafusa. A, Muramatsu. Y, Kaburagi. Y, Yoshida. A, Hishiyama. Y, Yang. W, Denlinger. J. D and Gullikson. E. M, App. Phys. Lett. 98, (2011) 184102.

[1.34] Yang. Z, Yao. Z, Li. G, Fang. G, Nie. H, Liu. Z, Zhou. X, Chen. X and Huang. S, ACS Nano 6, (2012) 205.

[1.35] H. Terrones, R. Lv, M. Terrones and M. S. Dresselhaus, Rep. Prog. Phys. 75, (2012) 062501.

Chapter 2

Catalyst-Free Synthesis of Carbon Nanofibers by Ultrasonic Spray Pyrolysis of Alcohol

2.1. Introduction

CNFs [2.1] have attracted considerable attention as promising carbon materials because of their high aspect ratio, small radii of curvature, low chemical activity, and mechanical toughness properties. They are expected to be applied for various applications such as in electron field emission source [2.2], probe tip [2.3], and fuel cells [2.4].

Chemical vapor deposition (CVD) is a promising technique for mass producing CNFs because it is a simple, low cost fabrication process. Synthesizing CNFs by CVD generally requires using transition metals as catalysts. Aoki *et al*. have grown amorphous CNFs by thermal CVD with CuNi alloy films as a catalyst in a mixture of acetylene and helium [2.5]. CNFs have also been synthesized by plasma-enhanced CVD using Fe, Ni, Co, and their alloys (e.g., FeCo) as catalysts CNF [2.6, 2.7].

Zhang *et al.* recently synthesized CNFs without using transition metal catalysts by ultra-sonic spray pyrolysis. CNFs that are several tens of nanometers in diameter have been produced using graphite, fullerene, or boron as nucleating site [2.8, 2.9]. Deng *et al*. developed a simple method for synthesizing CNFs that involves non-catalytic thermal decomposition of acetylene on a copper substrate [2.10]. From a view point of process simplification and product purification, catalyst-free synthesis is attractive. Several methods have been reported for synthesizing CNFs using

non-transition metal catalysts [2.8, 2.9], but the details of these methods have not been clarified. Therefore further study of catalyst-free CVD methods for synthesizing CNFs is required.

In this chapters, synthesis of CNFs by ultrasonic spray pyrolysis of alcohol only without using a catalyst were reported. The dependence of carbon deposition on the substrates, position of the substrate in the reaction tube and alcohols type were investigated.

2.2. Experimental Details

Figure 2.1 shows the schematic diagram of ultrasonic spray pyrolysis [2.11]. Alcohol was placed in a medication cup and pure nitrogen gas was used to transport the precursor mist generated in the atomization chamber to a quartz tube (length: 65 cm; diameter: 28 mm) in the electric furnace. Silicon and quartz substrates (size: 10 mm × 10 mm) were cleaned in acetone and methanol, washed in de-ionized water, and dried using nitrogen blower. Substrates were placed in quartz boats, which were placed at three different positions (position1, 2, and 3 in Figure 2.1). When the furnace temperature was set to 850 °C, a thermocouple measured temperature of 890 °C, 820 °C, and 570 °C at position 1, 2 and 3 in the quartz tube; respectively. Both ends of the quartz tube were then closed by quartz joints; one ends was connected to a nebulizer and other end was connected to water bubbler. A constant nitrogen flow with a flow rate of 0.5 l/min was applied until the temperature reached 700 °C -1000 °C. After the furnace reached the set temperature, the nitrogen flow rate was increased to 1l/min and this state was maintained for 5 min. An alcohol mist was passed through the reaction tube for 20 min – 120 min. After deposition, the furnace was turned off and allowed to

cool to room temperature. As-produced samples were characterized by atomic force microscopy (AFM, SII, SPA300), field emission scanning electron microscopy (FE-SEM, JEOL-7001F), scanning electron microscopy (SEM, Hitachi s-3000H), and transmission electron microscopy (TEM, Hitachi JEM-Z2500 and JEOL JEM-2100F) to check the quality and overall morphology. Raman spectroscopy was performed using JASCO NRS-1500W with 532-nm-wavelength excitation.

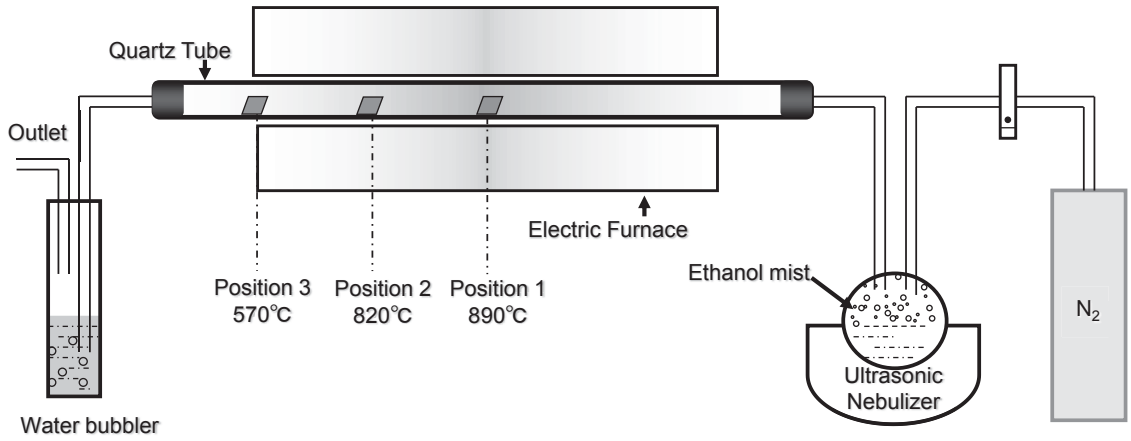

Figure 2.1 schematic diagram of ultrasonic spray pyrolysis of alcohol.

2.3. Results and Discussion

2.3.1 Substrates Dependence

Figure 2.2 (a-c) shows FE-SEM images of the as-grown samples on quartz substrates at positions 1, 2, and 3, respectively, at 850 °C using ethanol as carbon source. The samples at positions 1 and 2 have amorphous carbon films with carbonaceous nanoparticles on their surface, whereas the sample at position 3 clearly exhibit CNFs.

Substrates dependence of carbon deposition on silicon substrates were

investigated also. Figure 2.3 (a-d) show AFM images of the samples synthesized at 850 °C using ethanol as carbon source at positions 1 and 2 on silicon and quartz substrates, respectively. There is not so remarkable difference of surface morphology between the films formed on silicon and quartz substrates. Figure 2.4 show SEM images of CNFs synthesized at 850 °C on silicon substrates at position 3. Similar results were observed on the silicon substrates.

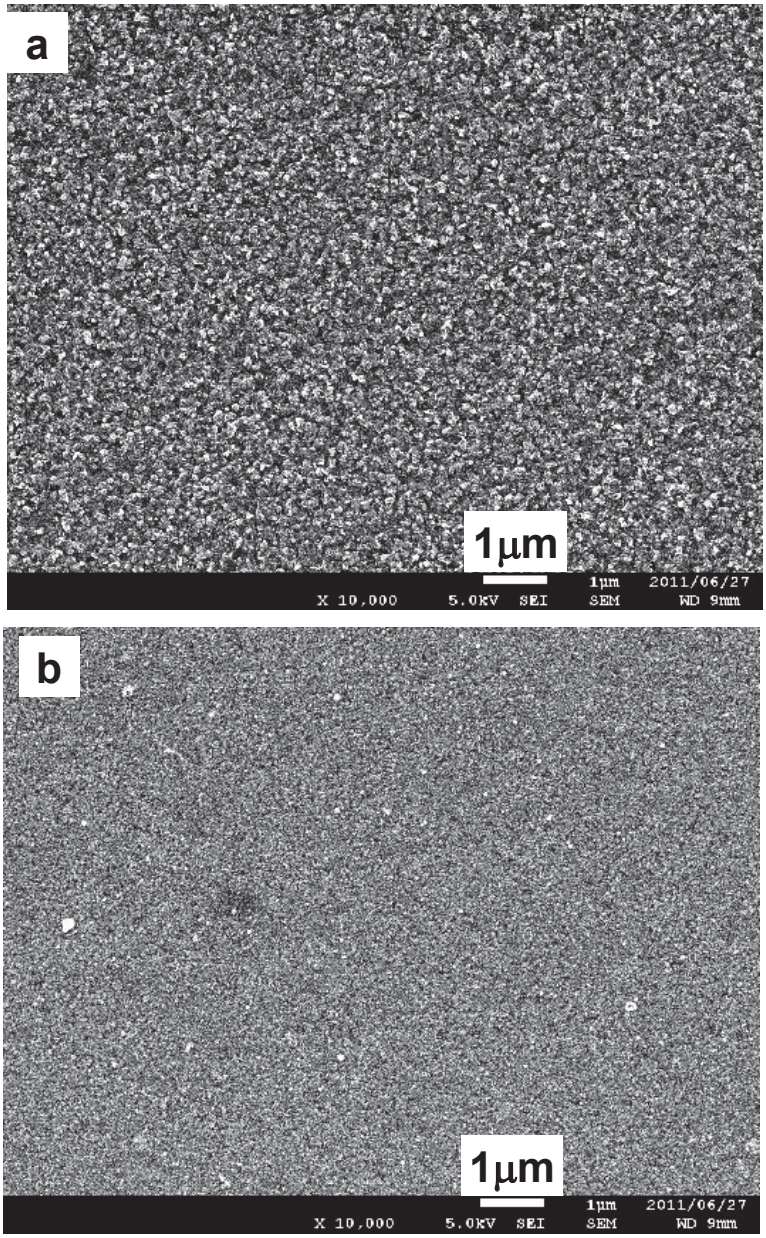

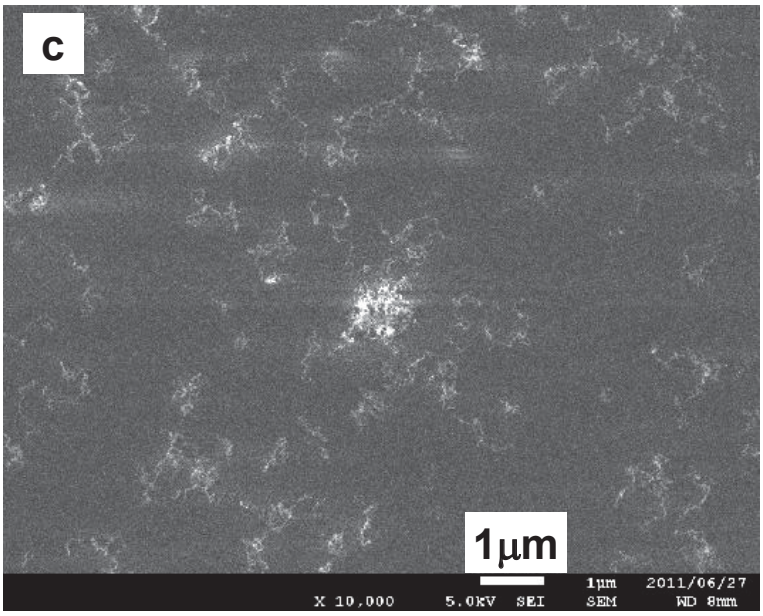

Figure 2.2 (a-c) FE-SEM images of the as grown samples on quartz substrates at position 1, 2, and 3, respectively, using ethanol as carbon source at 850 °C.

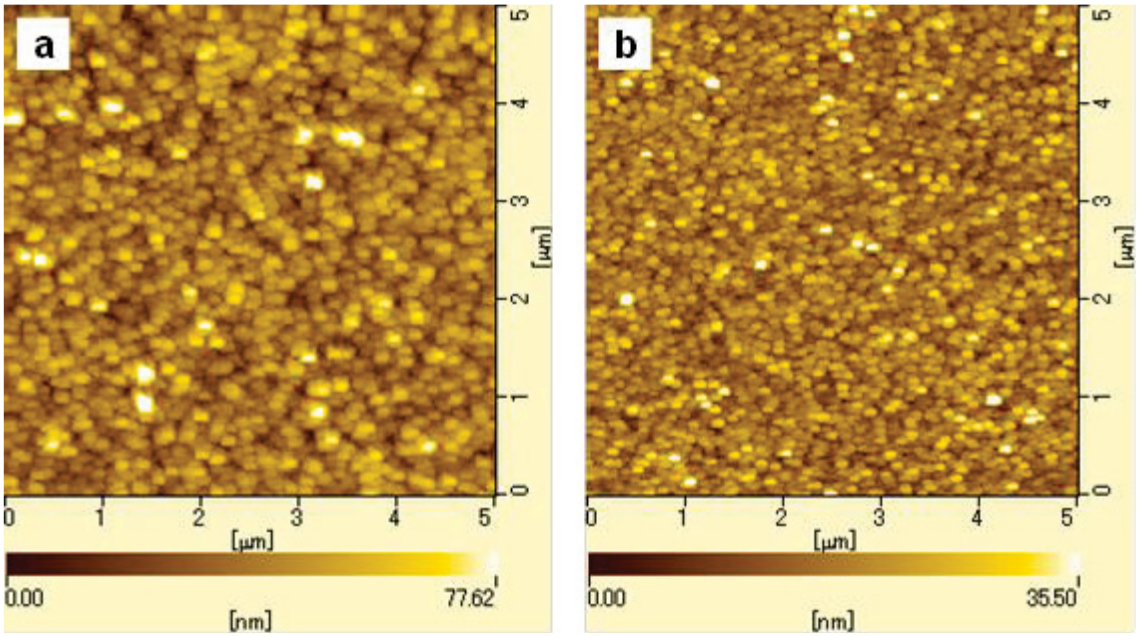

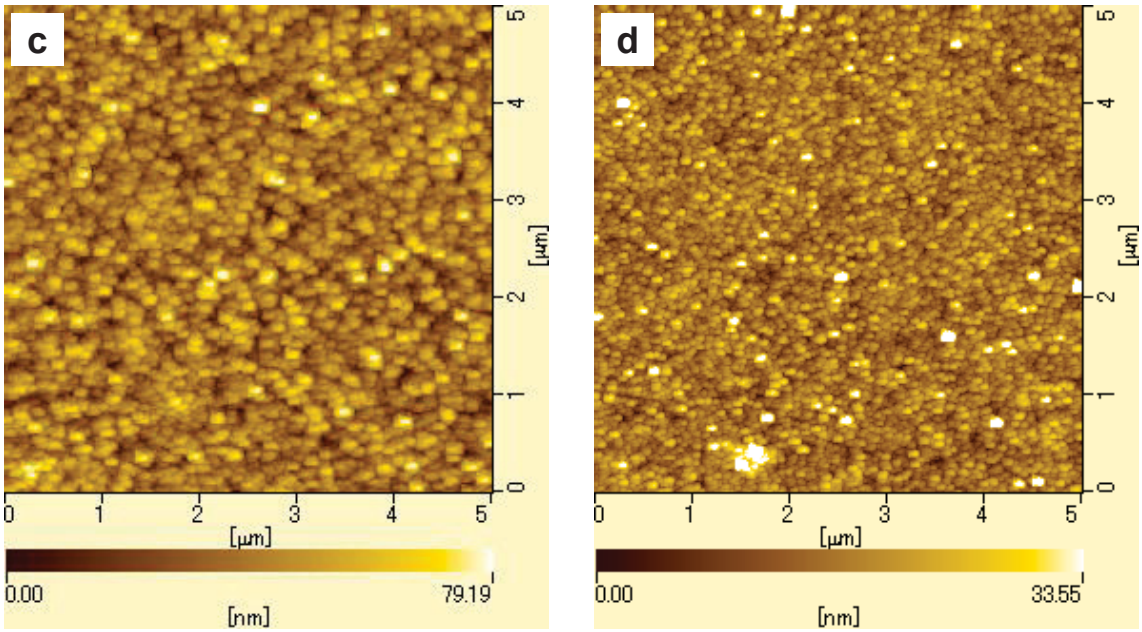

Figure 2.3 AFM images of the as-grown samples synthesized at 850 °C using ethanol as carbon source at position 1and 2 on (a, b) silicon and (c, d) quartz substrates, respectively.

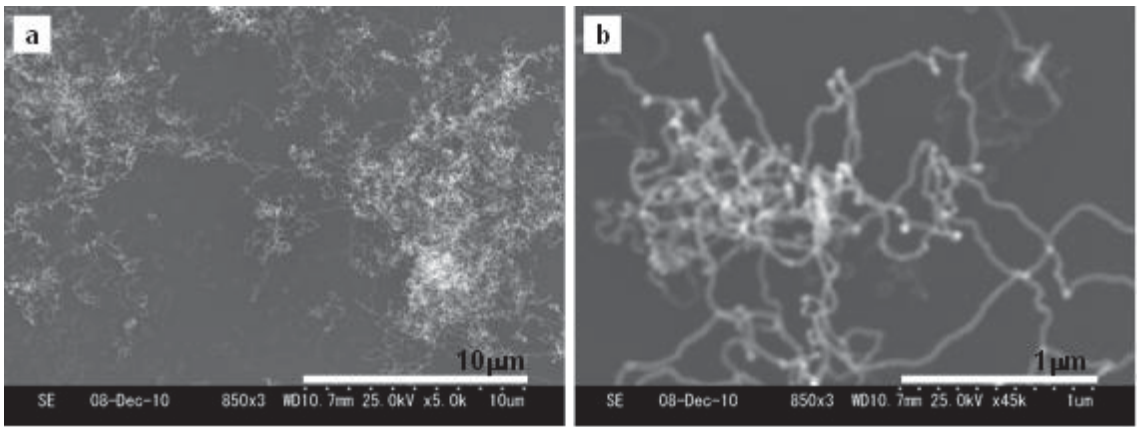

Figure 2.4 SEM images of the CNFs at position 3 on silicon substrates using ethanol as carbon source at 850 °C (a) low magnification (b) high magnification.

2.3.2 Deposition Temperature Dependence

To investigate the temperature dependence of carbon deposition, the furnace

temperature was varied in the range of 700 °C -1000 °C. Some carbon particles were formed at position 1 and 2 in the temperature 700 °C. Deposition of amorphous carbon films were observed on the samples at position 1 and 2 in the temperature range of 800 °C -1000 °C is shown in Figure 2.5 (a-j). In contrast, CNFs formed on the samples at position 3 for temperature between 800 °C and 900 °C is shown in Figure 2.6 (a-c).

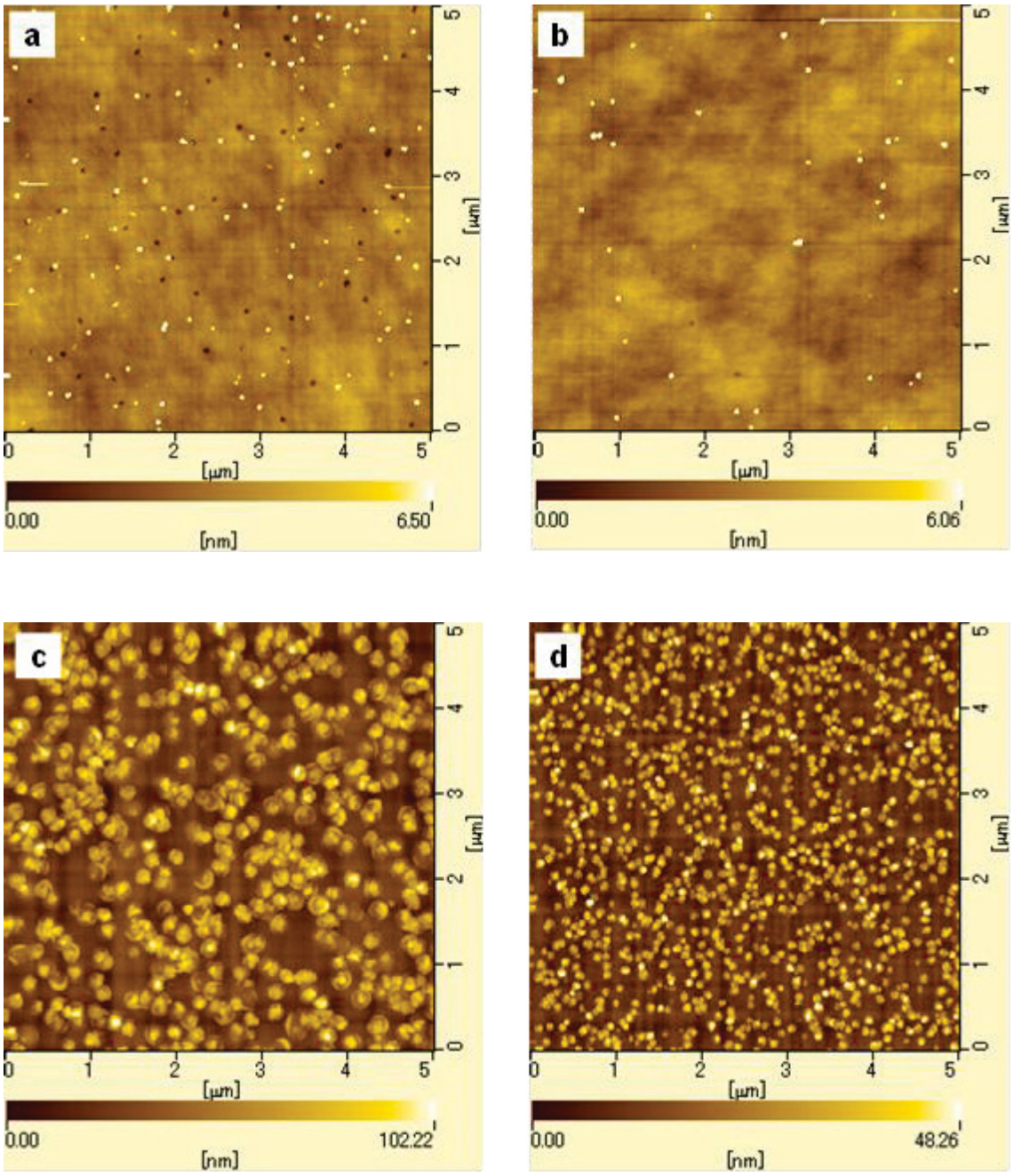

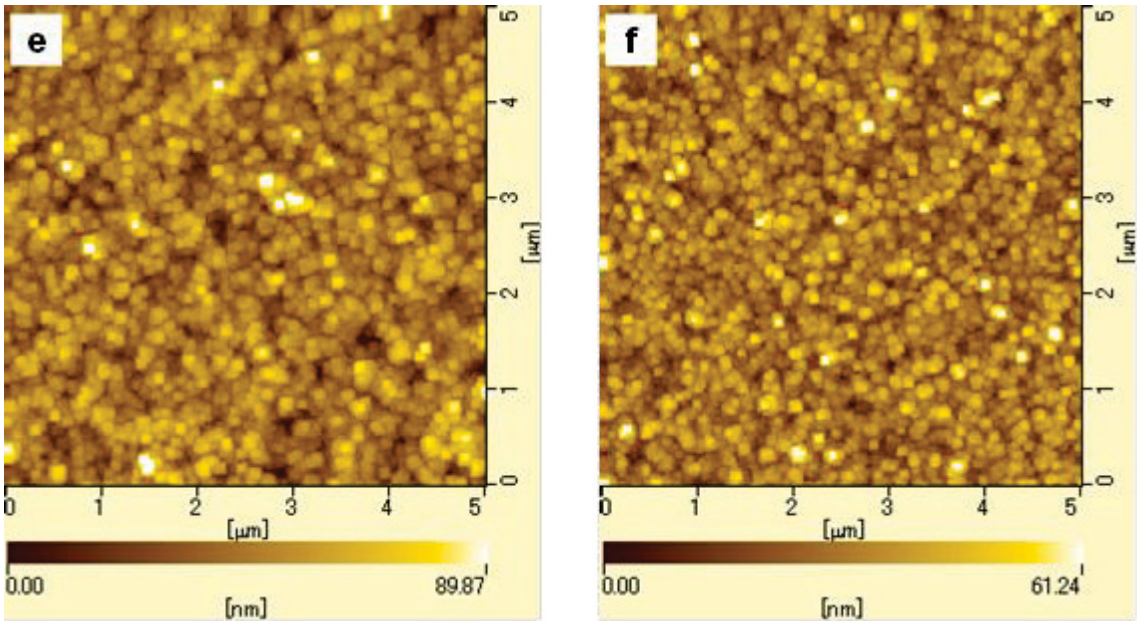
e
f
0
1
2
3
4
5
[µm]
0.00
89.87
61.24
[nm]

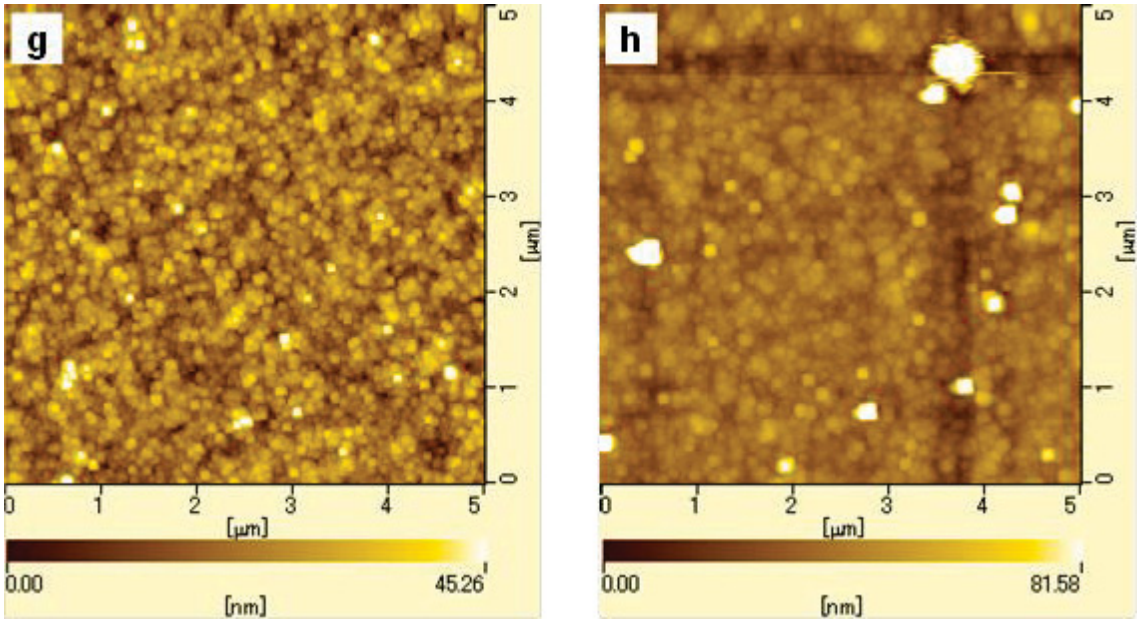
g
h
0
1
2
3
4
5
[µm]
0.00
45.26
81.58
[nm]

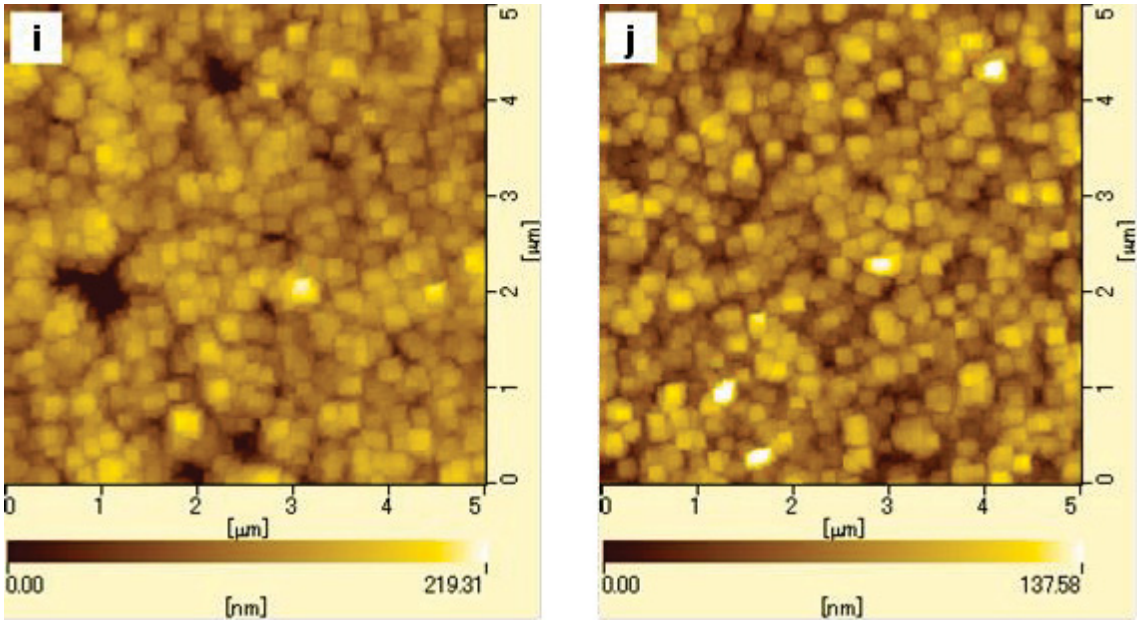

Figure 2.5 AFM images of as-grown samples on silicon substrates at position 1 and 2 at (a, b) 700 °C, (c, d) 800 °C, (e, f) 900 °C, (g, h) 950 °C, and (i, j) 1000 °C, respectively.

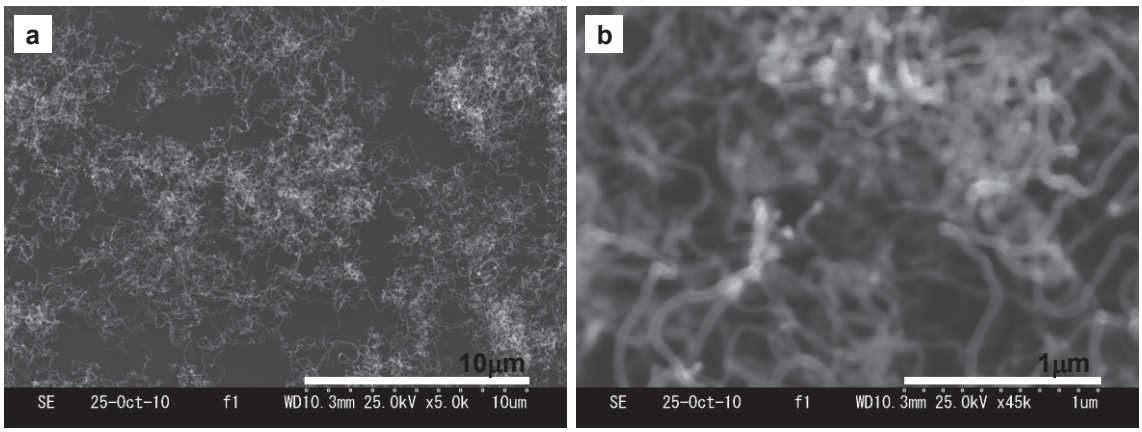

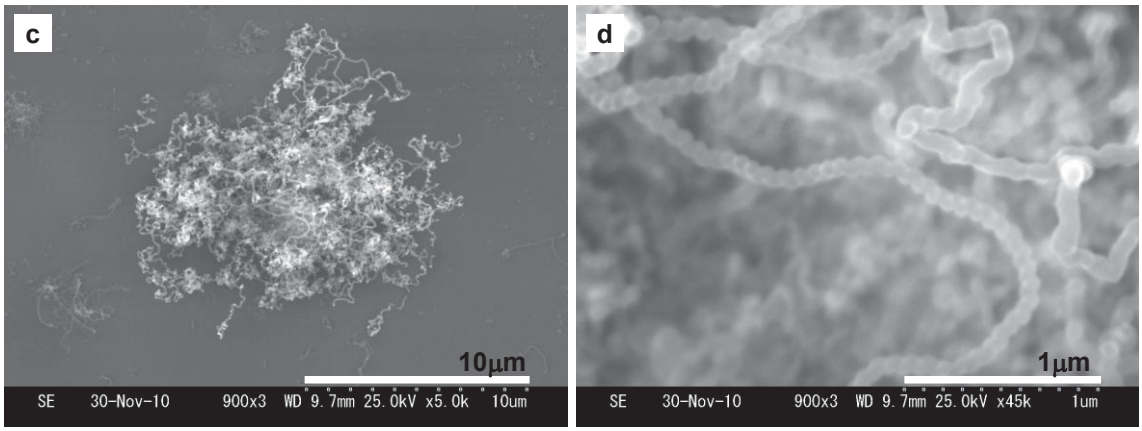

Figure 2.6 low and high magnification SEM images of CNFs synthesized on silicon substrates at position 3 using ethanol as carbon source at (a, b) 800 °C (c, d) 900 °C.

Figure 2.7 (a) shows a low-magnification TEM image of CNFs synthesized at 850 °C on silicon substrate; they exhibit bamboo-like (i.e., hollow fibril) morphology. The CNFs are about 20 nm in diameter. As shown in Figure 2.7 (b), these CNFs are open consisting of fringes with a low degree graphitization and small sheets.

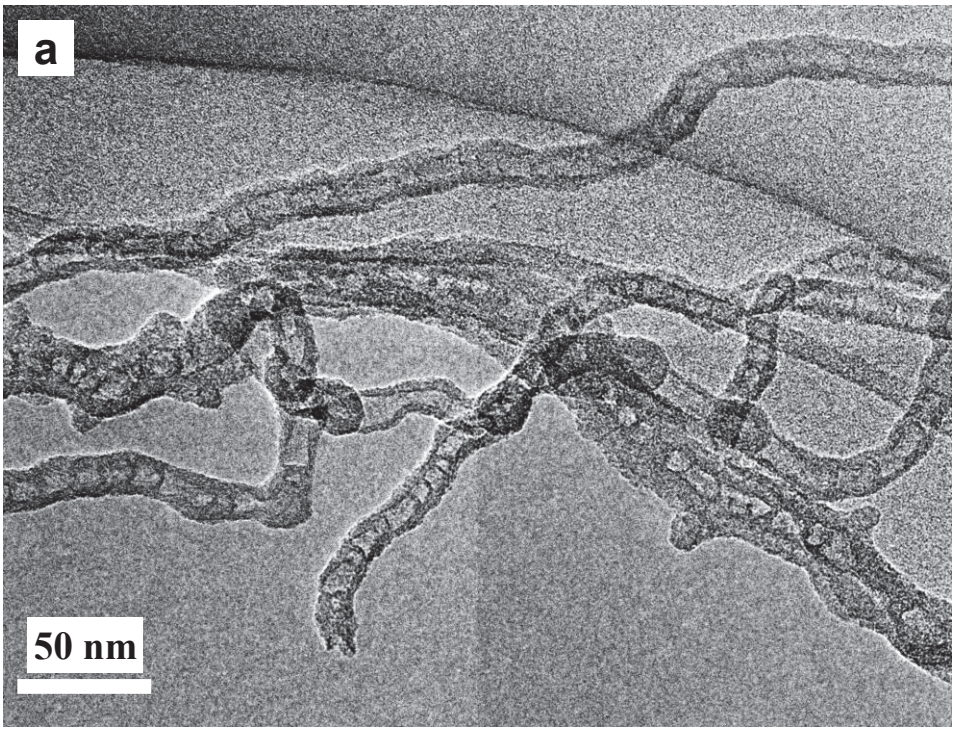

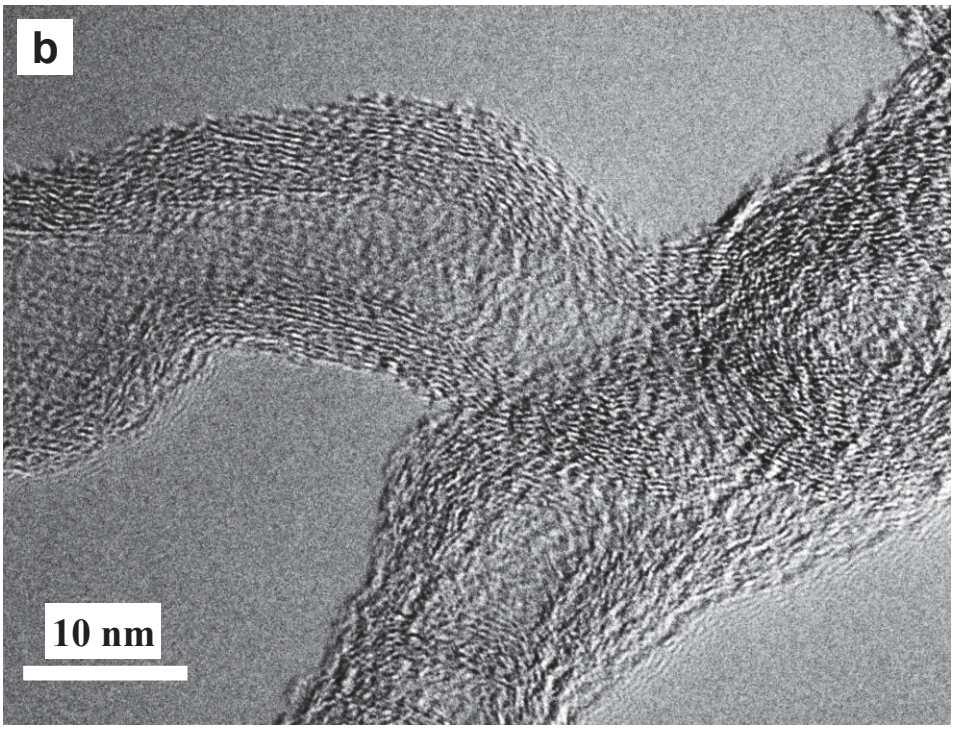

Figure 2.7 (a) low magnification and (b) high magnification TEM images of CNFs synthesized at position 3 using ethanol as carbon source. The furnace temperature was set to 850 °C.

Raman spectroscopy is a powerful tool to identify and evaluate the quality of as-grown carbon nanomaterial. The as-grown samples synthesized at 850 °C on quartz substrates were characterized by Raman spectroscopy. As shown in Figure 2.8, two distinct peaks were observed at about 1350 cm^{-1} and 1597 cm^{-1}, corresponding respectively to the D- and G-band of graphite materials. The broadening of these lines into bands implies that the CNFs have a low crystallinity and are composed of small sheets with a low degree of graphitization. The D-band maybe associated with structural defects and disorder in the CNFs. The G-band is due to vibration of sp^2 bonded carbons in a 2D hexagonal lattice [2.12]. The prominent D-band in Figure 2.8 indicates a low graphitization degree and presence of a many defects and disorder. Samples at positions

1, 2, and 3 have intensity ratio I_D/I_G of 1.19, 1.12, and 0.93, respectively; the ratio of the sample at position 3 is considerably lower than those position 1 and 2.

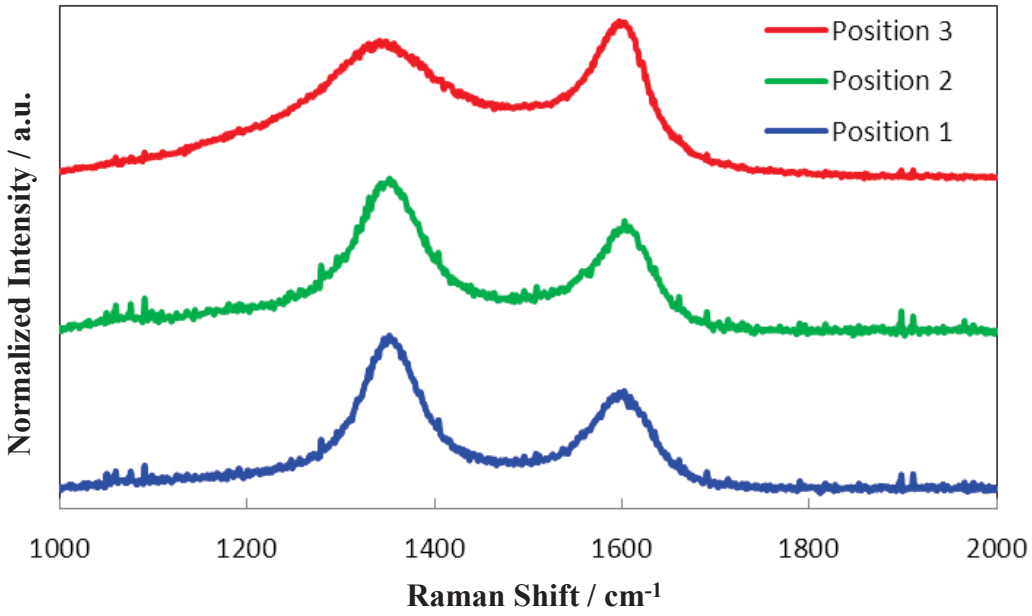

Figure 2.8 Raman spectra of as-grown samples located at position 1, 2, and 3, on quartz substrates using ethanol as carbon source at 850 °C.

2.3.3 Alcohol Type Dependence

The dependence of alcohols type for catalyst-free synthesis of CNFs was investigated. Figure 2.9 shows photograph of the as-produced samples were synthesized on the quartz substrates (1cm x 1cm) at 850 °C using methanol, ethanol, and 2-propanol, respectively. The carbon deposition clearly depends on alcohol type and the substrate position. The quartz substrates at position 1 and 2 appeared to be completely black when methanol ethanol and 2-propanol were used as the carbon source, whereas when methanol was used as the carbon source, the substrates at position 1 and 2 were transparent.

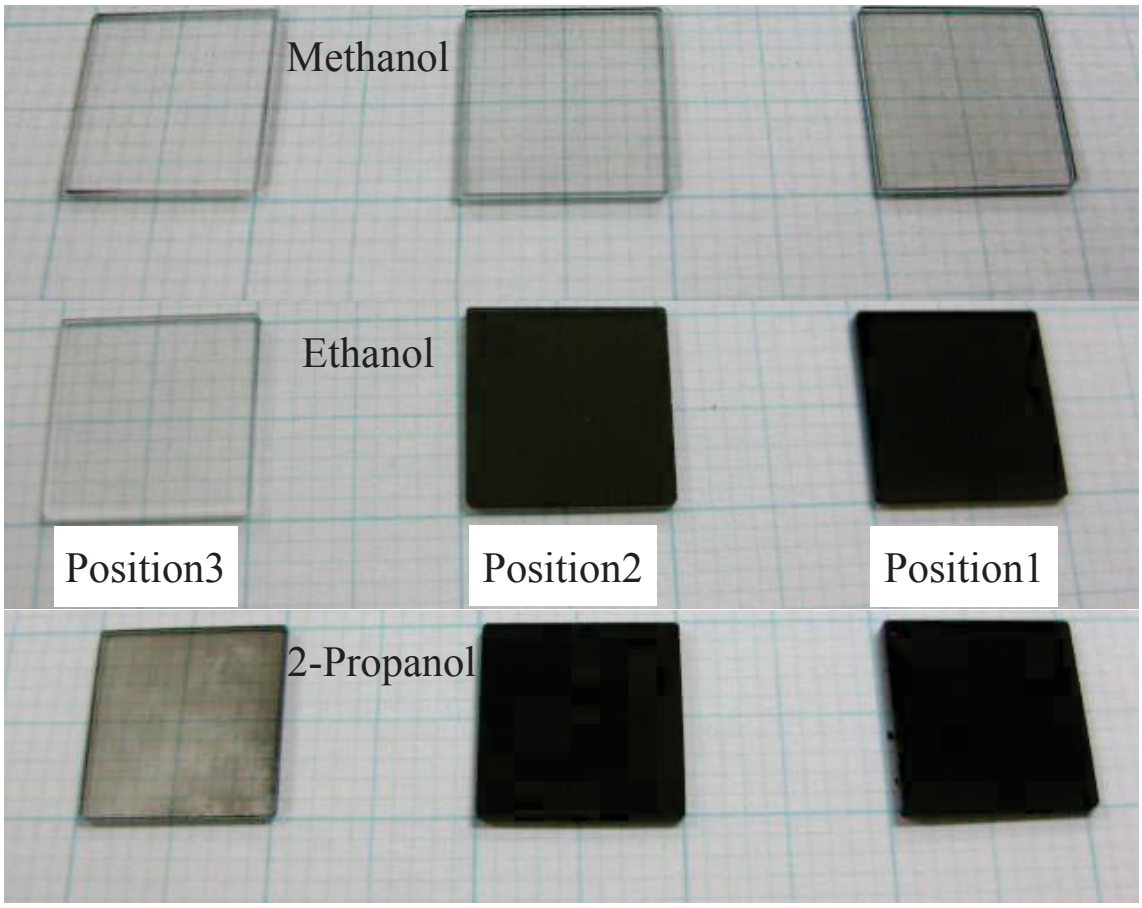

Figure 2.9 photograph of the as-produced samples were synthesized on quartz substrates (1cm x 1cm) at 850 °C using methanol, ethanol, and 2-propanol as carbon source.

Figure 2.10 shows SEM images of the samples formed by using different carbon source on silicon substrates at position 1, 2, and 3. When methanol used as the carbon source, CNFs were observed at position 1 and 2, whereas a few carbon particles were observed at position 3. In contrast, when ethanol and 2-propanol were used as the carbon source, the samples at positions 1 and 2 were amorphous carbon films with carbonaceous nanoparticle on their surface, whereas the sample at position 3 clearly exhibited CNFs.

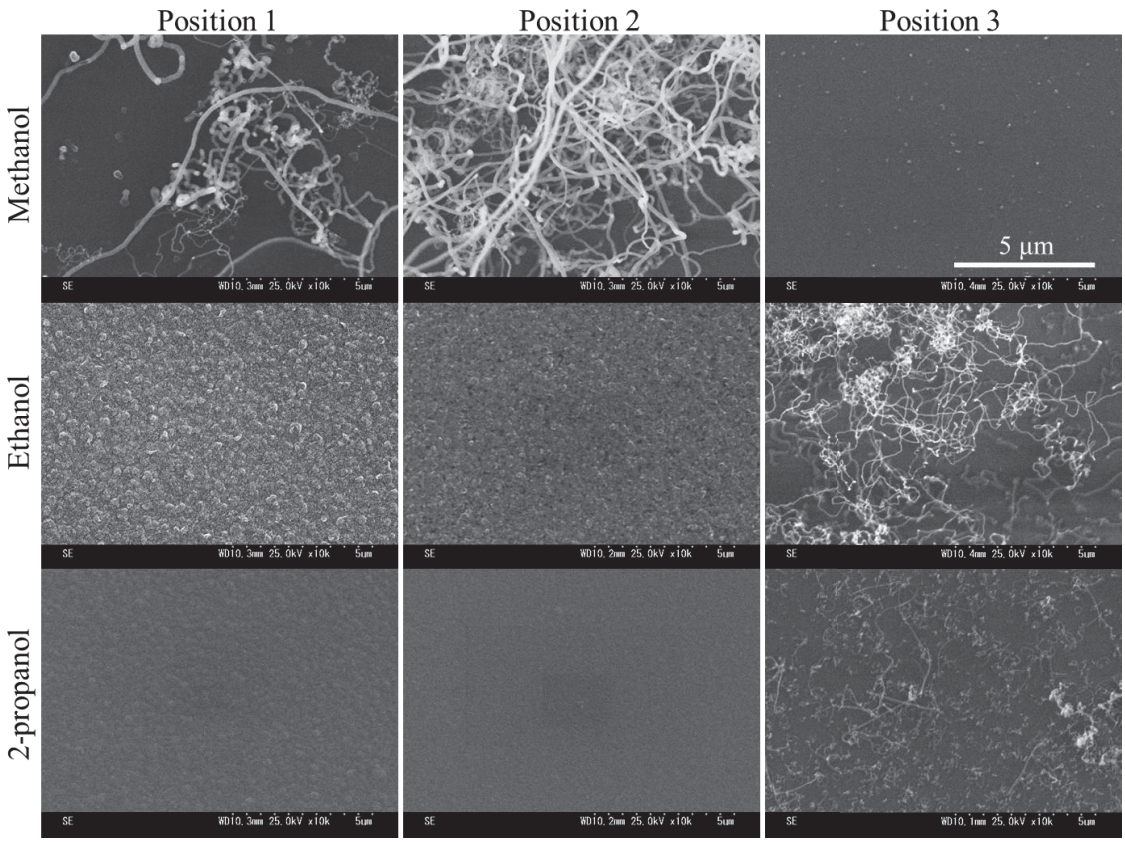

Figure 2.10 SEM images of as-grown samples on silicon substrates at position 1, 2, and 3, using methanol, ethanol, and 2-propanol, as carbon source.

To investigate the temperature dependence of CNFs using methanol and 2-propanol as carbon source, the furnace temperature was varied in the range 700 °C - 1000 °C. When methanol was used as carbon source, CNFs were observed at positions 1 and 2 in the range 850 °C - 1000 °C (Figure 2.11). In contrast, when 2-propanol was used as the carbon source, CNFs were observed at position 3 in the range 750 °C - 850 °C (Figure 2.12).

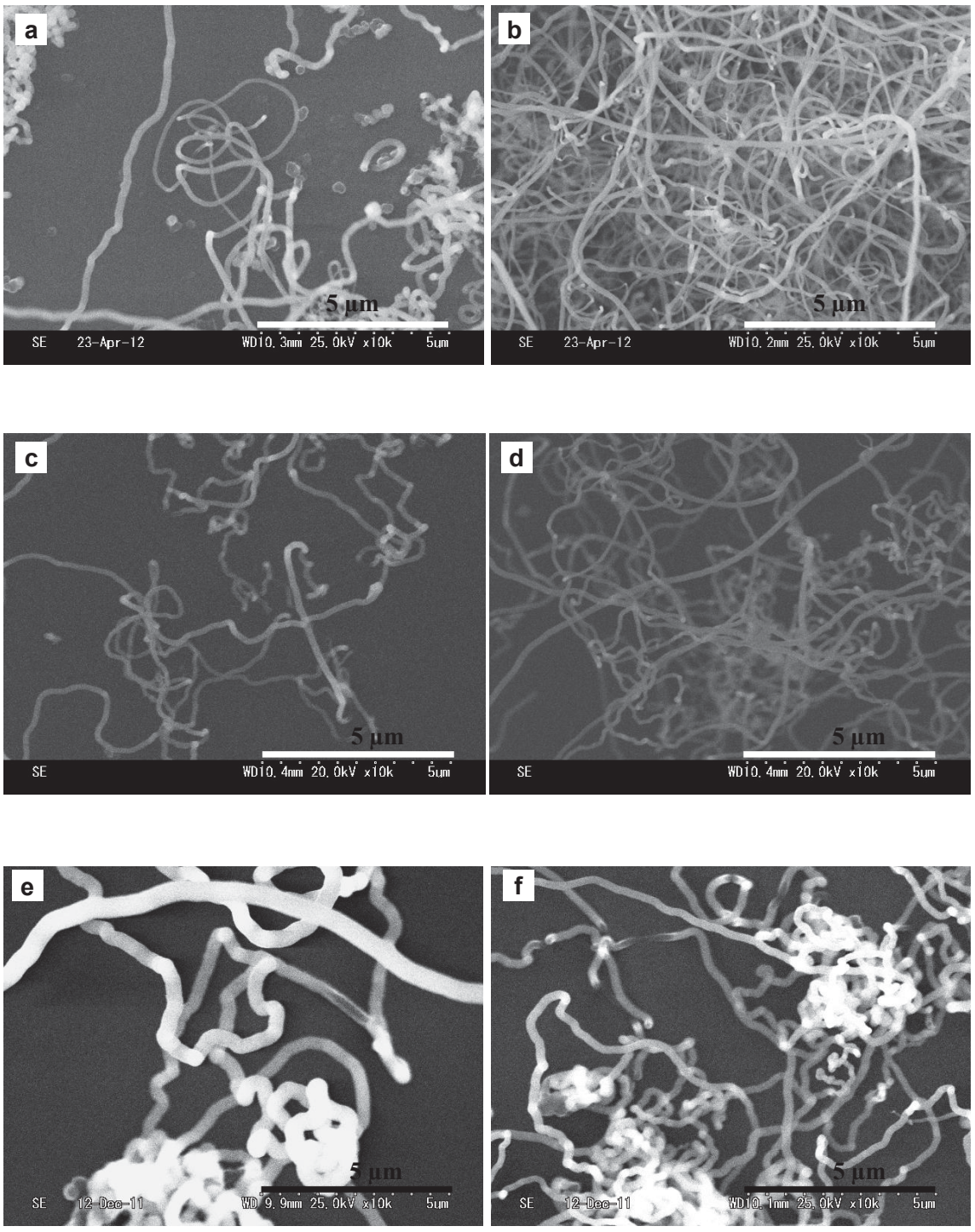

Figure 2.11 SEM images of CNFs synthesized on silicon substrates at position 1 and 2, using methanol as carbon source at (a, b) 900 °C, (c, d) 950 °C, and (e, f) 1000 °C, respectively.

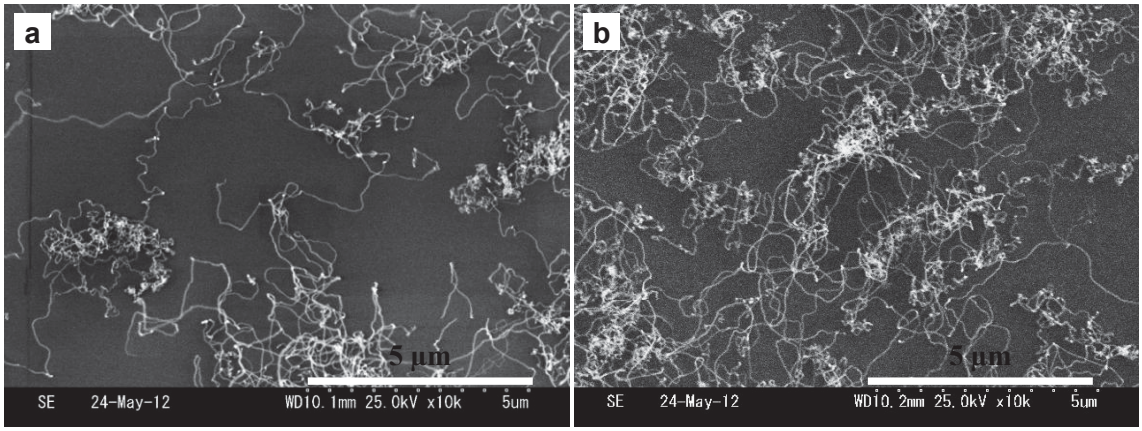

Figure 2.12 SEM images of CNFs synthesized on silicon substrates at position 3, using 2-propanol as carbon source at (a) 750 °C and (b) 800 °C.

Figure 2.13 shows a sample synthesized on silicon substrates at 850 °C on position 2 using methanol as carbon source, (a) low magnification and (b) high magnification TEM image. The CNFs are about 50-100 nm in diameter with solid amorphous carbon body surrounded with graphitized shell.

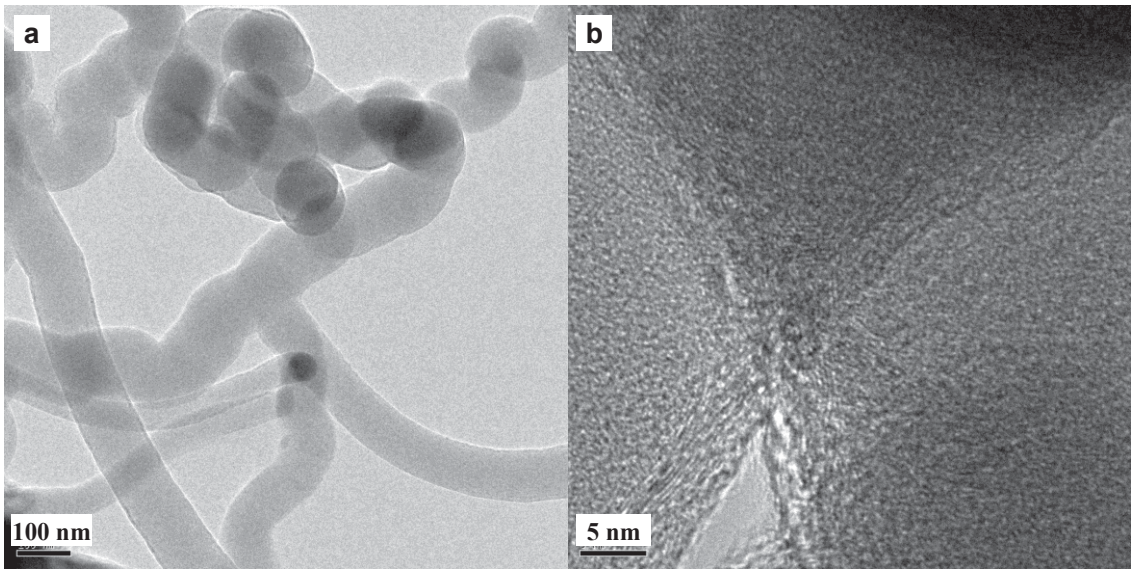

Figure 2.13 (a) low and (b) high magnification TEM images of CNFs synthesized on silicon substrates at position 2 using methanol as carbon source at 850 °C.

Figure 2.14 shows a sample synthesized on silicon substrates at 850 °C on position 3 using 2-propanol as carbon source, (a) low magnification and (b) high magnification TEM image. They similar to CNFs synthesized on silicon substrates at 850 °C on position 3 using ethanol as carbon source; exhibit some hollow structure. The CNFs are about 20-50 nm in diameter, thinner than using methanol as carbon source.

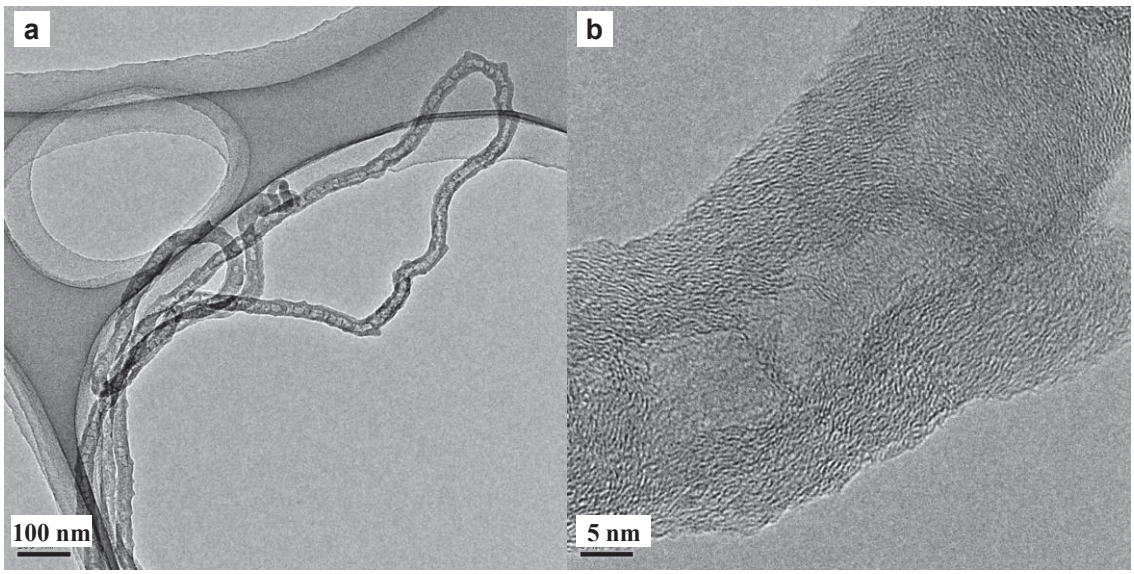

Figure 2.14 (a) low and (b) high magnification TEM images of CNFs synthesized on silicon substrates at position 3 using 2-propanol as carbon source at 850 °C.

Figure 2.15 (a-c) shows Raman spectra of the as-grown samples synthesized on the silicon substrates at 850 °C using methanol, ethanol, and 2-propanol, respectively, as the carbon source. Two distinct peaks were observed at about 1350 and 1597 cm^{-1}, corresponding to the D- and G-bands, respectively. The broadening of these lines into broad bands implies that the CNFs have poor graphitization or amorphous structure [2.12]. We also found that all of the D- and G-peak intensity ratio I_D/I_G of CNFs were smallest compared to samples without formed CNFs (shown in the left inset of Figure

2.15 (a-c)).

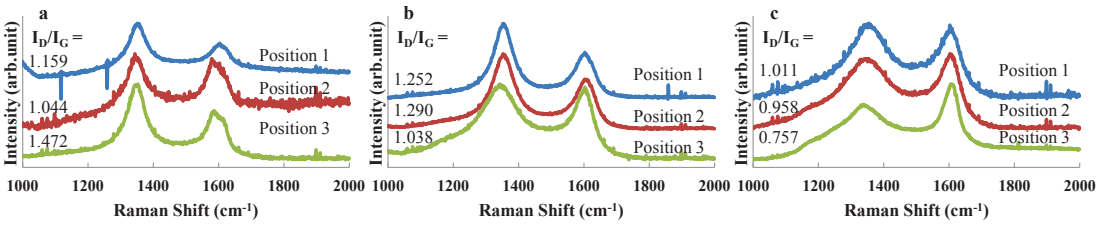

Figure 2.15 (a)-(c) Raman spectra of as-grown samples on silicon substrates located at positions 1, 2, and 3, using methanol, ethanol, and 2-propanol, respectively, as the carbon source. The furnace temperature was 850 °C.

To investigate a deposition time effects for CNFs growth, shorter deposition time experiment were performed. As shown in Figure 2.16, the nanoparticles were formed on the surface of substrates, and a few nanoparticles grow into filament morphologies. Recent experimental and theoretical studies show that hydrocarbon-molecule decomposition and graphite formation abilities are not essential and lead to a new interpretation of the role of catalyst particle in CNFs and CNTs growth: only a pore structures or nanoscale curvature would be necessary to grow CNFs and CNTs if carbon atoms are supplied to the nanocurvature [2.8, 2.9, 2.14].

On the basis of the results and discussion above, the mechanism of the catalyst-free CNFs synthesized by alcohol only is proposed that: first, alcohols were decomposed on the substrates and formed nanoparticles. Second, these nanoparticles play as a nucleation site and grow into CNFs.

The alcohols type and substrate's position dependence of the morphology of carbon deposition on the substrates are currently unclear. However, similar results in

both ethanol and 2-propanol were observed that large amount of carbon deposition was formed in the center of reaction tube whereas some hollow structure CNFs were formed in the downstream of reaction tube. On the other hand, amorphous structures CNFs were formed in the center of reaction tube when methanol was used as the carbon source. This was considered that the presence of the alkyl groups in the alcohols worked important role in the CNFs growth. Assuming that the bonds in alcohols dissociated thermally along the sequence of their bond energies, the C-C bonds should dissociate first as they were found to be the weakest in both ethanol and 2-propanol. In methanol, the weakest bond is H-C because of the absence of C-C bonds (shown in Table 2.1) [2.13]. Therefore, using methanol as the carbon source some different results compared to ethanol and 2-propanol were obtained.

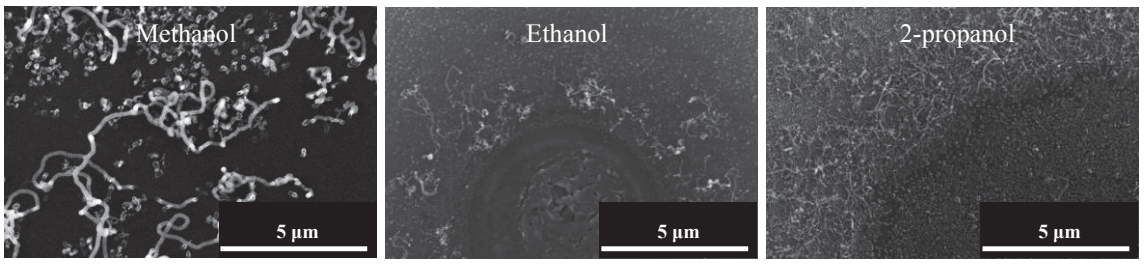

Figure 2.16 as-grown samples synthesized at 850 °C for 20 min using methanol, ethanol, and 2-propanol, respectively.

Alcohols	Bonds Energy (kJ mol^{-1})
Methanol CH_3OH	C–O: 385
	H–C: 335
	O–H: 437
Ethanol C_2H_5OH	C–O: 391
	C–C: 365
	H–C: 411
	O–H: 464
2-propanol C_3H_7OH	O–H: 438
	C–O: 392
	C–C: 370
	C–C: 356
	H–C: 422
	O–H: 443

Table 2.1 bond energies of alcohol molecules [2.13].

2.4. Summary

In this chapter, the CNFs synthesized on silicon and quartz substrates by catalyst-free ultrasonic spray-pyrolysis using alcohols only (methanol, ethanol, 2-propanol) were reported. The morphology of carbon deposition on the substrates strongly depended on the substrate location in the reaction tube and the carbon source species. Amorphous carbon films were formed on the center of the reaction tube

whereas some hollow structure CNFs were formed in the downstream area of the reaction tube when ethanol or 2-propanol was used as the carbon source. Amorphous carbon structures CNFs were formed at the center of the reaction tube when methanol was used as the carbon source, whereas similar results were in both ethanol and 2-propanol that some hollow structure with a thin diameter of CNFs were formed at the downstream of the furnace. Thus, it is concluded that the presence of the alkyl groups in the alcohols played important role in the CNFs growth with a different morphology. The mechanisms of catalyst-free CNFs synthesized by alcohols only were concluded that carbon nanoparticles were formed at the first stage, and these carbon nanoparticles were played to nucleation site grow into CNFs.

References

[2.1] A. Oberlin, M. Endo, and T. Koyama, J. Cryst. Growth 32, (1976) 335.

[2.2] K. B. K. Teo, M. Chhowalla, G. A. J. Amaratunga, and W. I. Milne, Appl. Phys. Lett 80, (2002) 2011.

[2.3] H. Cui, S. V. Kalinlin, X. Yang, and D. H. Lowndes, Nano Lett 4, (2004) 2157.

[2.4] Jui-Hsiang Lin, Tse-Hao Ko, Miao-Yu Yen, Energy &Fuels 23 (2009) 4042.

[2.5] Katsunori A, Tetsurou Y, Hiroshi F, Takashi I, Shinichi H, Mamoru F, Kenjiro O, Takashi H, Jpn. J. Appl. Phys 45, (2006) 5329.

[2.6] Vladimir l. Merkulov, A. V. Melechko, M. A. Guillorn, M. L. Simpson Appl. Phys. Lett 80, (2002) 4816.

[2.7] K. D. Sorge, K. L. Klein, A. V. Melechko, C. L. Finkel, O. Malkina, Th. Leventouri, J. D. Fowlkes, P. D. Rack, M. L. Simpson, J. Appl. Phys 104, (2008) 033909.

[2.8] Zhang J, Khatri I, Kishi N, Soga T, Jimbo T, IEICE Transactions on Electronics E92-C, (2009) 1432.

[2.9] Zhang J, Khatri I, Kishi N, Soga T, Jimbo T, Materials Letters 64, (2010) 1243.

[2.10] Da Deng, Jim Yang Lee, Chem. Mater 19, (2007) 4198.

[2.11] Khatri I, Soga T, Jimbo T, Adhikari S, Ram A H, Umeno M, Diamond Rel Mater 18, (2009) 319.

[2.12] A. C. Ferrari, J. Robertson, Phys. Rev. B 61, (2000) 14095.

[2.13] Y. L. Li, L. H. Zhang, X.H Zhong A. H Windle, Nanotechnology 18, (2007) 225604.

[2.14] J. H. Lin, C. S. Chen *et al*., Carbon 46, (2008) 1619.

Chapter 3

Synthesis of Nitrogen-Doped Carbon Nanotubes on Metal Substrates from a Single Liquid Precursor

3.1. Introduction

CNTs were first imaged by Iijima in 1991 [3.1], and are now being investigated worldwide for potential applications such as field emission, sensors, and fuel cells [3.2-3.4] because of their unique physical properties and morphology. Doping CNTs with other elements could be an interesting way to tune their properties [3.5]. This has led to an increasing interest in preparing nanotubes of other elements such as boron nitride [3.6, 3.7], and CNTs doped with other elements such as boron [3.8], nitrogen [3.9, 3.10], and phosphorous [3.11]. The advantage of such nanotubes is that their electronic properties are primarily determined by their composition, and are thus relatively easy to control. Nitrogen is considered the most effective dopant for CNTs. Doping with nitrogen is expected to enhance the conductivity of CNTs, because it provides additional electron carriers for the conduction band [3.12].

Two methods have generally been used to synthesize Nitrogen-doped CNTs (N-doped CNTs). One involves multiple steps including preparation of the catalyst and/or supporting materials and the growth process. The other uses two precursors (nitrogen and carbon sources and/or catalyst). Yun et al. synthesized N-doped CNTs by thermal chemical vapor deposition (CVD) of methane/ammonia and acetylene/ammonia mixtures on silicon substrates coated with $FeCl \cdot 4H_2O$ [13]. Hao et al. fabricated N-doped CNTs by floating catalyst CVD using a mixture of ferrocene and

melamine on silicon substrates with an aluminum buffer layer [3.14]. Recently, some interesting progress has been made in controlling the morphology and structure of N-doped CNTs using different liquid nitrogen precursors using an aerosol method [3.15, 3.16]. However, further development of simple methods to synthesize N-doped CNTs is required.

In this chapter, commercially available metal (Ni, Fe) substrates are investigated as alternative substrates to grow N-doped CNTs in the temperature range of 850-1000 °C. N-doped CNTs are synthesized by simple thermal CVD of monoethanolamine on Ni substrates without additional catalyst or processing. The structural characteristics of the N-doped CNTs are investigated by electron microscopy, and their composition is determined using X-ray photoelectron spectroscopy (XPS).

3.2 . Experimental Details

N-doped CNTs were synthesized on Ni and Fe substrates (thickness of 0.1 mm and area of 1 cm × 1 cm Nilaco) by CVD from a single precursor without additional catalyst. The deposition apparatus is showed in Figure 3.1. This is consisted of two horizontal furnaces fitted with a quartz tube (length of 120 cm and inner diameter of 26 mm). Monoethanolamine was placed at the center of the first furnace. Metal substrates were cleaned in acetone and methanol, washed in de-ionized water, and then dried under a stream of nitrogen. The cleaned metal substrates were inserted at the center of the second furnace. The CVD process was carried out at atmospheric pressure. The second furnace was raised to the desired reaction temperature under a flow of N_2 of 1 l/min, and then annealing at the reaction temperature for 10 min. After annealing, the temperature of the first furnace was raised to 120 °C. The reaction was carried out by introducing

monoethanolamine into the second furnace for 20 min. After the reaction, the furnace was cooled to room temperature. Scanning electron microscopy (SEM, Hitachi, S-3000H) and transmission electron microscopy (TEM, JEOL JEM-2100F) were used to check the quality, layer structure, and overall morphology of products. X-ray photoelectron spectroscopy (XPS, SSX-100 XPS spectrometer using Al K_α X-ray source with 1486.6 eV) to confirm nitrogen atoms doping levels and bonding configurations of incorporated nitrogen atoms in the N-doped CNTs. Annealed Ni substrates surface morphology were characterized by atomic force microscopy (AFM, SII, SPA300) to examine the dependence of growth temperature.

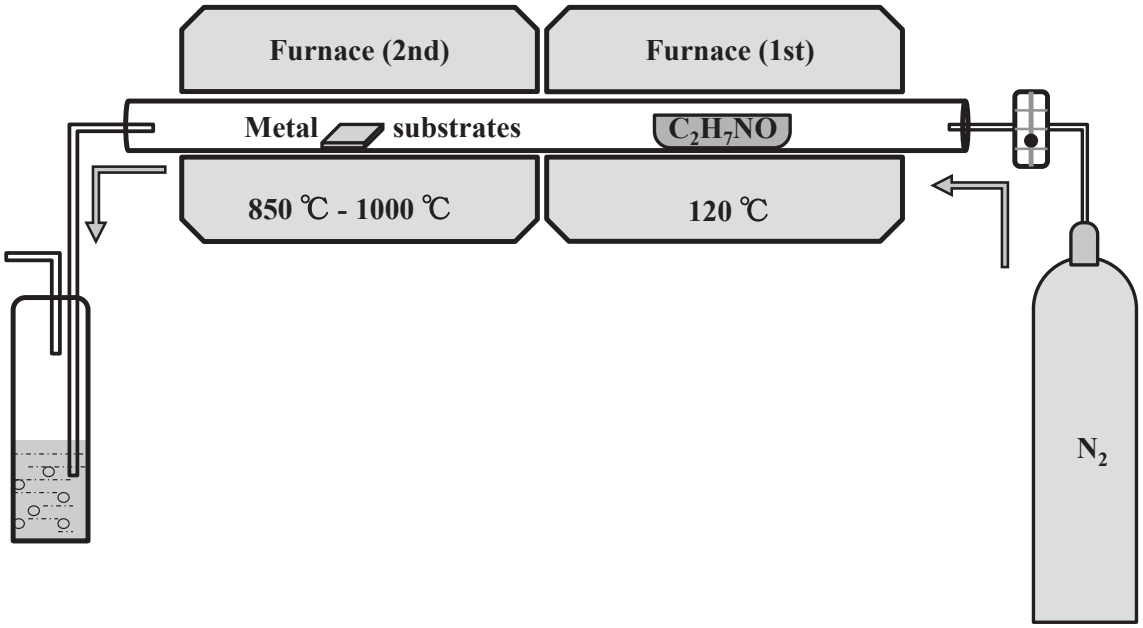

Figure 3.1 schematics diagram of thermal CVD set-up.

3.3 . Results and Discussion

3.3.1 Nitrogen-Doped Carbon Nanotubes Synthesized on Ni Substrates

SEM characterization was performed to check the products morphology on the Ni substrates. Figure 3.2 (a-d) show SEM images of the N-doped CNTs grown on Ni

substrates for 20 min at 850–1000 °C. As shown in Figure 3.2, the average diameter of the N-doped CNTs increased with increasing of synthesis temperature.

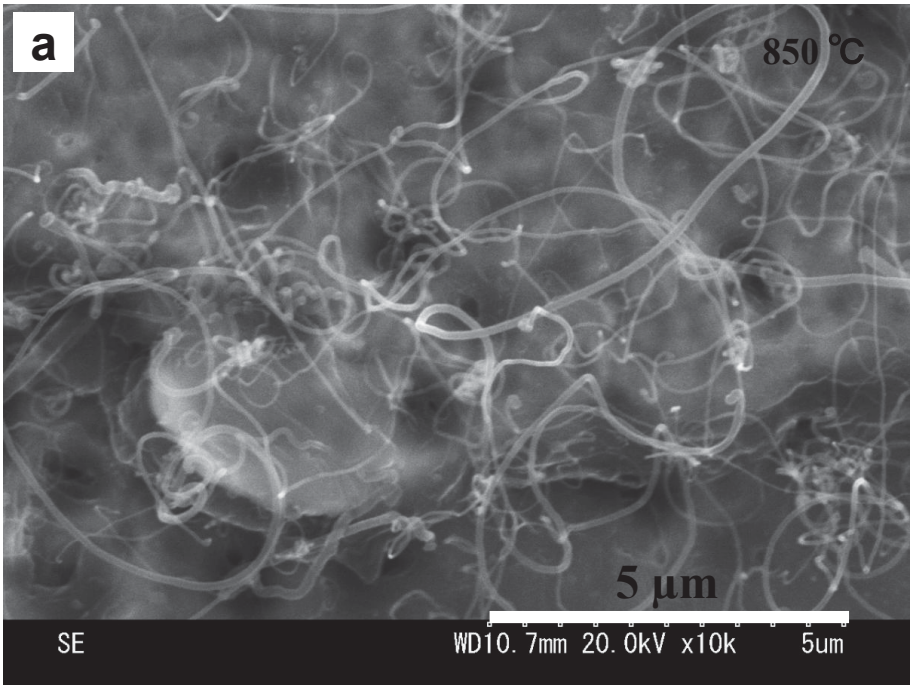

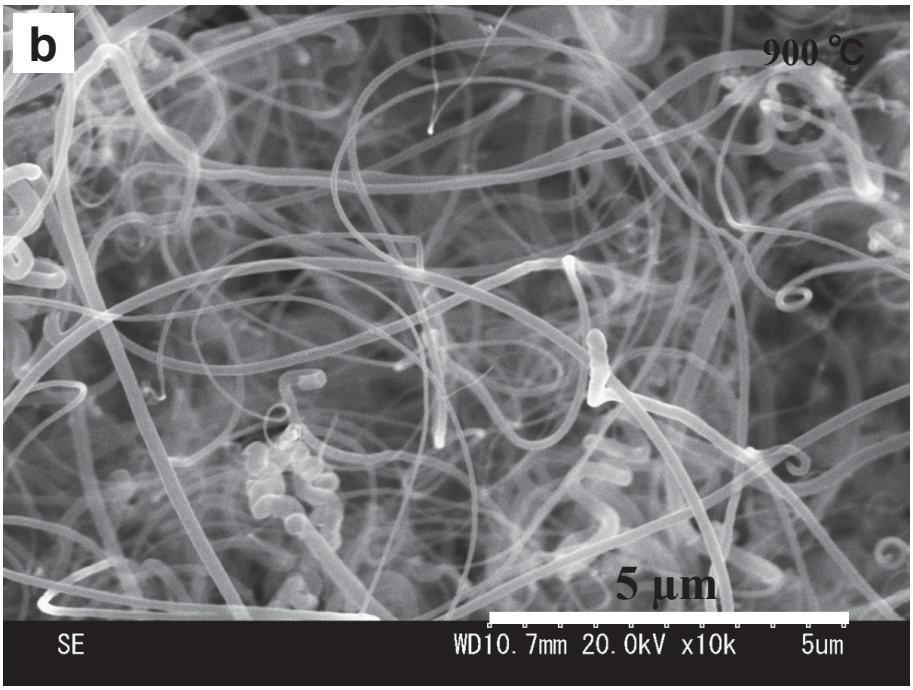

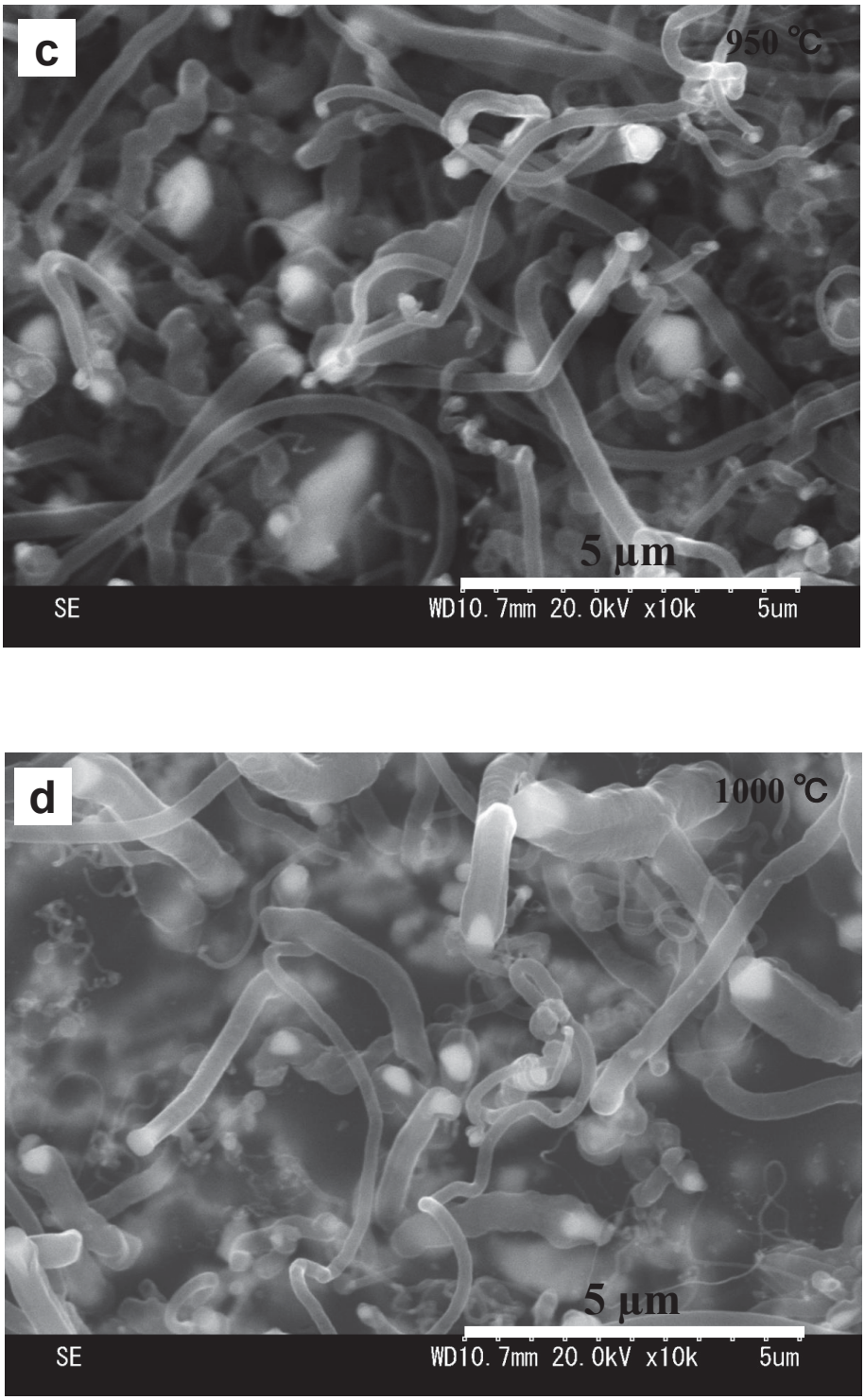

Figure 3.2 SEM images of N-doped CNTs synthesized on Ni substrates for 20 min using monoethanolamine at (a) 850 °C, (b) 900 °C, (c) 950 °C, and (d) 1000 °C, respectively.

To determine N-doping level and the bonding configurations of incorporated nitrogen atoms in the N-doped CNTs, XPS was performed on the N-doped CNTs samples. Figure 3.3 show a Survey scans of the N-doped CNT samples showed the presence of the principal C 1s, O 1s, and N 1s core levels (shown in Figure 3.3), and the atomic percentage of doped nitrogen level was about 2.5 at %, 2.3 at %, 2.5 at %, and 2.0 at % for the N-doped CNTs prepared at 850 °C, 900 °C, 950 °C, and 1000 °C, respectively. The C 1s, N 1s and O 1s peaks appear at 284.5 eV, 400.5 eV, and 533.5 eV, respectively, for all of the CNT samples. An intense, sharp peak at 284.5 eV confirms that the major component of the samples is carbon. The O peaks reflected the presence of oxygen in the air and/or adsorbed on the surface of the nanotubes. High-resolution N 1s spectra of the samples produced at 850 °C, 900 °C, 950 °C, and 1000 °C are presented in Figure 3.4 (a), (b), (c) and (d), respectively. The concentration of nitrogen in the N-doped CNTs did not depend on synthesis temperature. All of the N 1s spectra contain three components, which are fitted into peaks at 398.77 eV – 399.00 eV (N1), 401.02 eV – 401.35 eV (N2), and 404.16 eV – 404.76 eV (N3). The two peaks N1 and N2 are related to the two different chemical environment of the nitrogen atom in the as-grown samples. The peak N1 corresponds to ‘pyridine’ nitrogen whereas the peak N2 corresponds to ‘graphite’ nitrogen. The term ‘pyridine’ nitrogen is used to refer to the nitrogen atoms that contribute the o-system with one p-electron. The ‘graphitic’ nitrogen corresponds to highly coordinated nitrogen atoms substituting inner C atoms on the graphene layers. The peak N3 corresponds to molecular nitrogen encapsulated or intercalated in the nanotubes, respectively [3.14]. In this experiment results, the ratio of N1 to N2 increased with increasing the synthesis temperature.

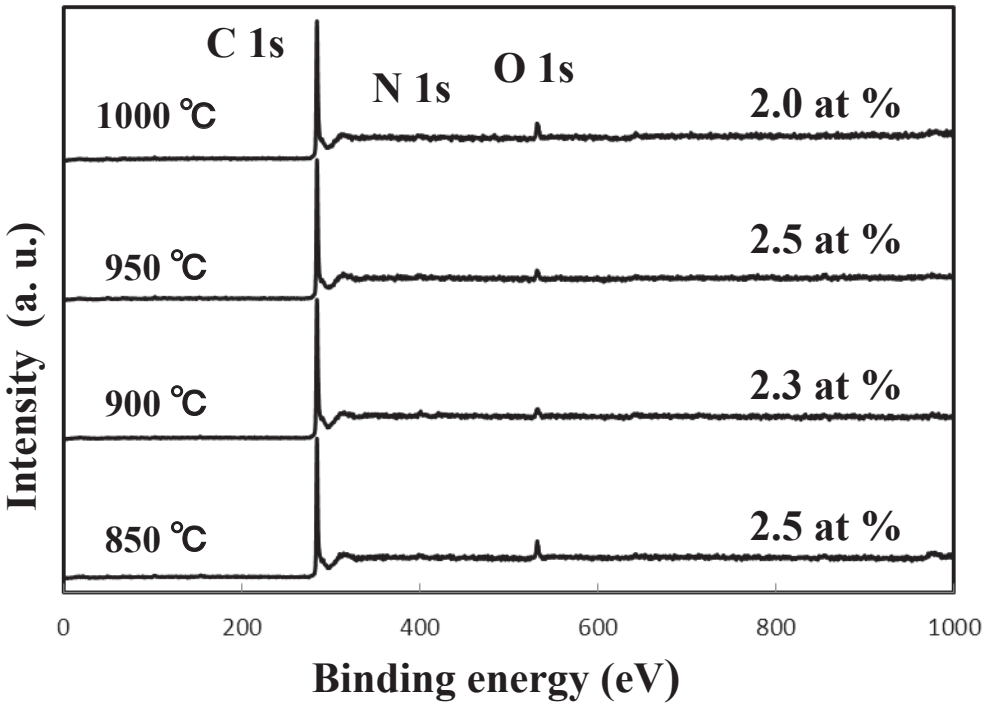

Figure 3.3 wide-range XPS spectra of N-doped CNTs synthesized on Ni substrates for 20 min using monoethanolamine at temperature range of 850 °C - 1000 °C.

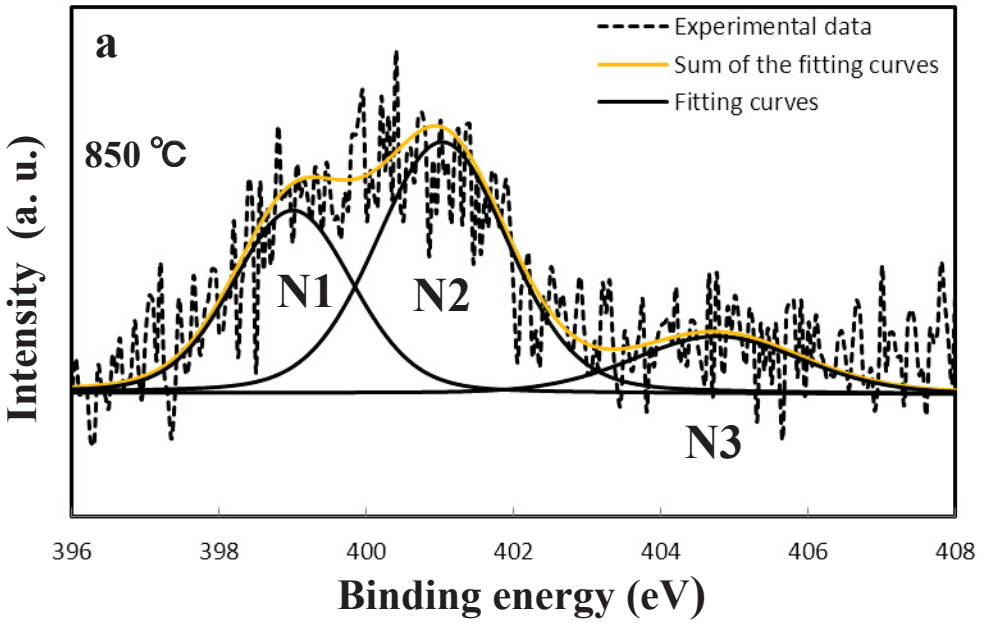

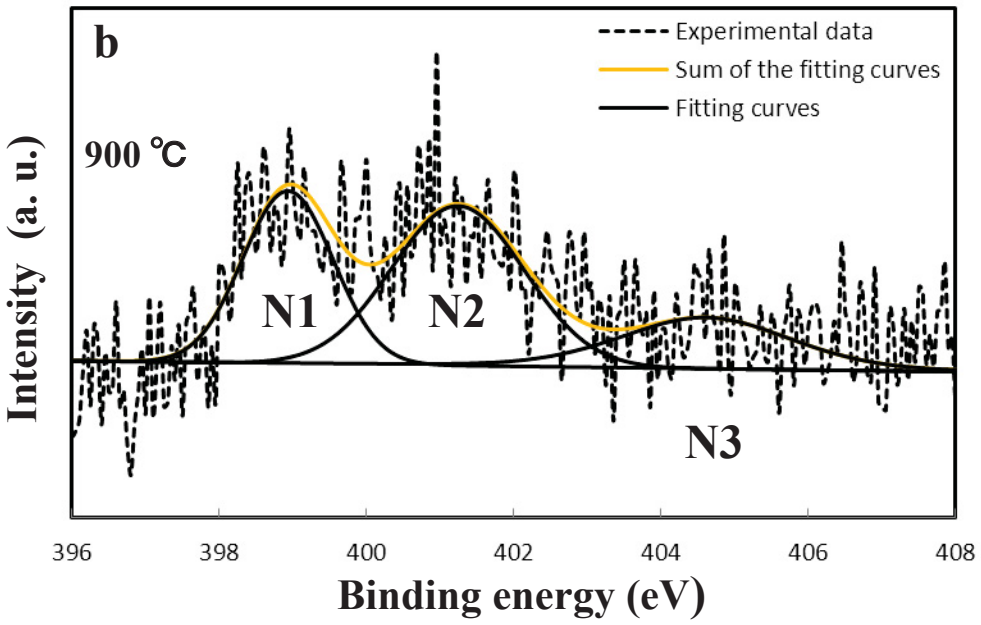
b
900 ℃
Experimental data
Sum of the fitting curves
Fitting curves
N1
N2
N3
Intensity (a. u.)
396
398
400
402
404
406
408
Binding energy (eV)

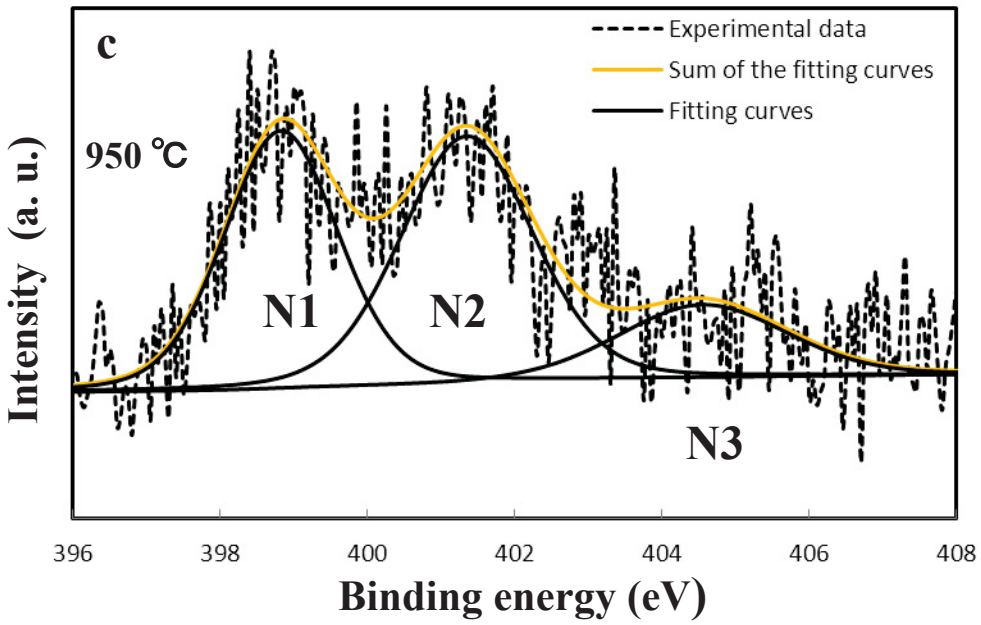
c
950 ℃
Experimental data
Sum of the fitting curves
Fitting curves
N1
N2
N3
Intensity (a. u.)
396
398
400
402
404
406
408
Binding energy (eV)

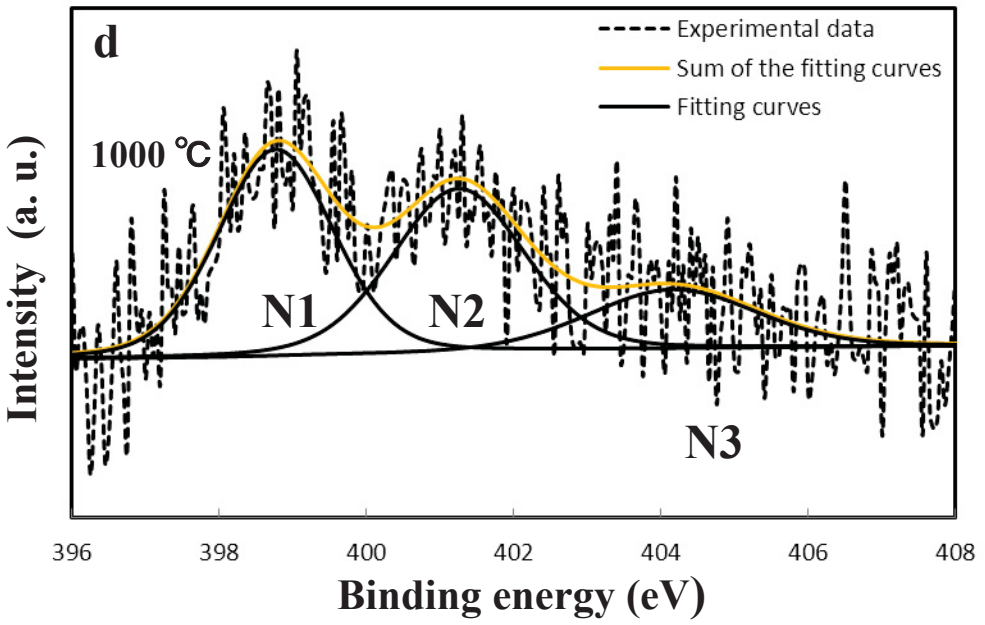

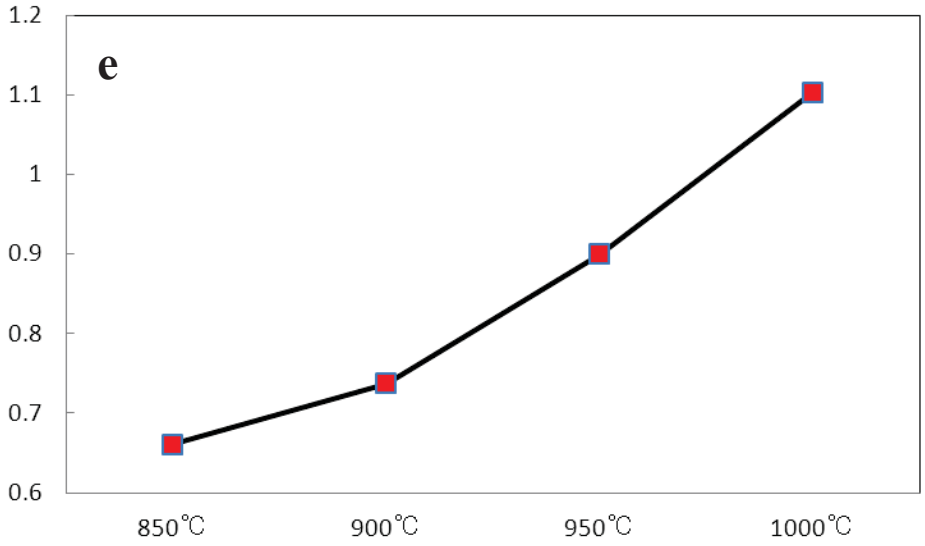

Figure 3.4 (a-d) high-resolution XPS spectra of the N 1s signal of N-doped CNTs synthesized on Ni substrates for 20 min at temperature of (a) 850 °C, (b) 900 °C, (C) 950 °C, and (d) 1000 °C, respectively. (e) Dependence of the ratio of pyridine-like to graphite-like nitrogen on synthesis temperature.

To investigate the structure morphology of the N-doped CNTs, they were characterized by TEM. TEM images of the N-doped CNTs prepared at different temperatures are depicted in Figure 3.5. The N-doped CNTs prepared at all temperatures exhibit bamboo-like, corrugated structures. High-resolution TEM images of N-doped CNTS grown at 850 °C and 950 °C are shown in Fig. 3(e) and (f), respectively. The N-doped CNTs synthesized at 850 °C contain ridged graphitic sheets over a large area, showing a lower degree of crystallinity than those synthesized at 950 °C whereas have a same nitrogen doping level in both N-doped CNTs synthesized at 850 °C and 950 °C. Therefore, this is concluded that the crystallinity of the N-doped CNTs was improved with increasing the synthesis temperature.

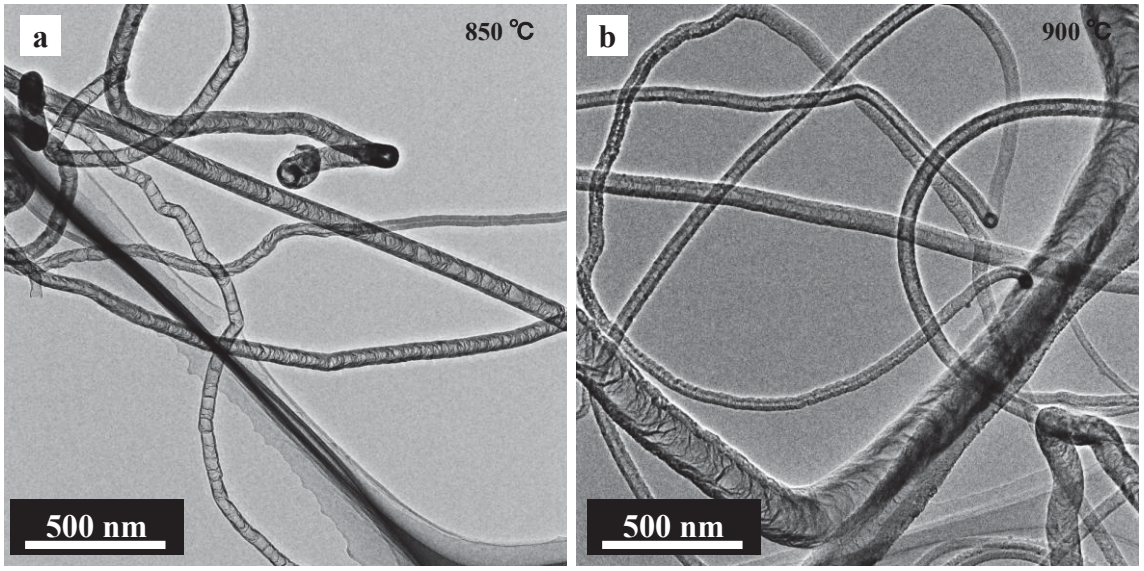

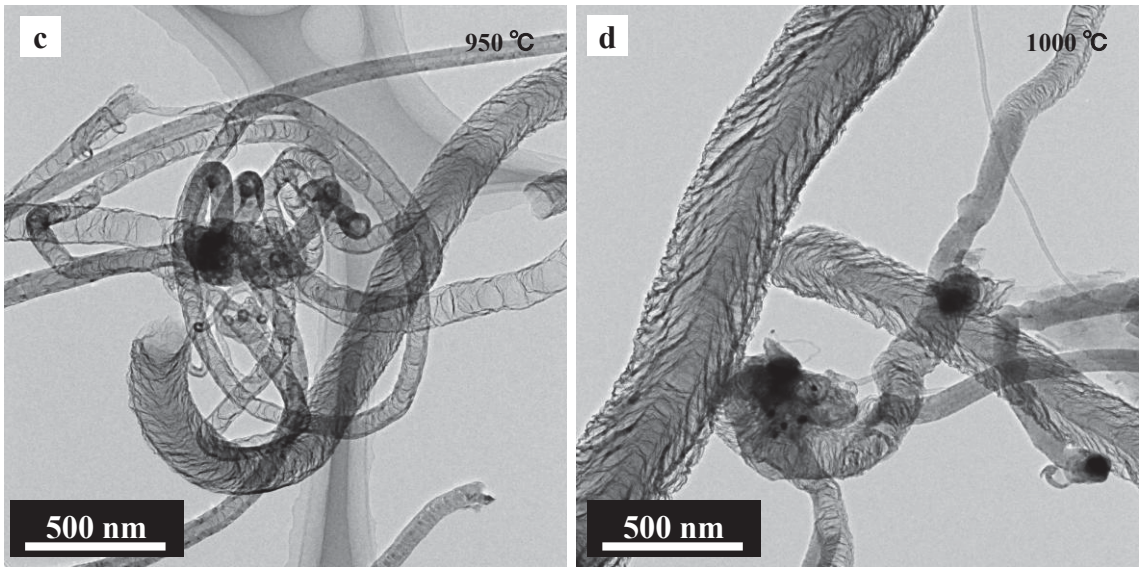

Figure 3.5 TEM images of N-doped CNTs synthesized on Ni substrates for 20 min using monoethanolamine at temperature of (a) 850 °C, (b) 900 °C, (c) 950 °C, and (d) 1000 °C, respectively.

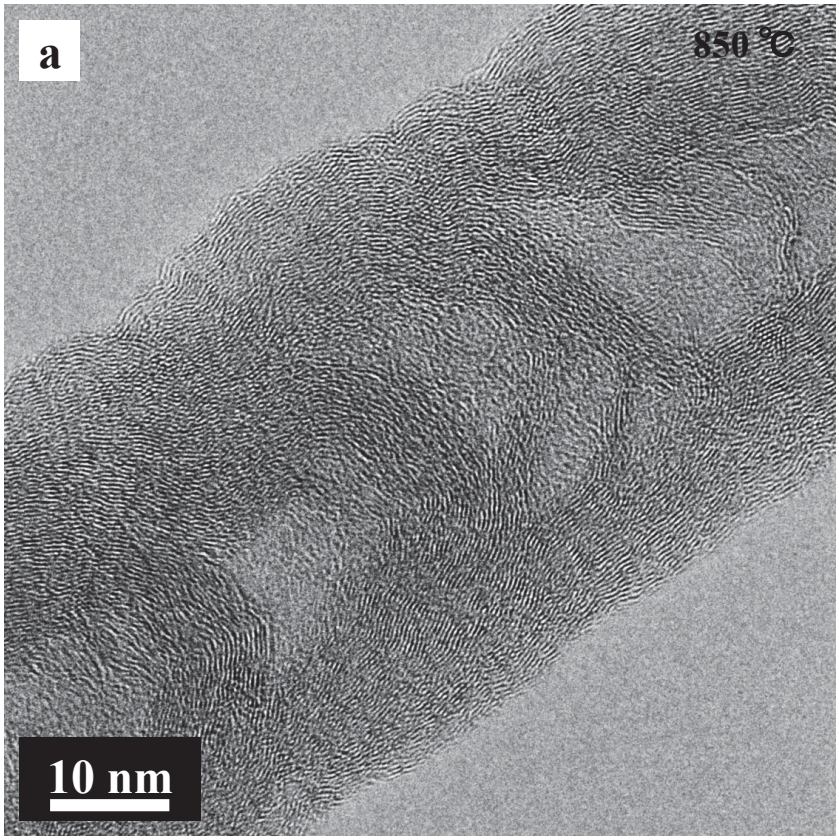

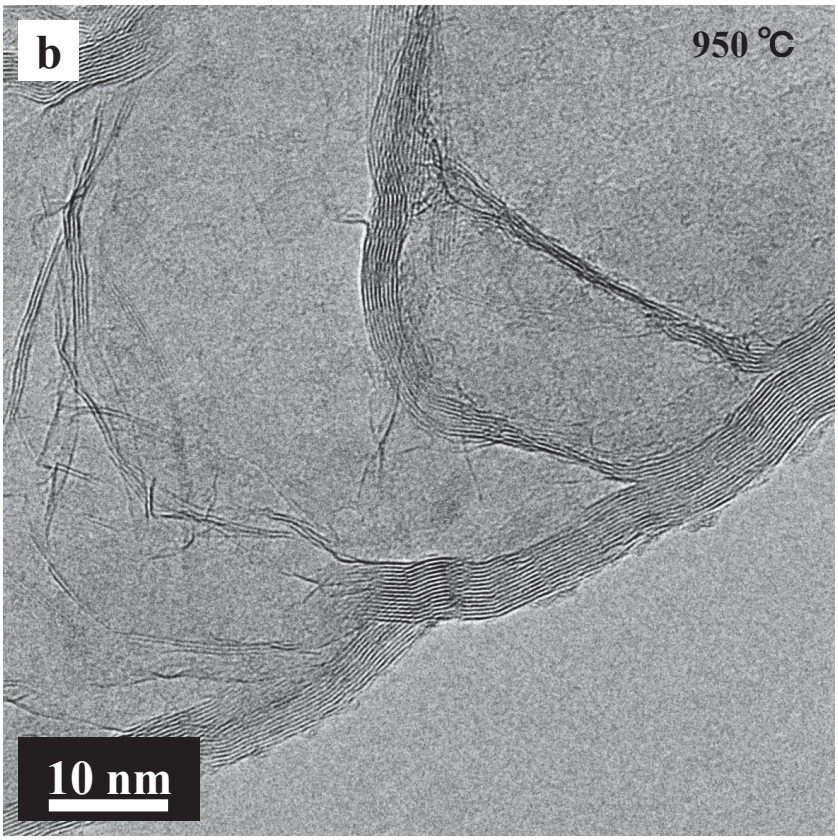

Figure 3.6 high magnification TEM images of N-doped CNTs on Ni substrates for 20 min at temperature of (a) 850 °C and (b) 950 °C.

To investigate annealing temperature influence for Ni substrates surface AFM measurement were carried out. AFM images of the Ni substrates after annealing for 10 min under a flow of N_2 of 1 l/min at temperatures of 850 °C, 900 °C, 950 °C, and 1000 °C are presented in Fig. 3.7 (a-d). As the annealing temperature increased from 850 °C to 1000 °C, the root mean square (RMS) roughness of the Ni substrates increased considerably. This is indicates that Ni substrates surface became more roughly and some large curvature Ni island were formed. Therefore, this is considered that increasing of Ni substrates surface RMS were result to average diameter of N-doped CNTs became large with increasing the synthesis temperature.

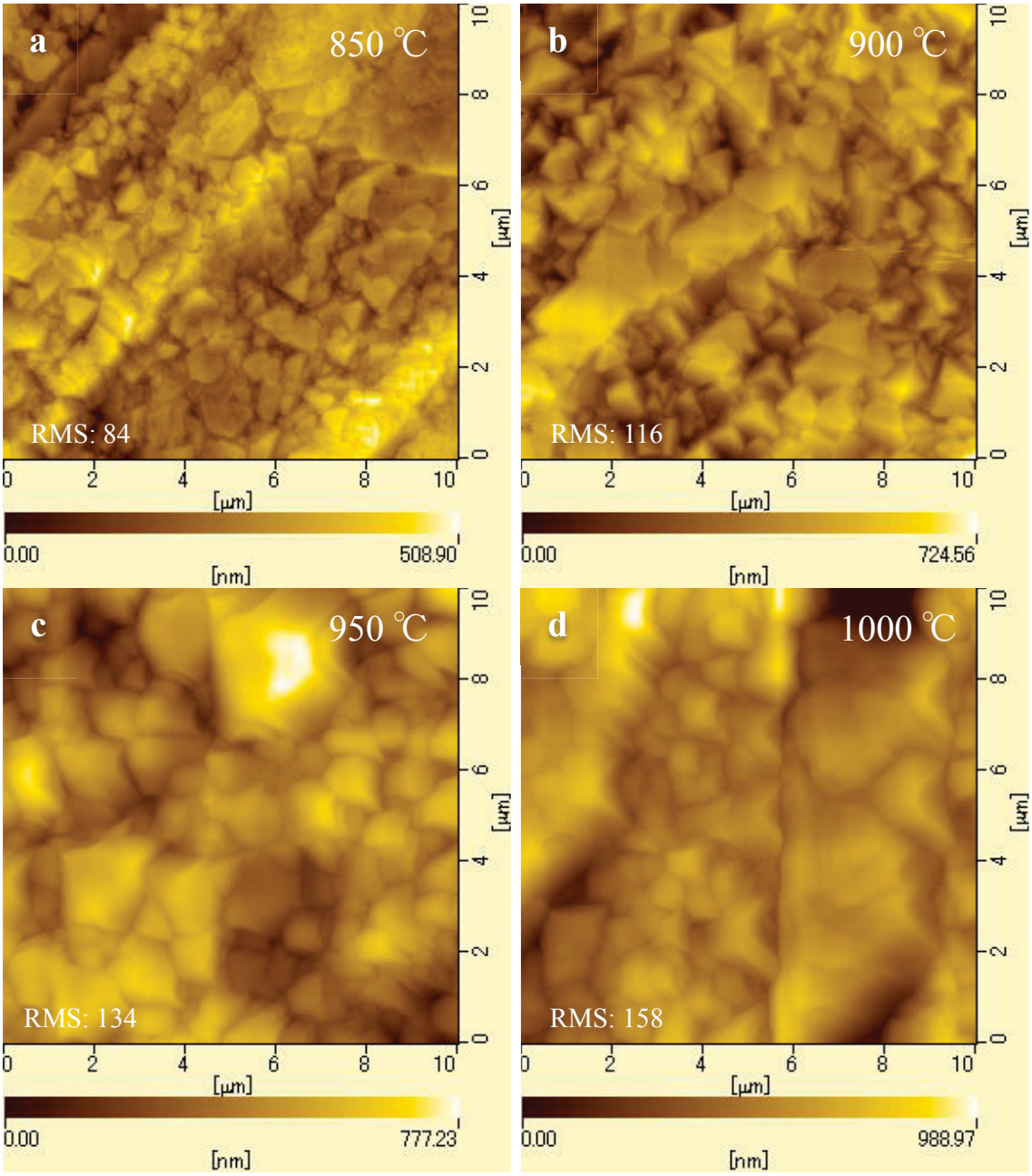

Figure 3.7 AFM images of Ni substrates surface annealed in the nitrogen atmosphere for 10 min at temperature of (a) 850 °C, (b) 900 °C, (c) 950 °C, and (d) 1000 °C, respectively.

3.3.2 Nitrogen-Doped Carbon Nanotubes Synthesized on Fe Substrates

Syntheses of N-doped CNTs on the Fe substrates from a monoethanolamine

were carried out at temperature 900 °C and 1000 °C. Figure 3.8 show SEM images of N-doped CNTs synthesized on the Fe substrates for 20 min at temperature of (a) 900 °C and (b) 1000 °C. The average diameter of N-doped CNTs synthesized on Fe substrates were slightly decreased with increasing the synthesis temperature.

To further investigate the structure morphology of the N-doped CNTs synthesized on Fe substrates, they were characterized by TEM. Figure 3.9 show a TEM images of N-doped CNTs synthesized on Fe substrates for 20 min at 900 °C (a) low magnification and (b) high magnification. The N-doped CNTs synthesized at 900 °C exhibits bamboo-like and corrugated structure.

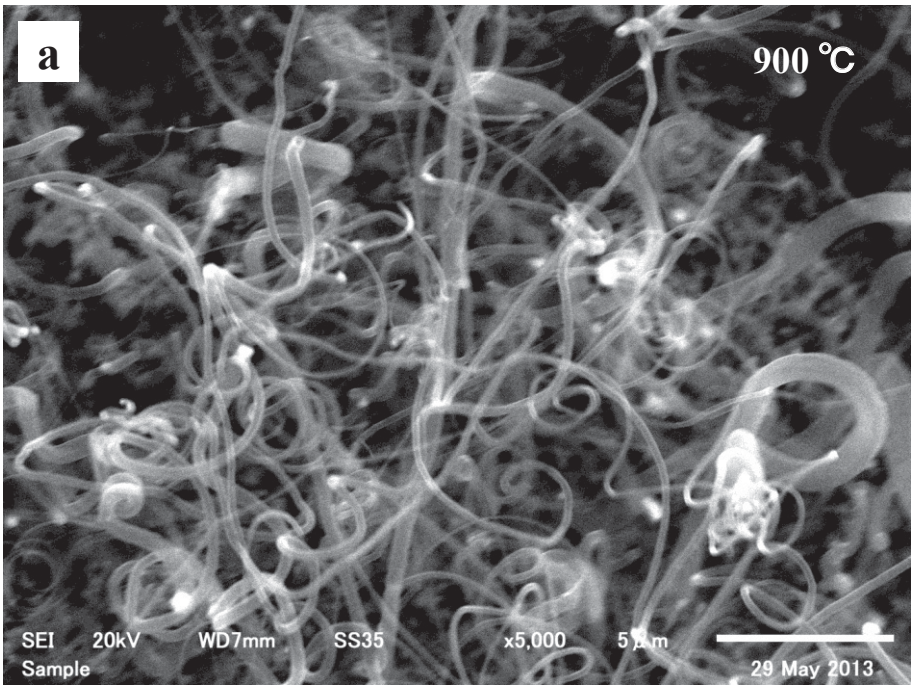

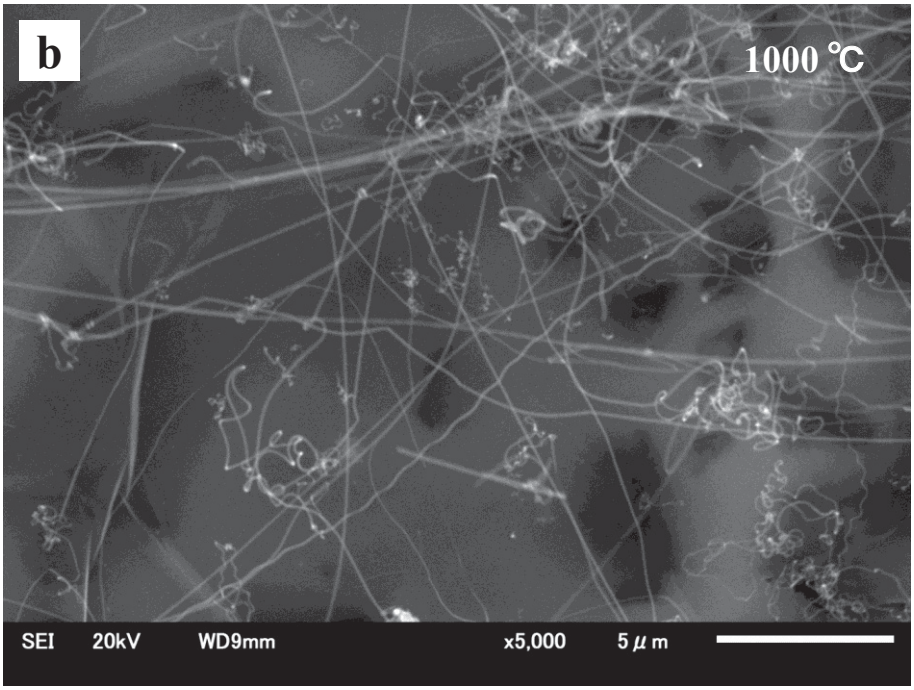

Figure 3.8 SEM images of the N-doped CNTs synthesized on Fe substrates for 20 min using monoethanolamine at temperature of (a) 900 °C and (b) 1000 °C.

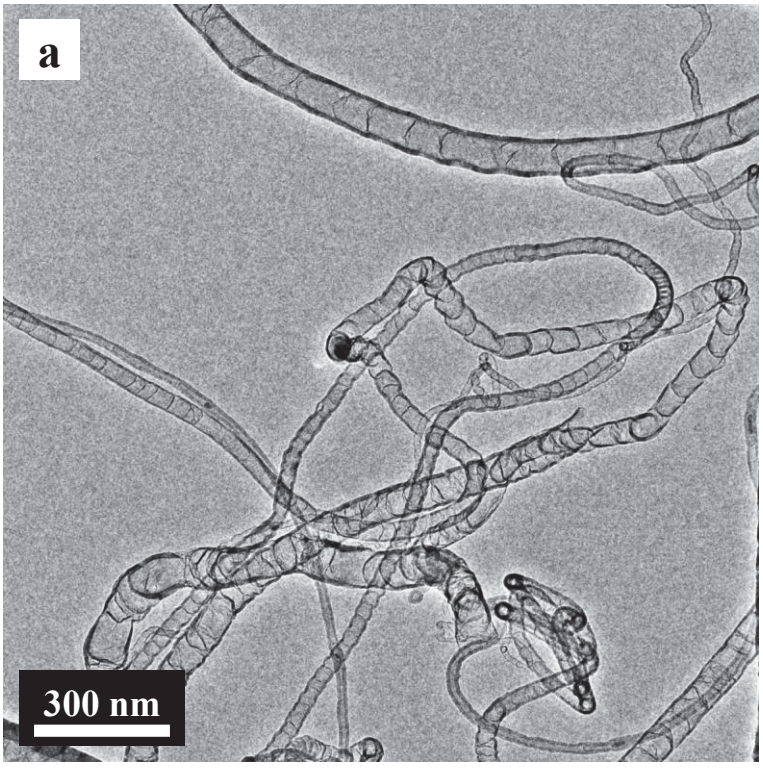

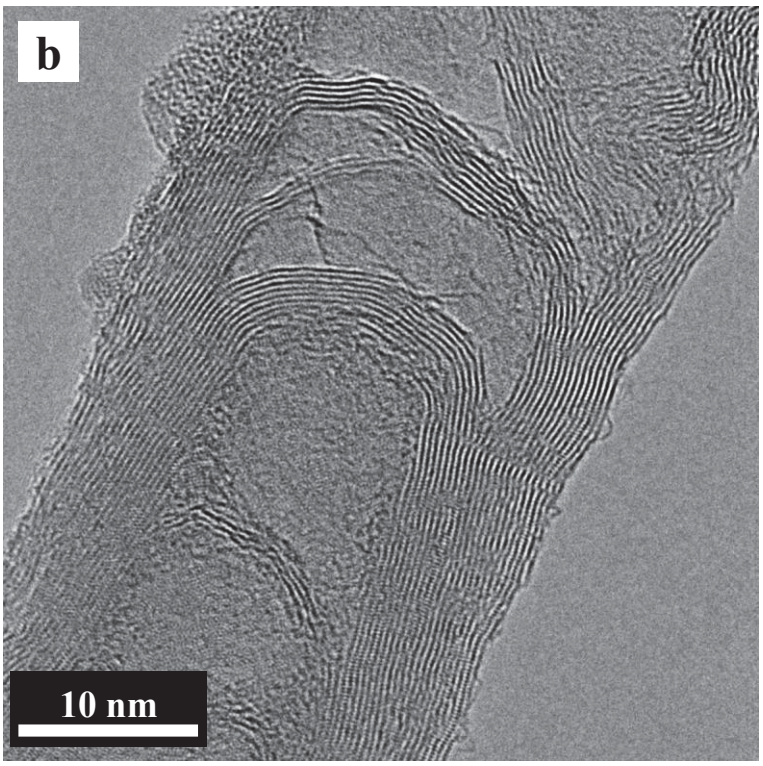

Figure 3.9 TEM images of N-doped CNTs synthesized on Fe substrates for 20 min at 900 °C (a) low magnification and (b) high magnification.

In order to measure the doping concentration and understand the doping level and chemical states of the doped nitrogen atoms, XPS was applied to study the N-doping CNTs synthesized at 900 °C for 20 min on Fe substrates. The survey scan spectra of the samples were presented at Figure 3.10 (a). The C 1s, N 1s and O 1s peaks appear at 284.5eV, 400.5 eV, and 533.5 eV, respectively, and nitrogen doping level is 2.3 at %. An intense, sharp peak at 284.5 eV confirms that the major component of the samples is carbon. The O peaks reflected the presence of oxygen in the air and/or adsorbed on the surface of the nanotubes. High resolution N 1s spectra of the sample produced at 900 °C was presented at Figure 3.10 (b). From XPS spectra it has been revealed that N 1s signal was split into three peaks at 398.8 eV, 401.5 eV, and 404.7 eV.

The peak at 398.8 eV and 401.5 eV are corresponding to pyridine-like and graphite-like nitrogen. The peak around the 404.5 eV corresponds to molecular nitrogen encapsulated or intercalated in the nanotubes [3.14].

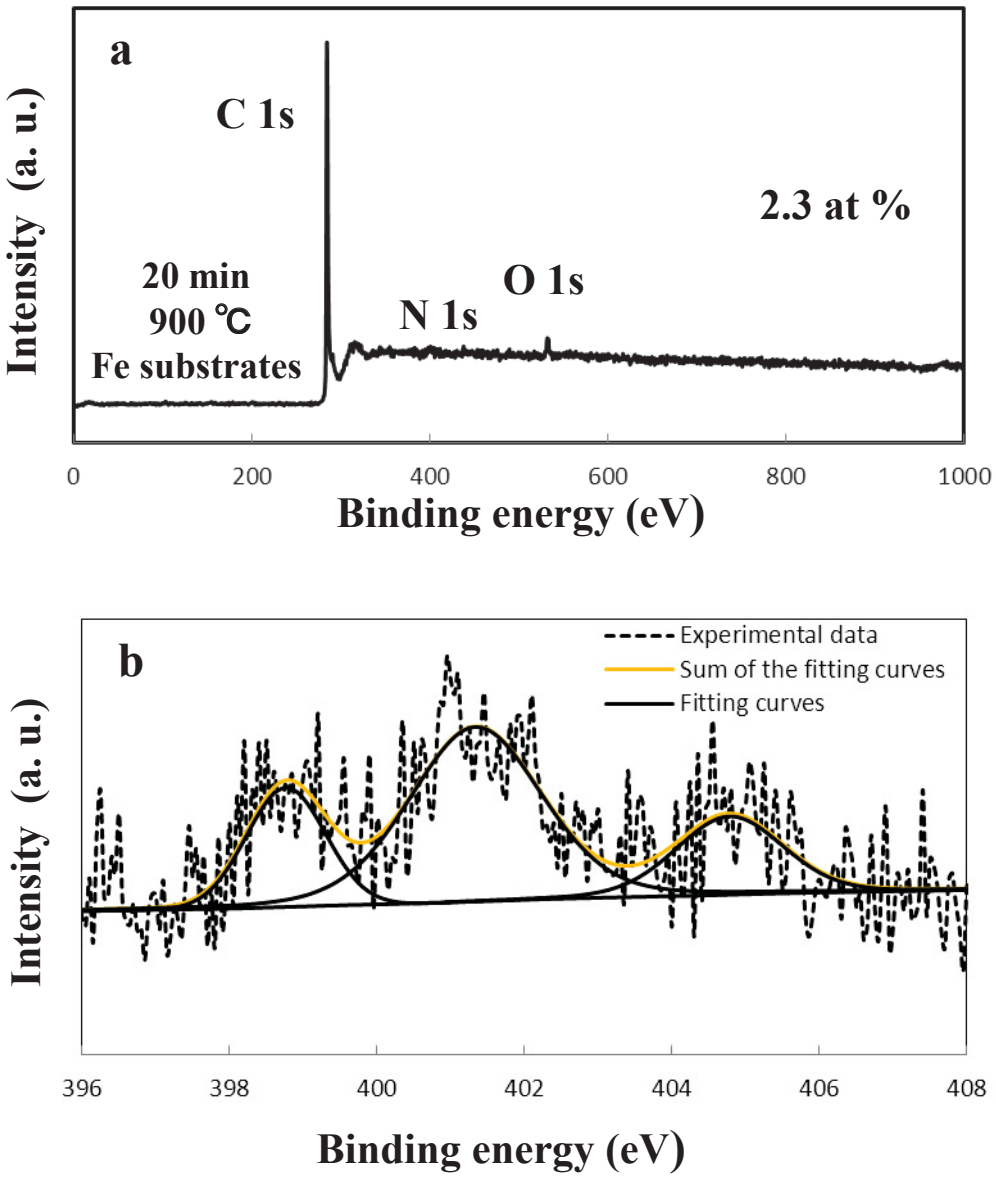

Figure 3.10 (a) wide-range XPS spectra and (b) high-resolution XPS spectra of the N1s signal of N-doped CNT synthesized on Fe substrates for 20 min at 900 °C.

3.4. Summary

In this chapter, N-doped CNTs with a nitrogen concentration of 2.0–2.5 at % were synthesized on Ni substrates by simple thermal CVD of monoethanolamine without any additional catalyst or processing at temperature range of 850 °C-1000 °C. The N-doped CNTs exhibited a bamboo-like, corrugated structure independent of synthesis temperature, whereas the ratio of pyridine-like nitrogen to graphite-like nitrogen increased with increasing the synthesis temperature. The degree of crystallinity increased with increasing of synthesis temperature whereas have a same nitrogen concentration (2.5 at %). The average diameters of the N-doped CNTs synthesized on Ni substrates increased as the growth temperature were increased from 850 °C to 1000 °C. Thus this is concluded that large curvature Ni islands were formed at higher growth temperature. The N-doped CNTs synthesized on Fe substrates with a nitrogen doping level of around 2.3 at % at 900 °C and exhibit bamboo-like, corrugated structure also. Compared to samples synthesized on Ni substrates the average diameter of N-doped CNTs decreased with synthesis temperature increasing.

References

[3.1] S Iijima, Nature 354, (1991) 56.

[3.2] Guillorn M A, Simpson M L, Bordonaro G J, Merkulov V I, Baylor L R, Lowndes D H, J. Vac. Sci. Technol.19, (2001) 573.

[3.3] Wang J, Electroanalysis 17, (2005) 7.

[3.4] X Wang, M Waje, Y S Yan, Electrochem and Solid State Lett. 8, (2005) 42.

[3.5] X Blase, J C Charlier, A De Vita, R Car, Appl. Phys. A 68, (1999) 293.

[3.6] R S Lee, J Gavillet, et al. Phys. Rev. B 64, (2001) 121405.

[3.7] R Ma, Y Bando, T Sato, Chem. Phys. Lett. 337, (2001) 61.

[3.8] M Terrones, N Grobert, H Terrones, Carbon 40, (2002) 1665.

[3.9] J Liu, S Webster, D L Carroll, J. Phys. Chem. B 109, (2005) 15769.

[3.10] P. Ghosh, M. Zamari et al., Journal of Physics D: Applied Physics 41, (2008) 155405.

[3.11] Cruz-Silva E, Cullen D A, et al, ACS Nano 2, (2008) 441.

[3.12] Terrones M, Ajayan P, et al, Appl. Phys. A 74, (2002) 355.

[3.13] Yun T L, Nam S K, et al, J. Phys. Chem. B 107, (2003) 12958.

[3.14] Hao L, Yong Z, et al, carbon 48, (2010) 1498.

[3.15] Koos AA, Dowling M, et al, Carbon 47, (2009) 30.

[3.16] Ayala P, Gruneis A, et al, J. Chem. Phys. 127, (2007) 1847091.

Chapter 4

Synthesis of Nitrogen-Doped Graphene by Thermal Chemical Vapor Deposition from a Single Liquid Precursor

4.1. Introduction

Graphene, a monolayer of carbon atoms arranged in a two-dimensional honeycomb lattice, has attracted much attention because of its unique properties and many potential applications [4.1-4.5]. Doping of graphene by foreign atoms [4.6-4.9] is of interest because this doping allows modification of the band structure and physicochemical properties of the materials, further extending the potential applications. Among numerous potential dopants, nitrogen is considered to be an interesting element for chemical doping of graphene with a wide variety of potential applications for the materials, including lithium batteries [4.8], electrochemical biosensor [4.10] and fuel cells [4.11, 4.12].

A number of approaches have been proposed to synthesize nitrogen-doped graphene, such as heat treatment of graphene oxide under an ammonia atmosphere [4.13], nitrogen plasma treatment of graphene [4.10], and wet chemical reactions [4.14]. Recently, CVD growth has been demonstrated using hydrocarbon gases in an ammonia atmosphere [4.11], or using a single precursor compounds that contain both carbon and nitrogen [4.15, 4.16]. Development of liquid precursors based on nitrogen and carbon containing material may be expected to be a milestone in nitrogen-doped graphene synthesis because of their ease of use.

In this chapter, the synthesis of nitrogen-doped graphene by an ambient pressure

thermal CVD technique using monoethanolamin as the sole source of both carbon and nitrogen were reported. The dependence of the growth temperature and deposition time on the nitrogen/carbon composition, number of layers, and the quality of nitrogen-doped graphene were investigated.

4.2. Experimental Details

Nitrogen-doped graphene were synthesized on polycrystalline Ni substrates (thickness of 0.1 mm, Nilaco) using thermal CVD of monoethanolamin. The deposition apparatus consist of two horizontal furnaces fitted with a quartz tube having length of 120 cm and an internal diameter of 26 mm. monoethanolamin was placed at the center of the first furnace. The Ni substrates were inserted at the center of the second furnace. The CVD process was carried out under nitrogen atmosphere at ambient pressure. The second furnace was raised to the desired temperature (1000 °C -1100 °C) under a nitrogen flow of 500 ml/min, and then annealed at the reaction temperature for 10 min. After annealing, the temperature of the first furnace was raised to 120 °C. The reaction was carried out by introducing monoethanolamin into the second furnace for the desired deposition time (3 min - 12 min) after the reaction, the furnaces were turned off and the Ni substrates were pushed mechanically to the cool temperature zoon and a cooled to around 100 °C at a rate of 200 °C/min. after cooling, the products were characterised by SEM (JEOL JSM7001FF), atomic force microscopy (AFM, SII, SPA300), TEM (JEOL JEM-2100F), X-ray photoelectron spectroscopy (XPS, SSX-100 using an Al Kα X-ray source at 1486.6 eV), and spatially resolved Raman spectroscopy (JASCO; NRS-3300). The Raman mappings were measured over 50 μm × 50 μm in 5 - μm steps. The excitation wavelength of the laser used in the Raman measurement was 532 nm.

4.3. Results and Discussion

4.3.1 Deposition Temperature Dependence

First of all we investigated temperature dependence on the number of layers and the quality of nitrogen-doped graphene from 1000 °C to 1100 °C. Raman measurements were carried out to determine the number of layers and the graphene materials quality. The intensity ratio of the G peak at around 1580 cm^{-1} to the 2D peak at around 2700 cm^{-1} (I_G/I_{2D}) and full width at half maximum (FWHM) of the 2D peak provide information on the number of graphene layers [4.17, 4.18]. Figure 4.1 (a-c) shows the Raman mappings for the FWHMs of the 2D peaks of samples synthesized at 1000 °C, 1050 °C, and 1100 °C on polycrystalline Ni substrates with 7 min. The samples synthesized at 1000 °C and 1050 °C show broader 2D-FWHMs. Compared with the samples synthesized at 1000 °C and 1050 °C, there were smaller 2D-FWHM regions, coloured in red, in the mapping of the sample synthesized at 1100 °C. Figure 4.1 (d-f) shows the maps of I_G/I_{2D} in the same area. Comparisons between the 2D-FWHM and I_G/I_{2D} maps reveal that narrower 2D-FWHM regions are almost consistent with smaller I_G/I_{2D} regions. As the growth temperature increased from 1000 °C to 1100 °C, smaller 2D-FWHM and I_G/I_{2D} were increased. This indicates that with increasing the growth temperature decrease the number of graphene layers on Ni substrates.

Figure 4.2 (a-c) shows the Raman mappings results for the intensity ratio of the D- and G-band (ID/IG) with the same area in Figure 4.2. There was an obvious decrease, with increasing synthesis temperature (coloured in red). Figure 4.2 (d) show Raman spectra taken from circles A marked in Figure 4.2 (a-c). We infer that increasing the growth temperature both improves the quality and decrease the number of graphene layers formed on Ni substrates.

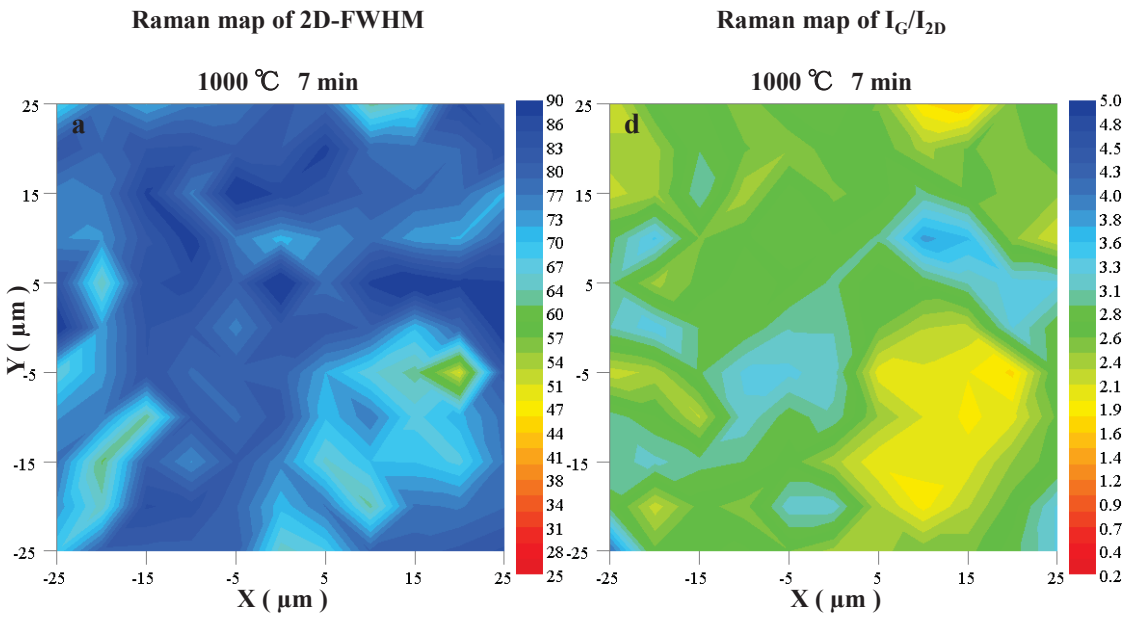
Raman map of 2D-FWHM
1000 ℃ 7 min
a
Y (μm)
X (μm)
Raman map of I_G/I_{2D}
1000 ℃ 7 min
d
X (μm)

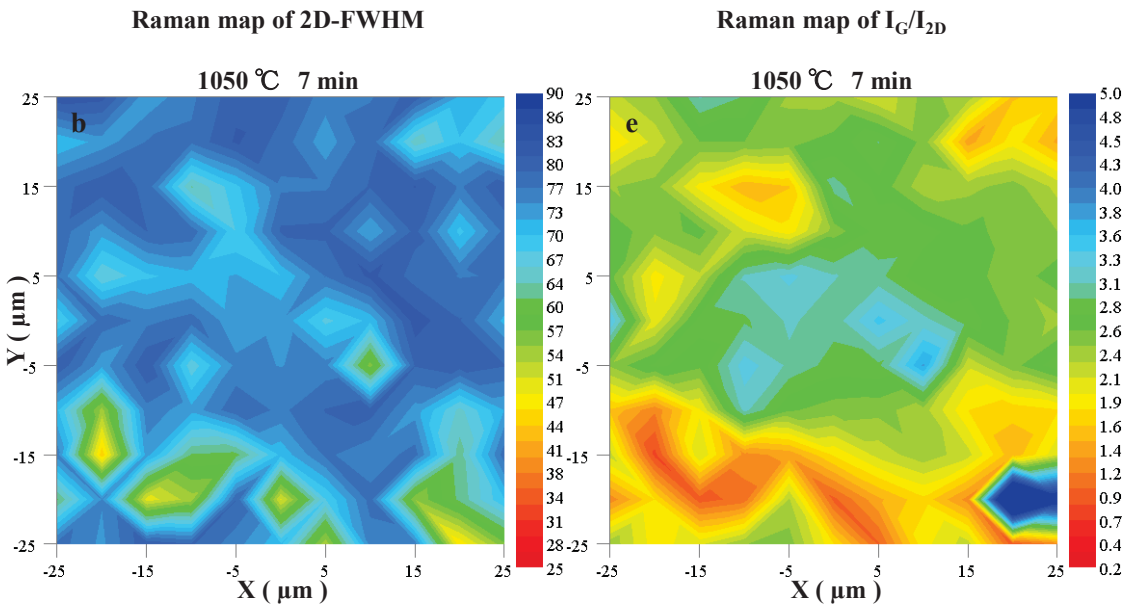
Raman map of 2D-FWHM
1050 ℃ 7 min
b
Y (μm)
X (μm)
Raman map of I_G/I_{2D}
1050 ℃ 7 min
e
X (μm)

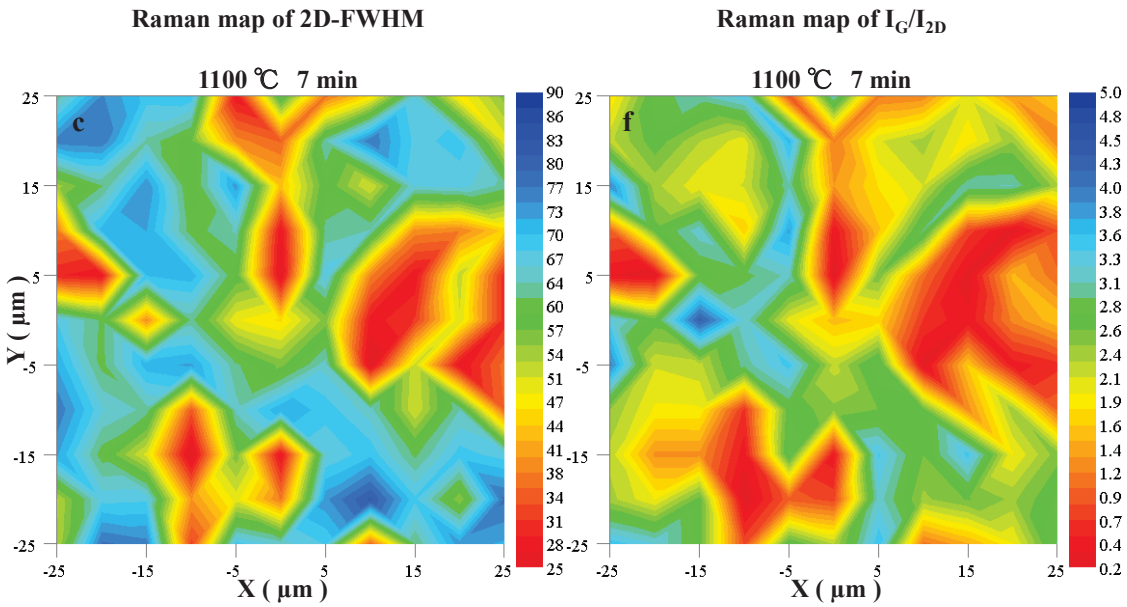

Figure 4.1 Raman mapping results of (a-c) 2D-FWHM (d-f) I_G/I_{2D} values as-grown samples on polycrystalline Ni substrates using monoethanolamine for 7 min at 1000 °C, 1050 °C, and 1100 °C, respectively.

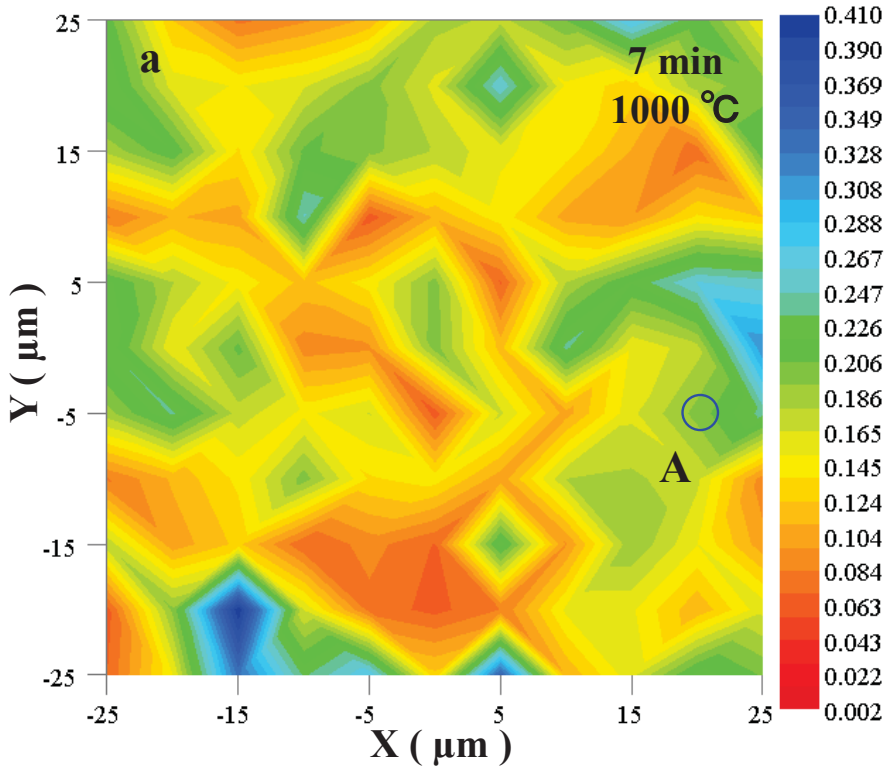

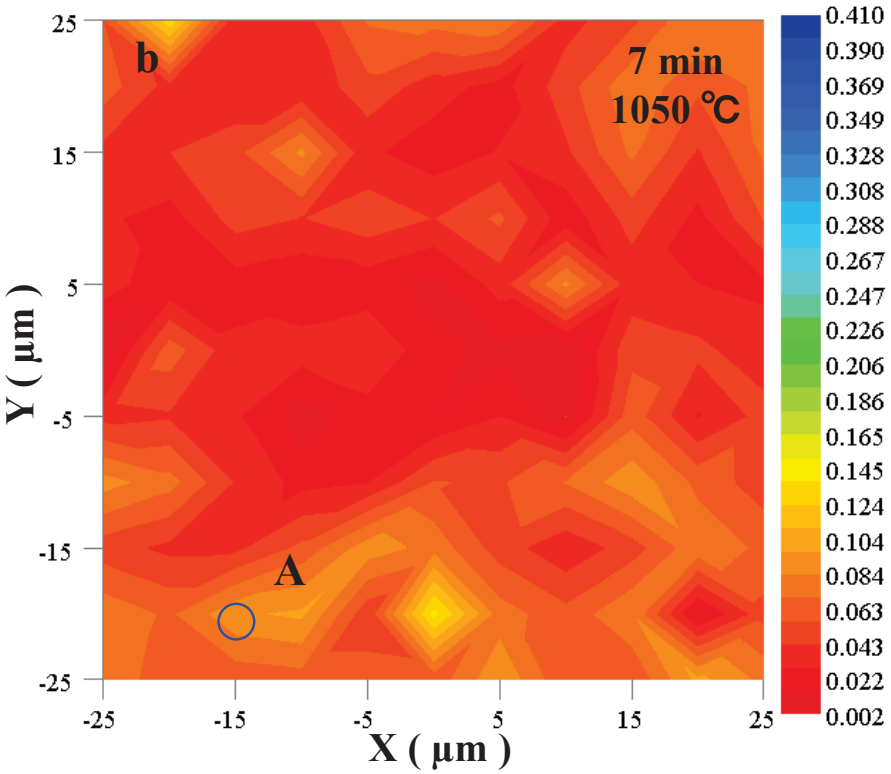
b
7 min
1050 ℃
A
Y (μm)
X (μm)
25
15
5
-5
-15
-25
0.410
0.390
0.369
0.349
0.328
0.308
0.288
0.267
0.247
0.226
0.206
0.186
0.165
0.145
0.124
0.104
0.084
0.063
0.043
0.022
0.002

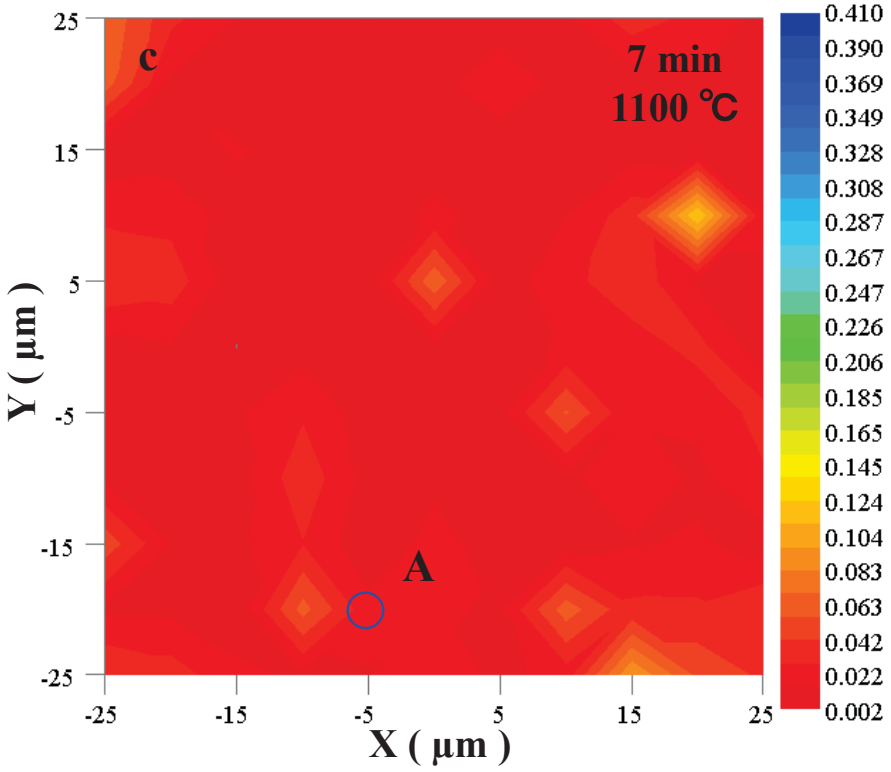
c
7 min
1100 ℃
A
Y (μm)
X (μm)
25
15
5
-5
-15
-25
0.410
0.390
0.369
0.349
0.328
0.308
0.287
0.267
0.247
0.226
0.206
0.185
0.165
0.145
0.124
0.104
0.083
0.063
0.042
0.022
0.002

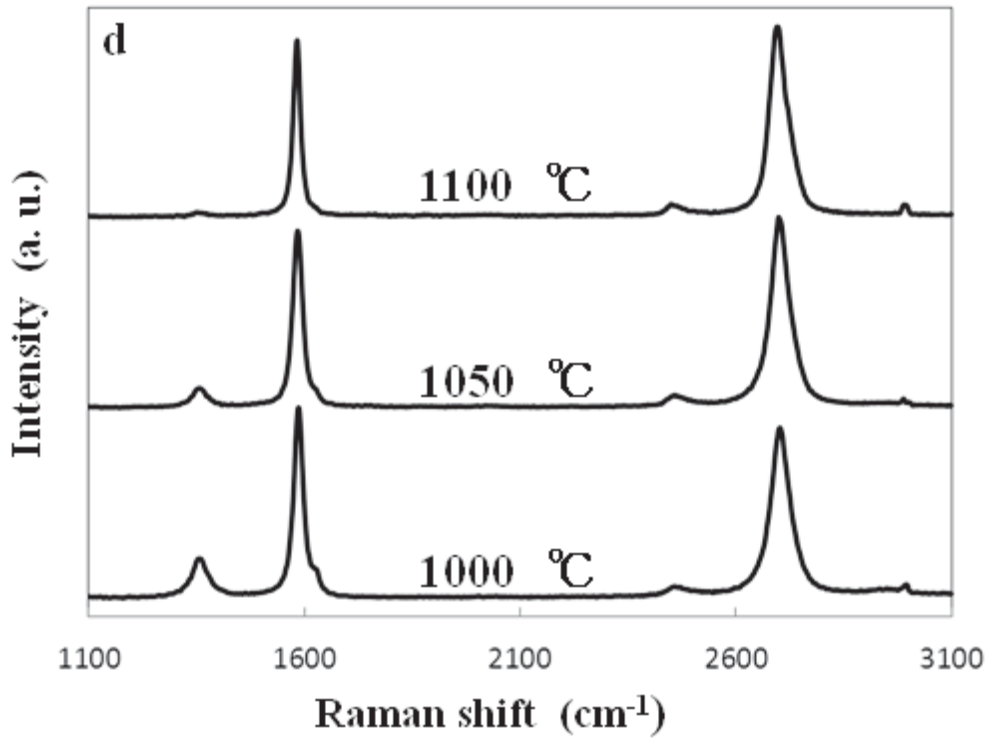

Figure 4.2 (a-c) shows Raman mapping results of I_D/I_G values correspond to same area in Figure 4.1. Figure 4.2 (d) shows the Raman spectra obtained at the circles A marked in Figure 4.2 (a-c).

To investigate surface morphology SEM characterization were carried out. Figure 4.3 (a-c) shows SEM images of nitrogen-doped graphene sheets synthesized on polycrystalline Ni substrates at 1000 °C, 1050 °C, and 1100 °C with deposition time of 7 min, at low magnification. Figure 4.3 (d-f) shows high magnification SEM images of the regions in Figure 4.3 (a-c). As increasing the growth temperature large area homogenous films were formed.

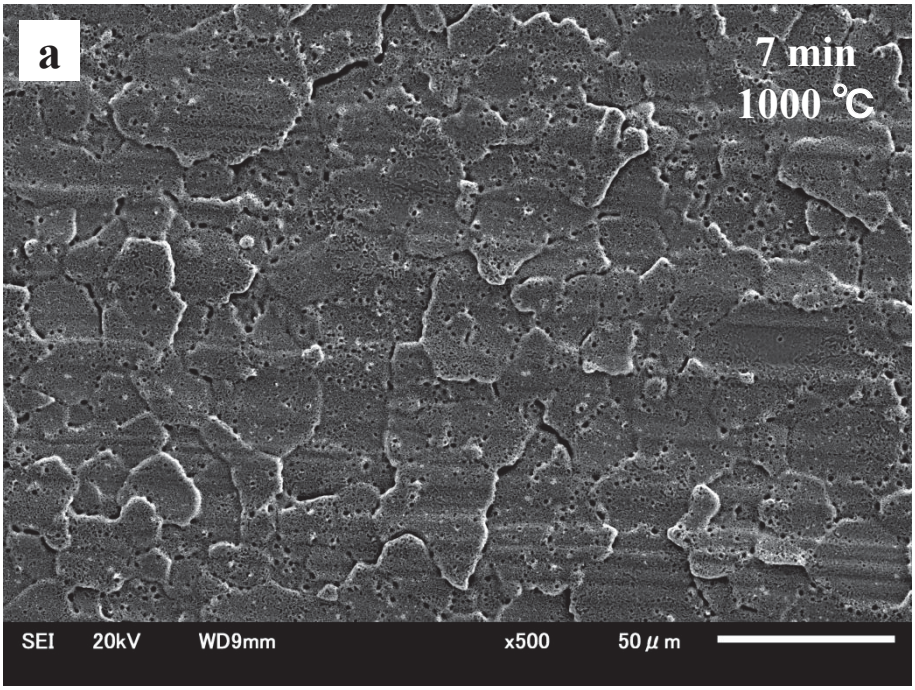
a
7 min
1000 ℃
SEI 20kV WD9mm x500 50 μ m

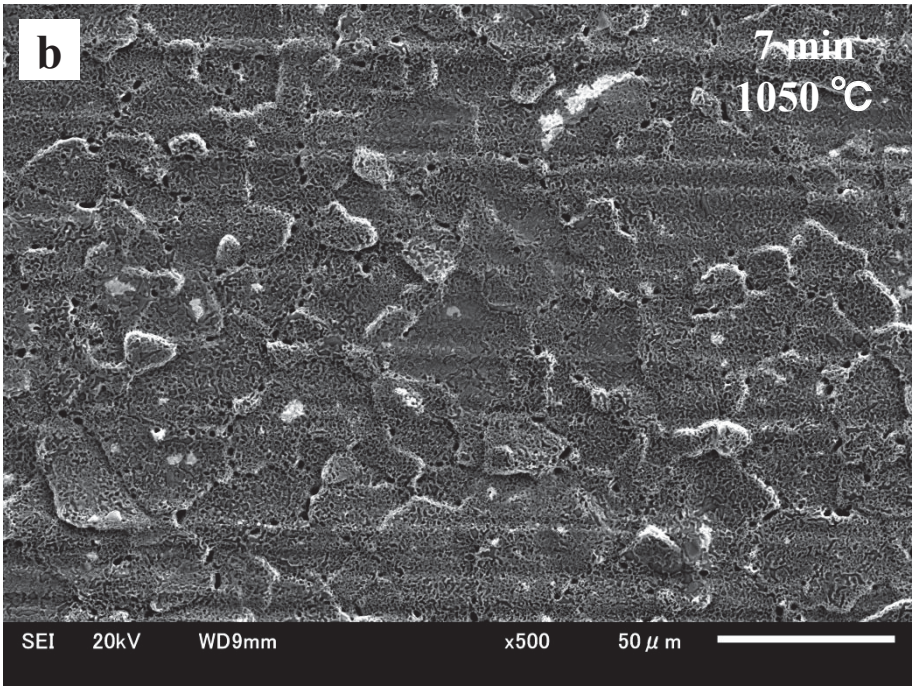
b
7 min
1050 ℃
SEI 20kV WD9mm x500 50 μ m

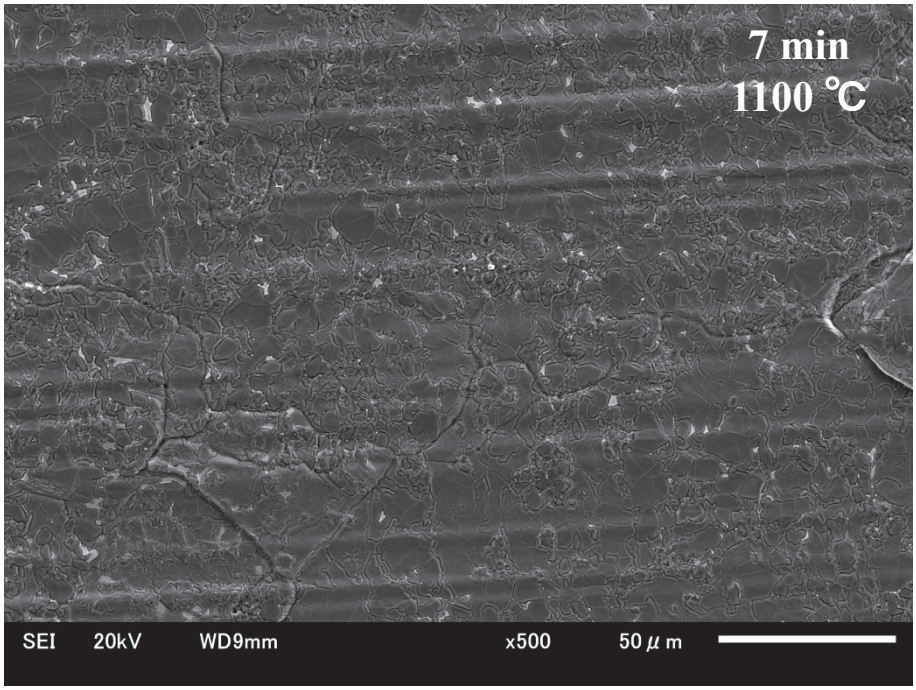
7 min
1100 ℃
SEI 20kV WD9mm x500 50 μ m

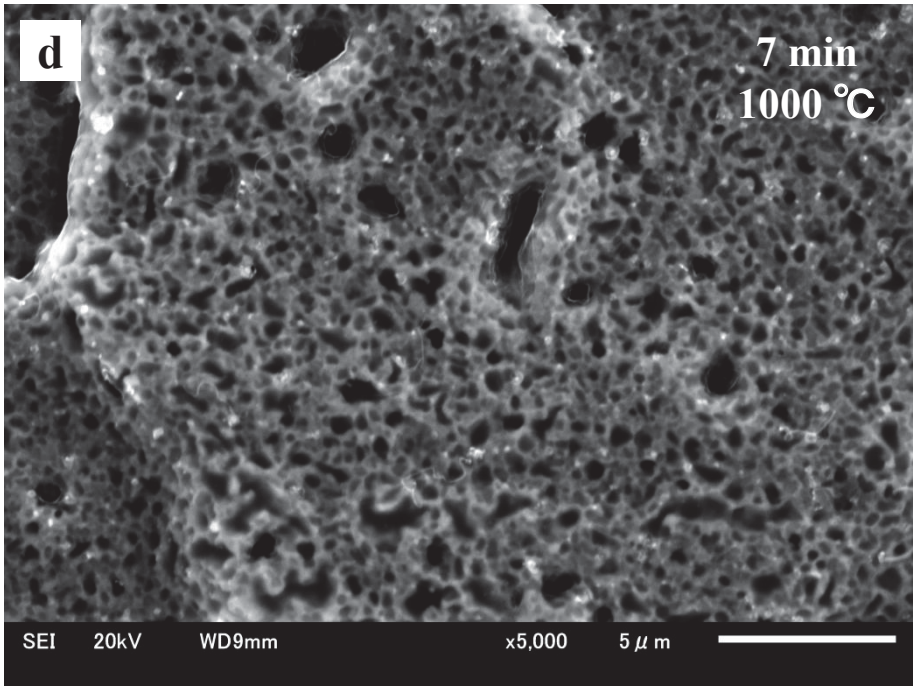
d
7 min
1000 ℃
SEI 20kV WD9mm x5,000 5 μ m

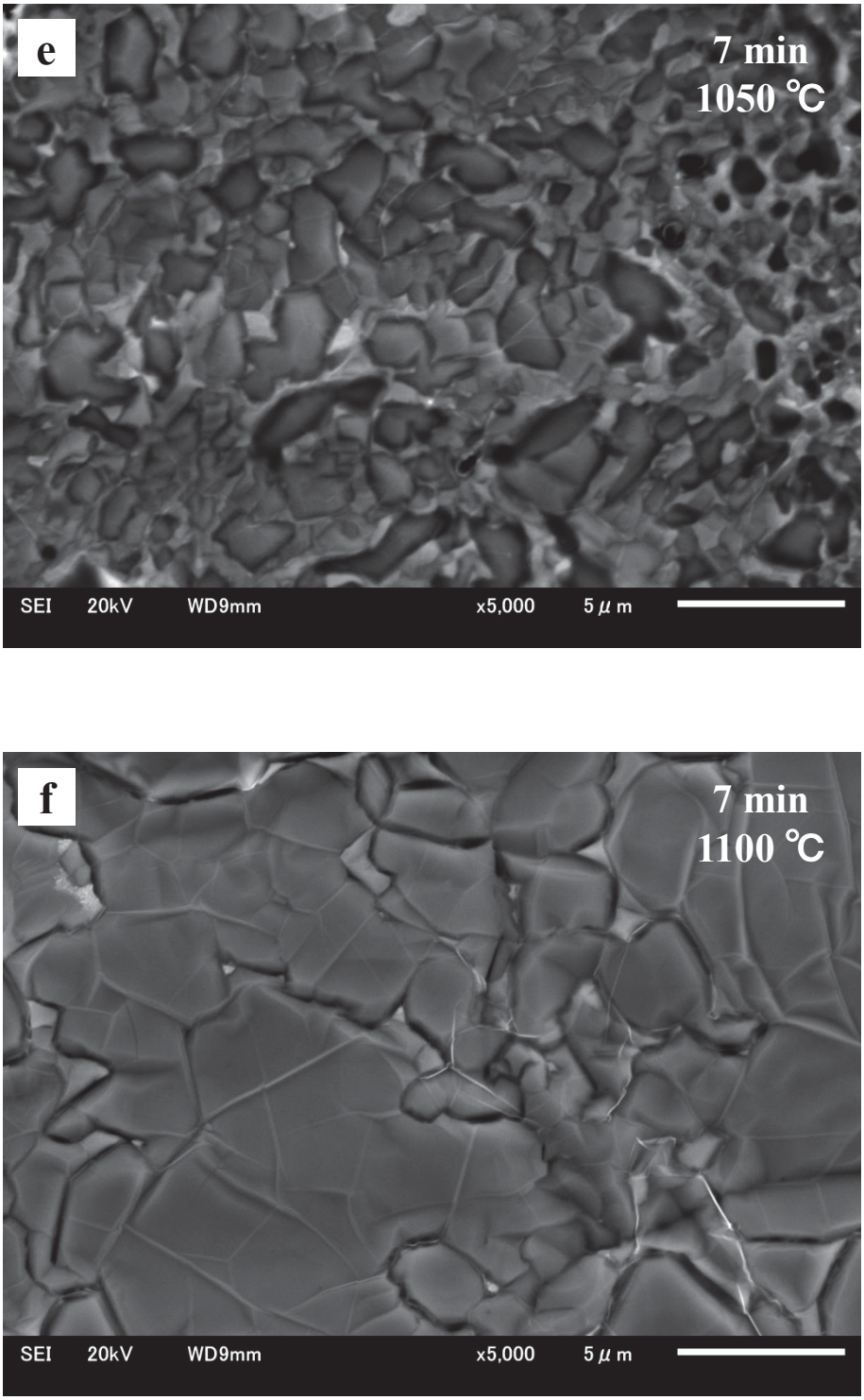

Figure 4.3 SEM images of as-grown samples synthesized on polycrystalline Ni substrates for 7 min at 1000 °C, 1050 °C, and 1100 °C (a-c) low magnification (d-f) high magnification.

4.3.2 Deposition Time Dependence

Deposition time dependence for quality, layer numbers, and nitrogen-doping levels of the nitrogen-doped graphene formation from 3 min to 12 min were investigated. To investigate the synthesized graphene materials composition, XPS was performed on the graphene materials formed at 1100 °C and various deposition times. The survey scans from the XPS analysis in Figure 4.4 (a) shows the C 1s peak at 284.5 eV, the N 1s peak 401.3 eV, and the O 1s peak at 534.5. The nitrogen-doping levels were 0 at %, 1.5 at %, and 2.9 at %, at deposition times of 3 min, 7 min, and 12 min, respectively. The nitrogen content clearly increased with increasing a deposition time. Figure 4.4 (b-d) shows the high-resolution scan of the N 1s signals, no N 1s peaks were observed for the sample synthesized at a deposition time of 3 min (shown in Figure 4.4 (b)). As shown in Figure 4.4 (c, d), the N1s peaks were observed for the samples grown at longer deposition times and could be fitted by three components, centred at ~399.2 eV, ~401.3 eV, and ~402.6 eV, corresponding to pyridine-like, pyrrole-like, and graphite-like nitrogen atoms doped into the graphene, respectively [4.8]. Figure 4.5 (e-g) shows high-resolution scans of the C1s peaks. All the C1s peaks could be fitted by five components centred at ~284.8 eV, ~285.4 eV, ~286.5 eV, ~288.6 eV, and ~291.3 eV, corresponding to sp^2C-sp^2C, N-sp^2C, N-sp^3C, carboxyl functionalities, and the π-π^* satellite peak, respectively [4.7, 4.8]. Increasing the doping level of nitrogen reduced the proportion of sp^2 bonded carbon. This indicates that the graphene sheets were partially substituted nitrogen atoms.

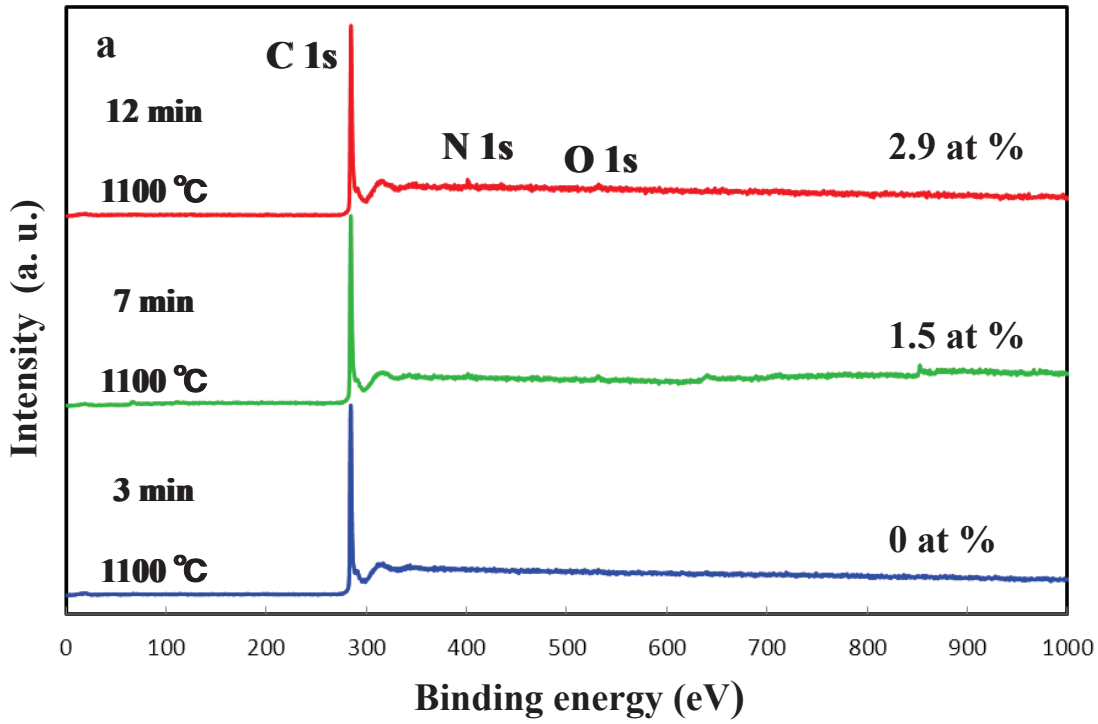
a
C 1s
12 min
1100 ℃
N 1s
O 1s
2.9 at %
7 min
1100 ℃
1.5 at %
3 min
1100 ℃
0 at %
Intensity (a. u.)
0
100
200
300
400
500
600
700
800
900
1000
Binding energy (eV)

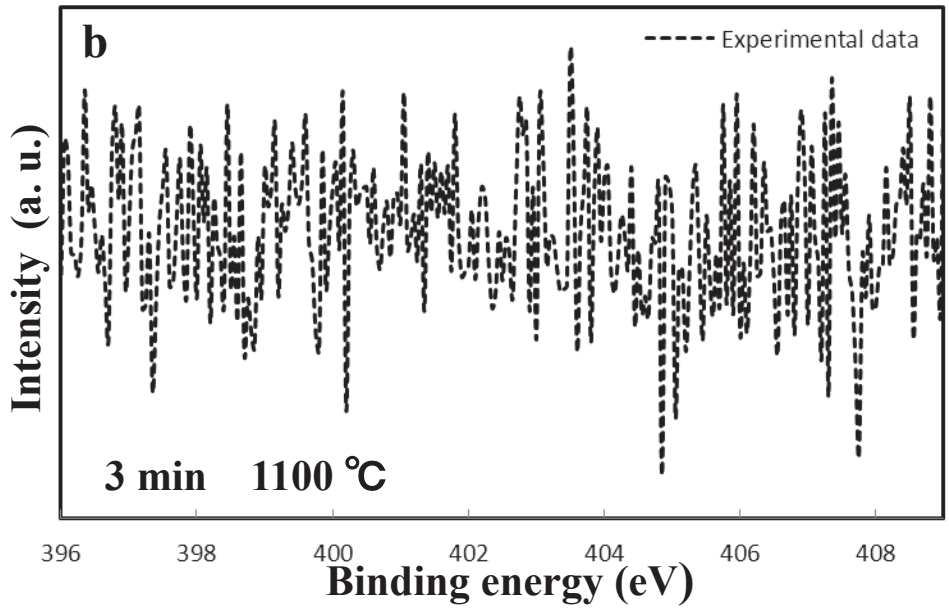
b
Experimental data
3 min 1100 ℃
Intensity (a. u.)
396
398
400
402
404
406
408
Binding energy (eV)

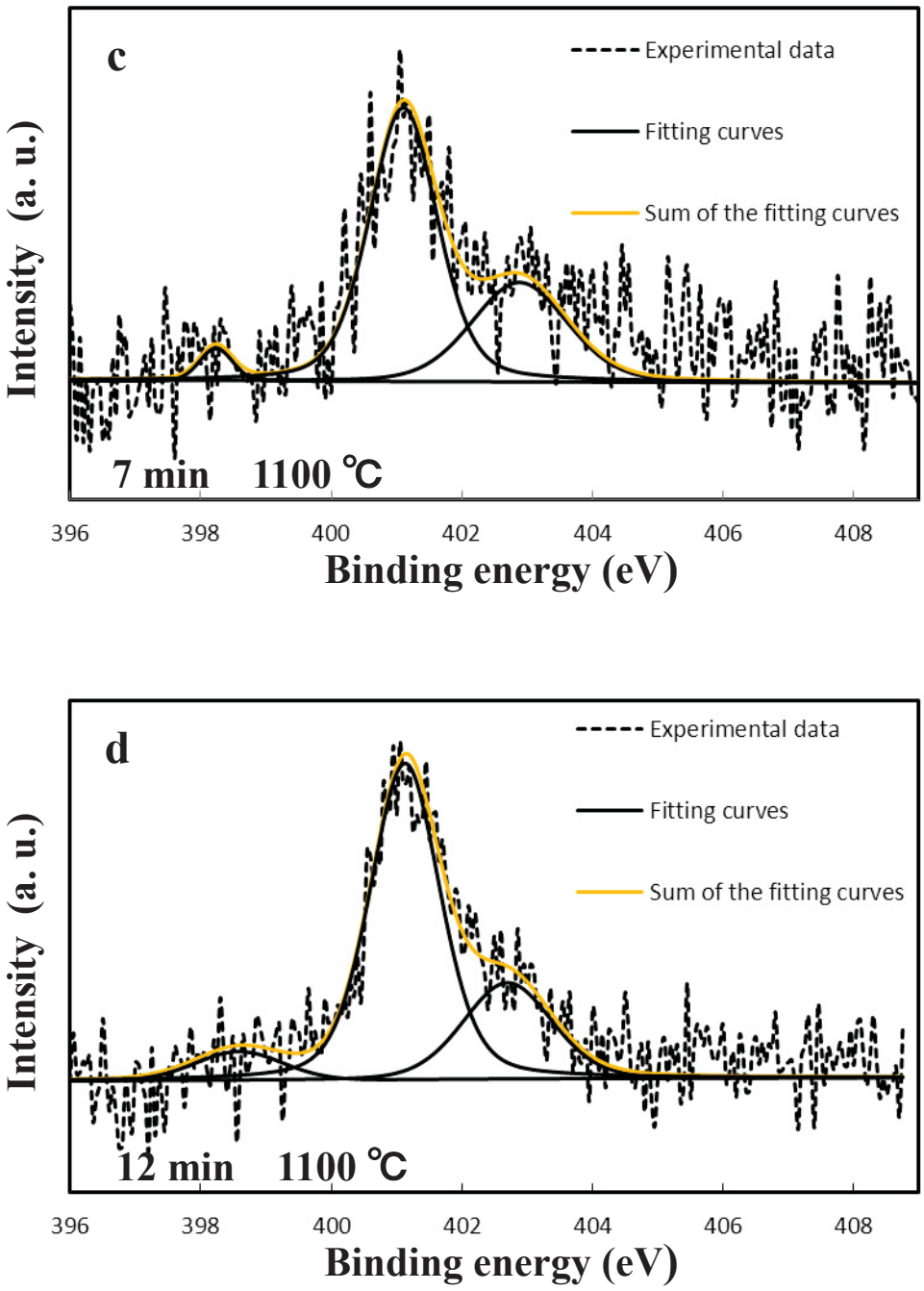

Figure 4.4 (a) wide-range XPS spectra of as-grown sample synthesized on Ni substrates at 1100 °C for 3 min, 7 min, and 12 min. High-resolution XPS spectra of N 1s signal for (b) 3 min, (c) 7 min, and (d) 12 min.

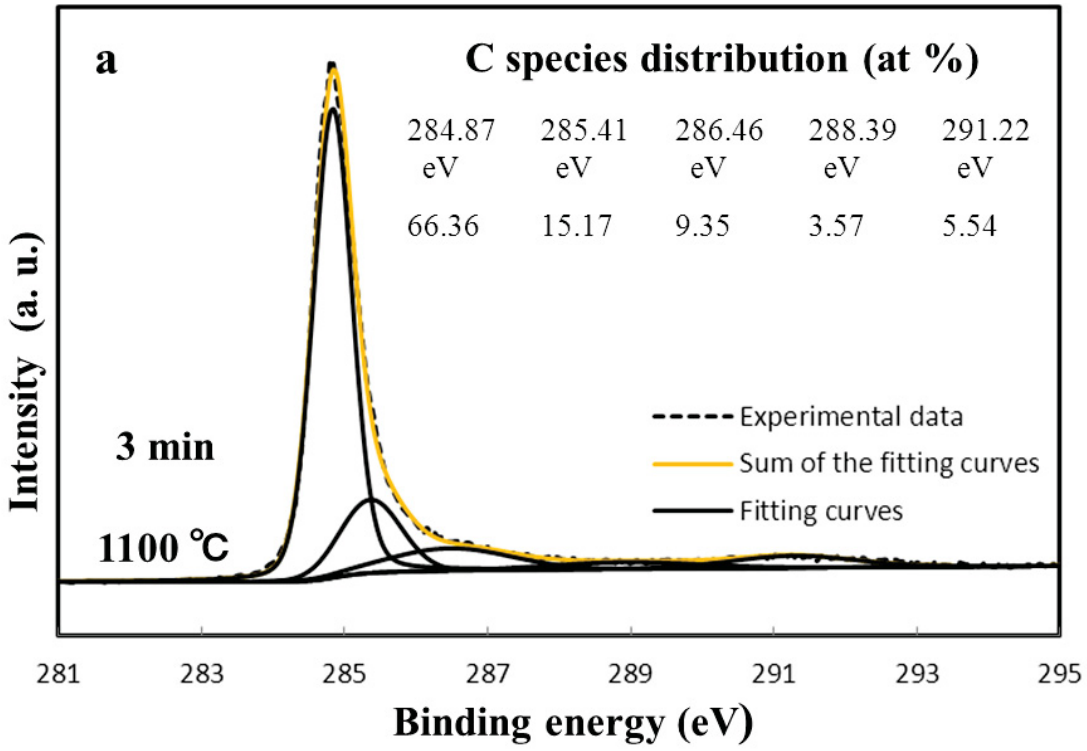
a
C species distribution (at %)
284.87 eV
285.41 eV
286.46 eV
288.39 eV
291.22 eV
66.36
15.17
9.35
3.57
5.54
3 min
1100 ℃
Experimental data
Sum of the fitting curves
Fitting curves
Intensity (a. u.)
281
283
285
287
289
291
293
295
Binding energy (eV)

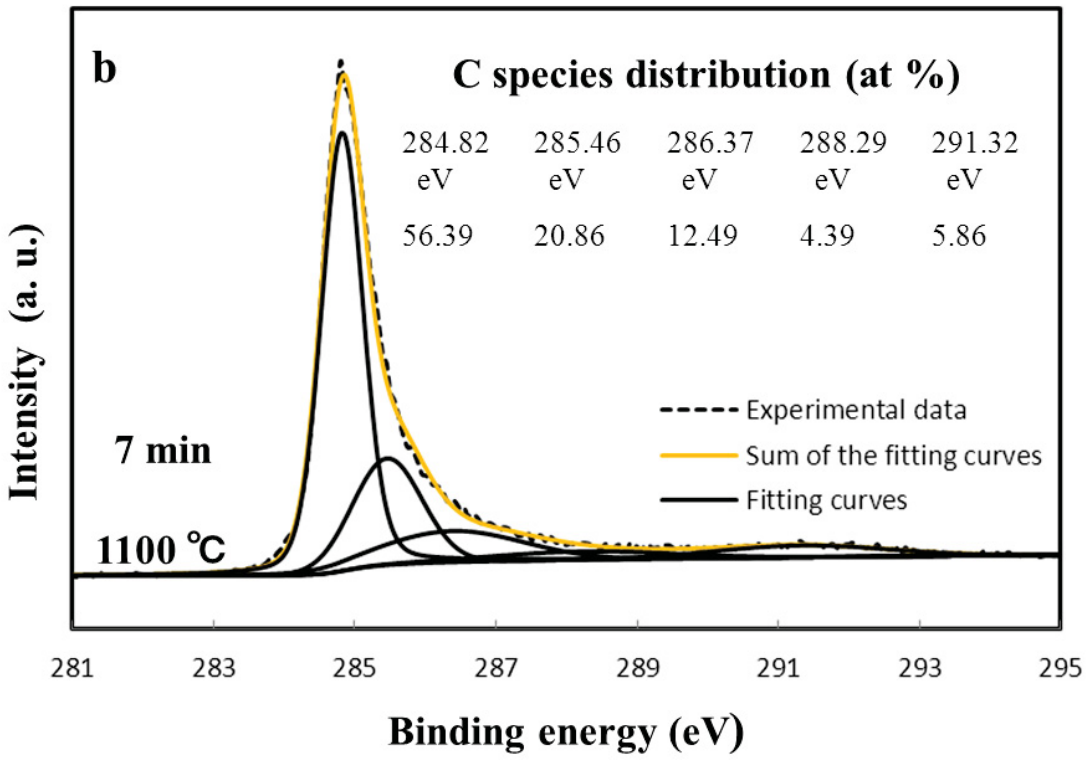
b
C species distribution (at %)
284.82 eV
285.46 eV
286.37 eV
288.29 eV
291.32 eV
56.39
20.86
12.49
4.39
5.86
7 min
1100 ℃
Experimental data
Sum of the fitting curves
Fitting curves
Intensity (a. u.)
281
283
285
287
289
291
293
295
Binding energy (eV)

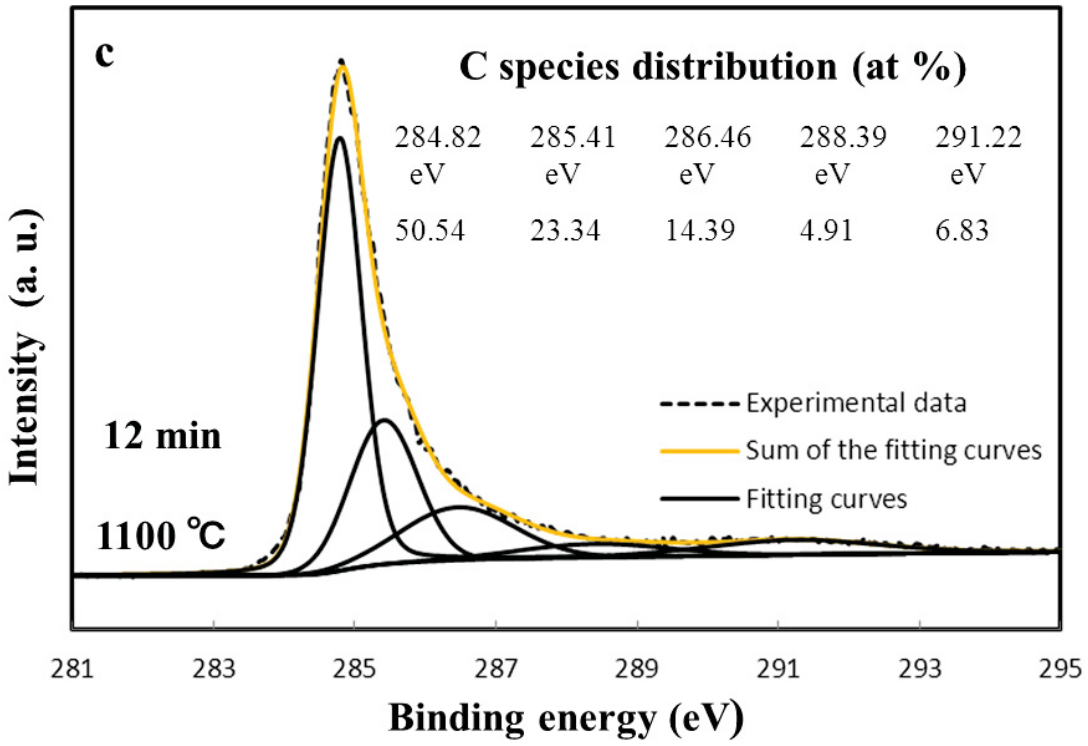

Figure 4.5 high-resolution XPS spectra of C 1s signal corresponding to Figure 4.4 (b-d) and C 1s species distribution.

Figure 4.6 (a-c) shows the Raman mappings results for the 2D-FWHM of nitrogen-doped graphene synthesized at 1100 °C with deposition times of 3, 7, 12 min, on polycrystalline Ni substrates. In Figure 4.6 (a) the samples synthesized with a deposition time of 3 min shows a smaller 2D-FWHM regions over a large area of the substrate, coloured red. In Figure 4.6 (b), smaller 2D-FWHM regions were decreased compared with the samples synthesized at a deposition time of 3 min. Extending the deposition time broadened the 2D-FWHM (coloured blue) in Figure 4.6 (c). This indicates that the number of nitrogen-doped graphene layers increased with the deposition time. Figure 4.6 (d-f) shows the Raman spectra obtained at circles A and B

marked in Figure 4.6 (a-c). As the deposition time increased from 3 min to 12 min, the intensity of the D-band peak increased. This indicates that nitrogen atoms doped into the sheet introduced topological defects.

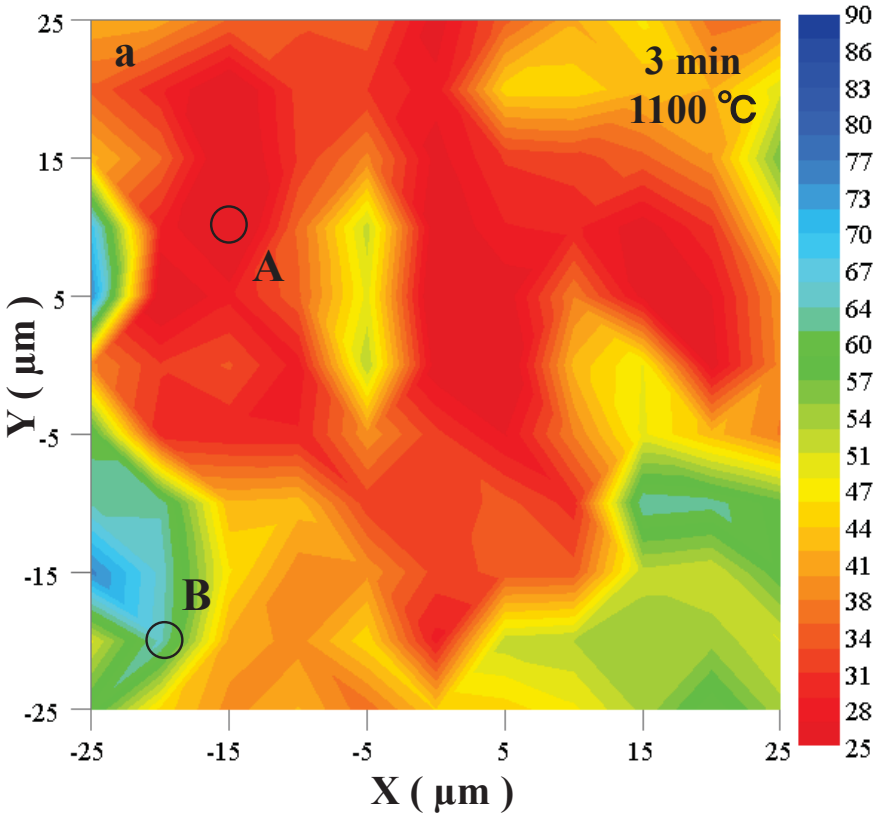

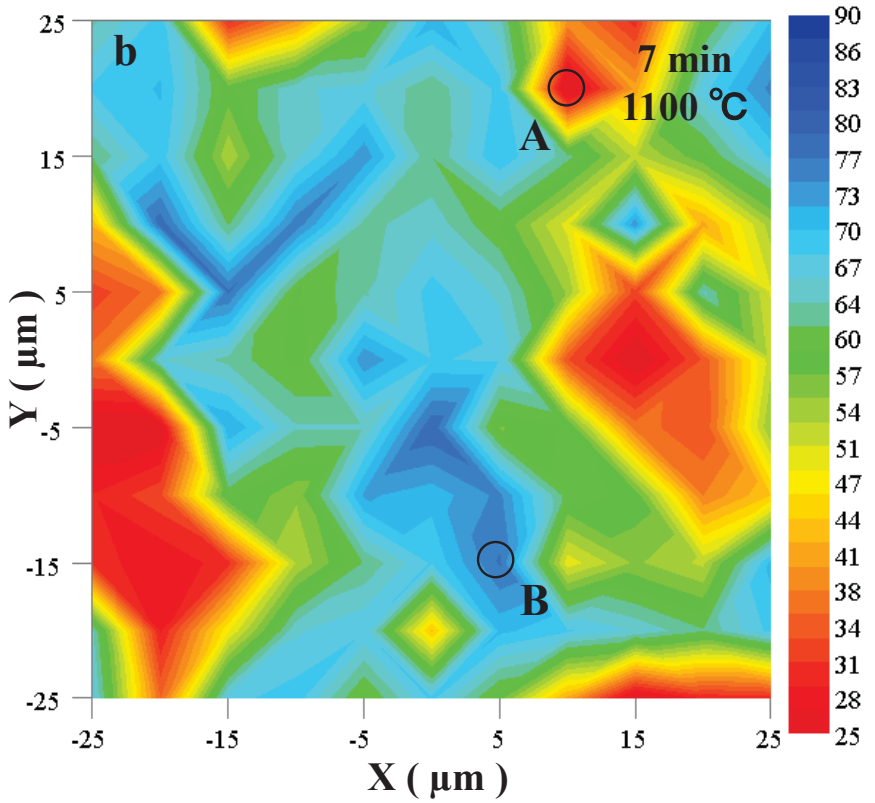
b
7 min
1100 ℃
A
B
25
15
5
-5
-15
-25
Y (μm)
-25
-15
-5
5
15
25
X (μm)
90
86
83
80
77
73
70
67
64
60
57
54
51
47
44
41
38
34
31
28
25

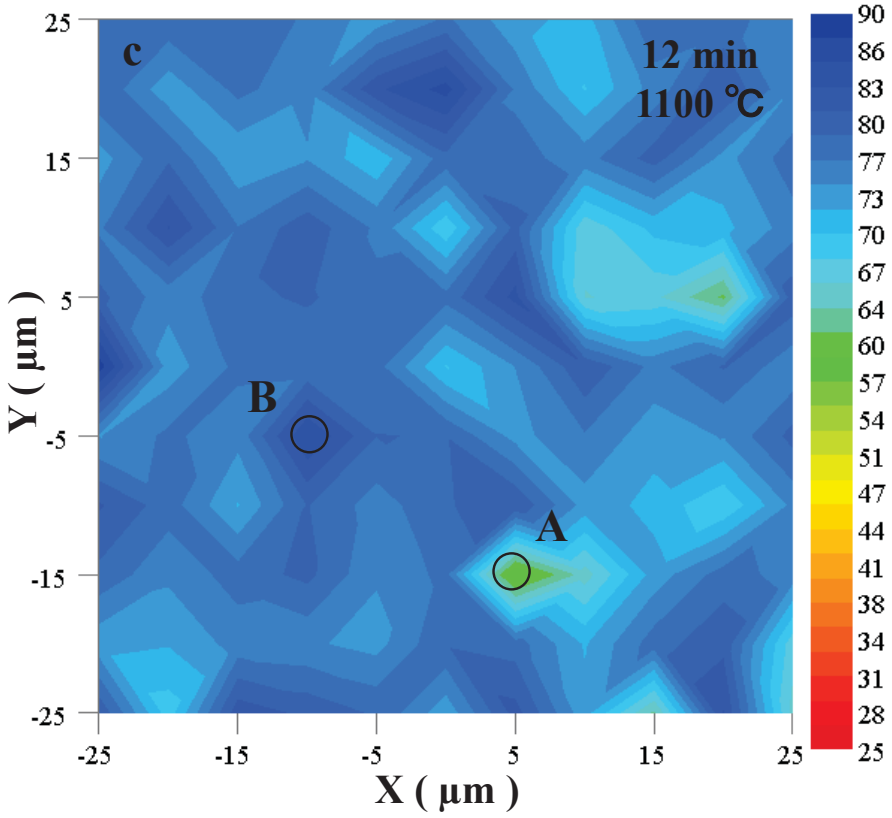
c
12 min
1100 ℃
B
A
25
15
5
-5
-15
-25
Y (μm)
-25
-15
-5
5
15
25
X (μm)
90
86
83
80
77
73
70
67
64
60
57
54
51
47
44
41
38
34
31
28
25

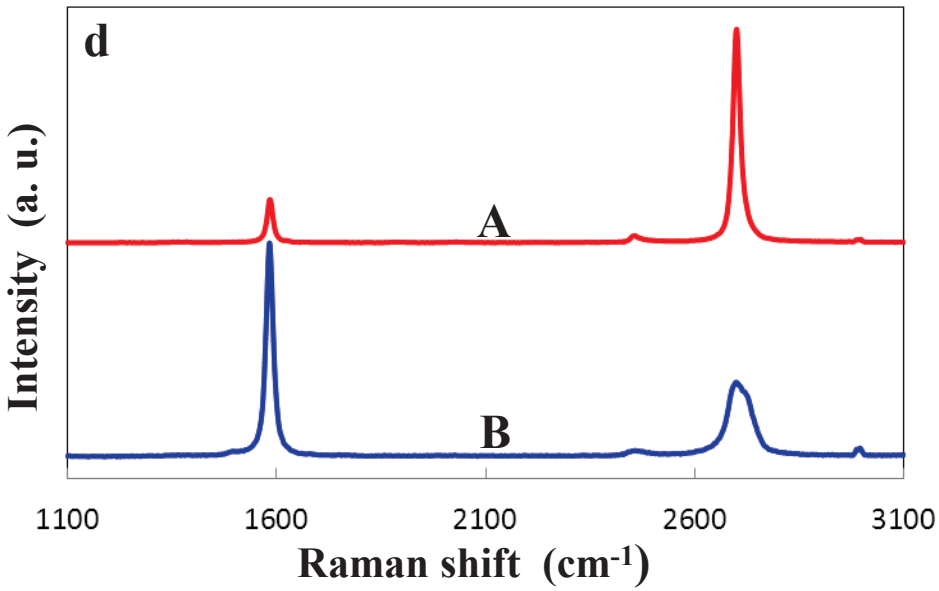
d
Intensity (a. u.)
A
B
1100
1600
2100
2600
3100
Raman shift (cm-1)

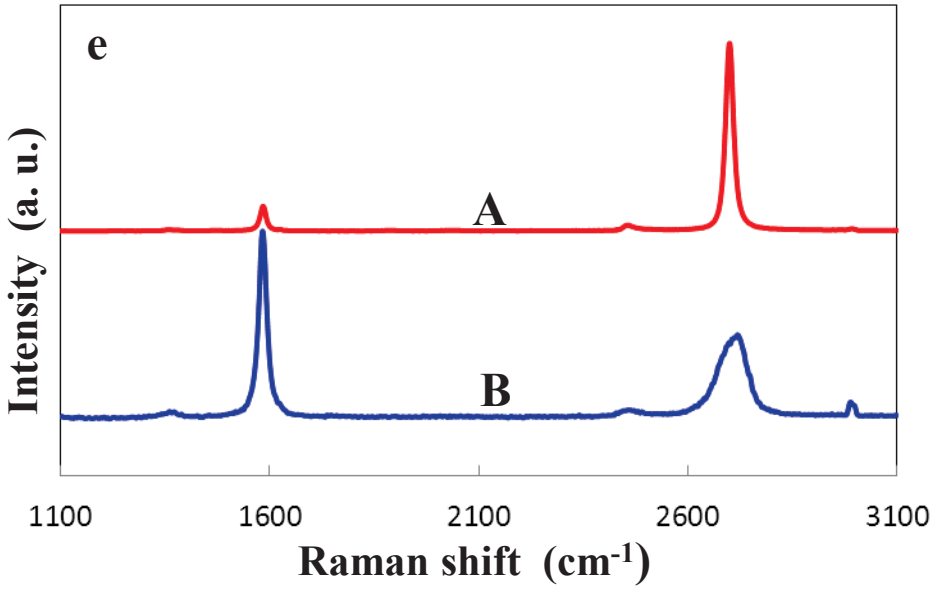
e
Intensity (a. u.)
A
B
1100
1600
2100
2600
3100
Raman shift (cm-1)

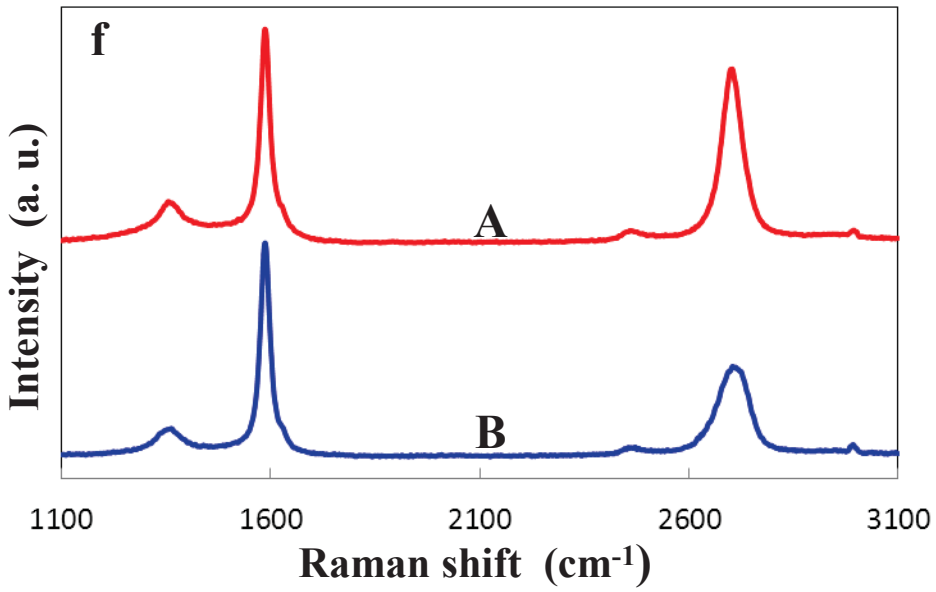

Figure 4.6 Raman mapping results of 2D-FWHM for samples synthesized on polycrystalline Ni substrates at 1100 °C for (a) 3 min, (b) 7 min, and (c) 12 min. (d-f) Raman spectra taken at circle A and B marked in Figure 4.6 (a-c).

Figure 4.7 (a-c) shows SEM images of nitrogen-doped graphene sheets synthesized on polycrystalline Ni substrates at 1100 °C with deposition time of 3, 7, and 12 min, at low magnification, and Figure 4.7(d-f) shows high magnification SEM images of the regions in Figure 4.7 (a-c). Large area homogenous films were formed at shorter deposition times.

Figure 4.8 (a-f) show AFM images of as-grown samples synthesized at 1100 °C for 3 min, 7 min, and 12 min on polycrystalline Ni substrates. At shorter deposition time, large size grain were observed compared to samples synthesized at longer deposition time.

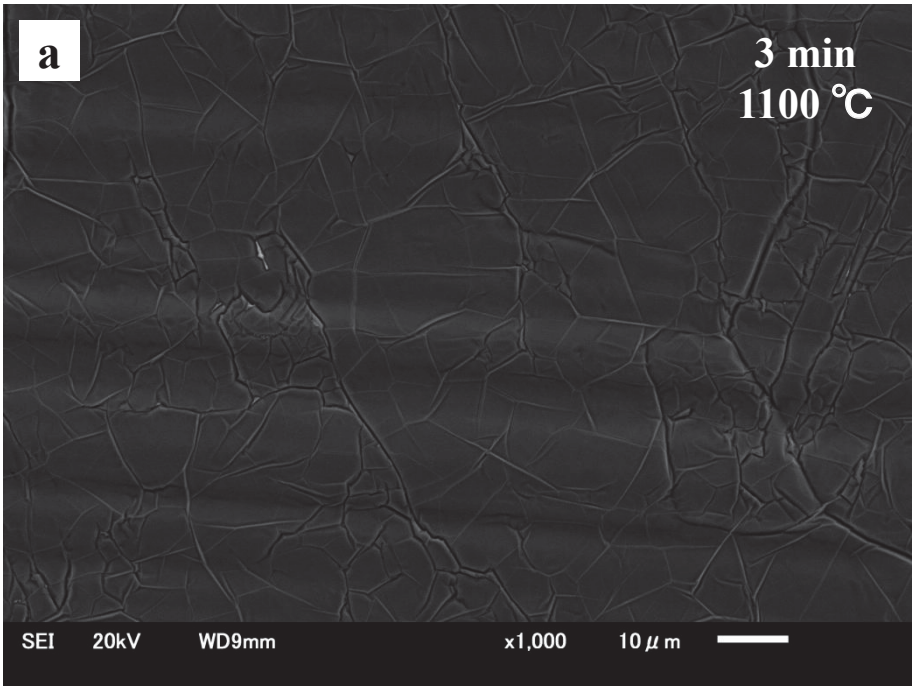
a
3 min
1100 ℃
SEI 20kV WD9mm x1,000 10 μ m

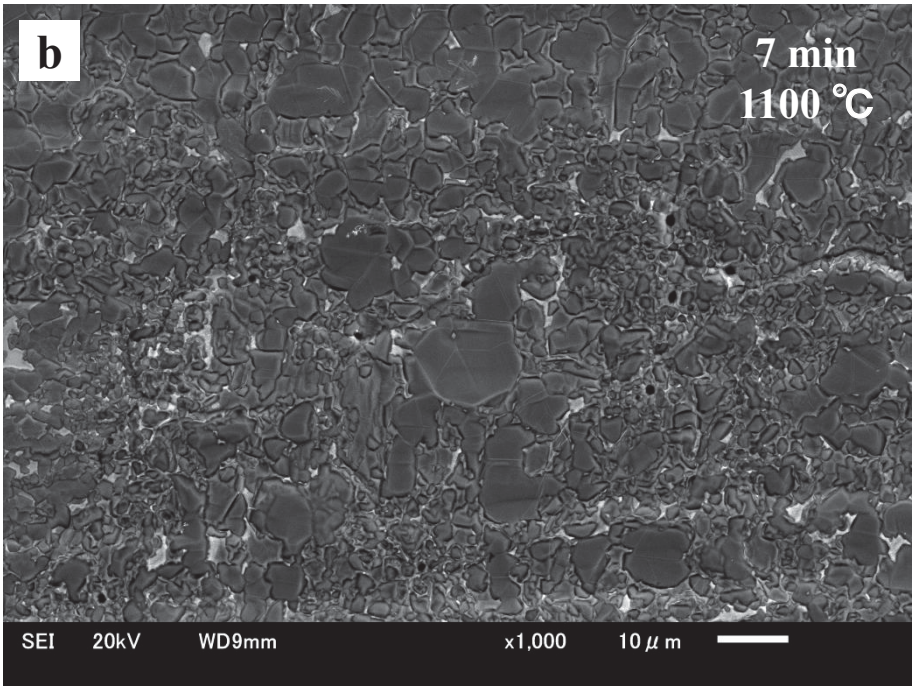
b
7 min
1100 ℃
SEI 20kV WD9mm x1,000 10 μ m

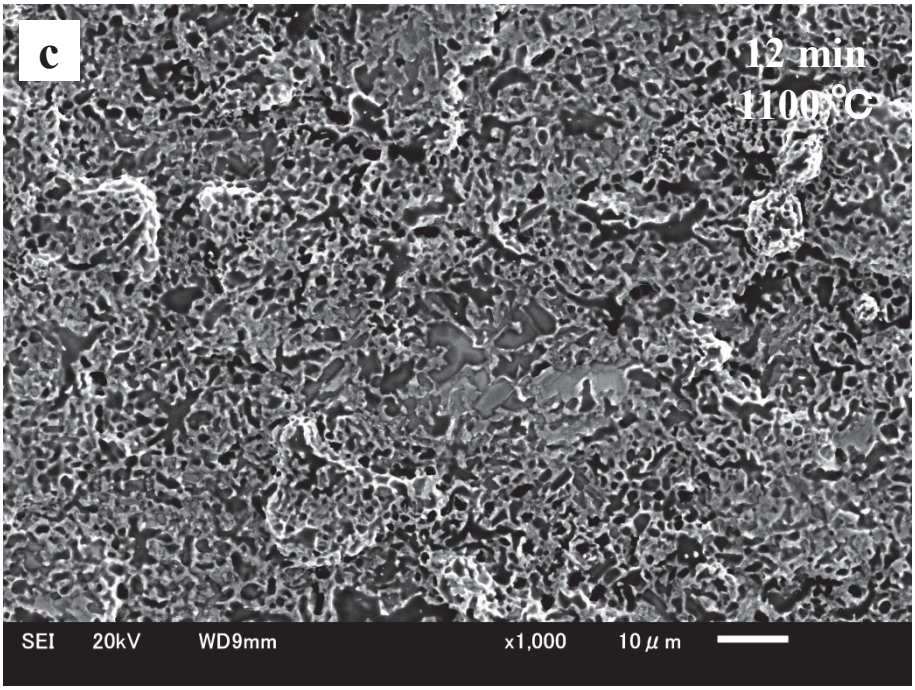
c
12 min
1100℃
SEI 20kV WD9mm x1,000 10 μ m

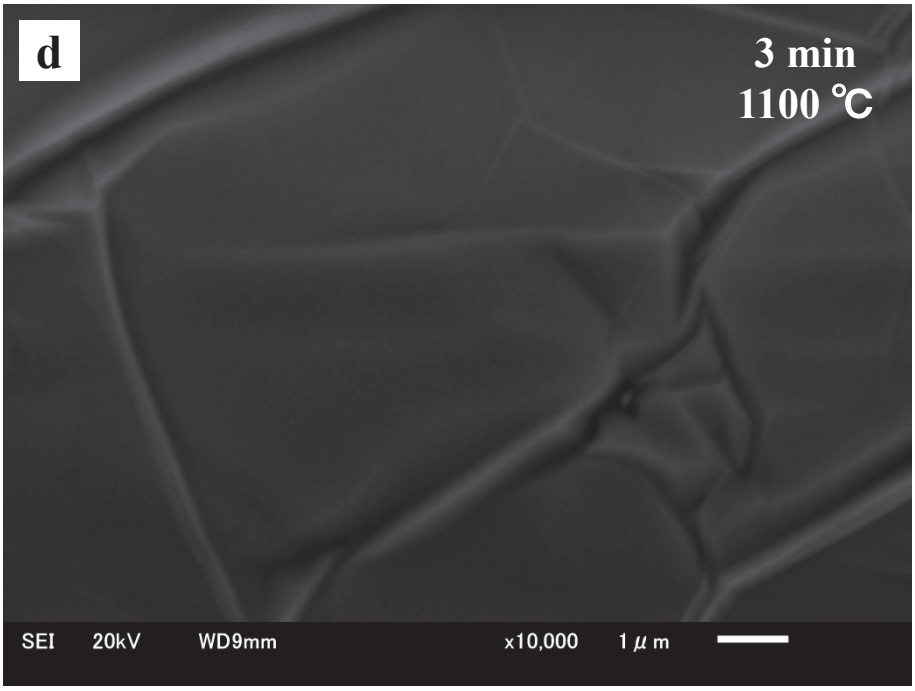
d
3 min
1100 ℃
SEI 20kV WD9mm x10,000 1 μ m

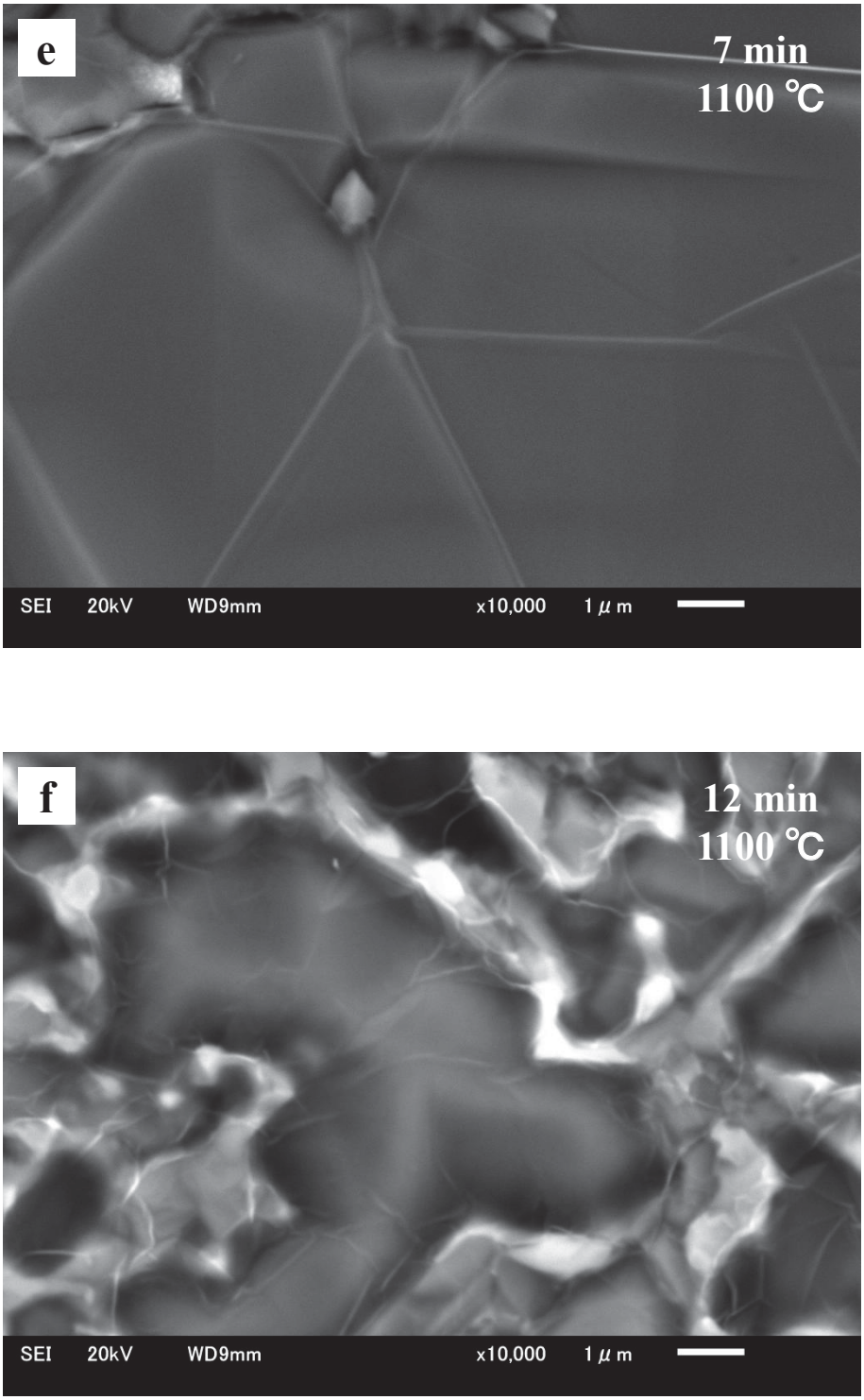

Figure 4.7 SEM images of nitrogen-doped graphene synthesized on polycrystalline Ni substrates at 1100 °C for 3 min, 7 min, and 12 min at (a-c) low magnification and (d-f) high magnification.

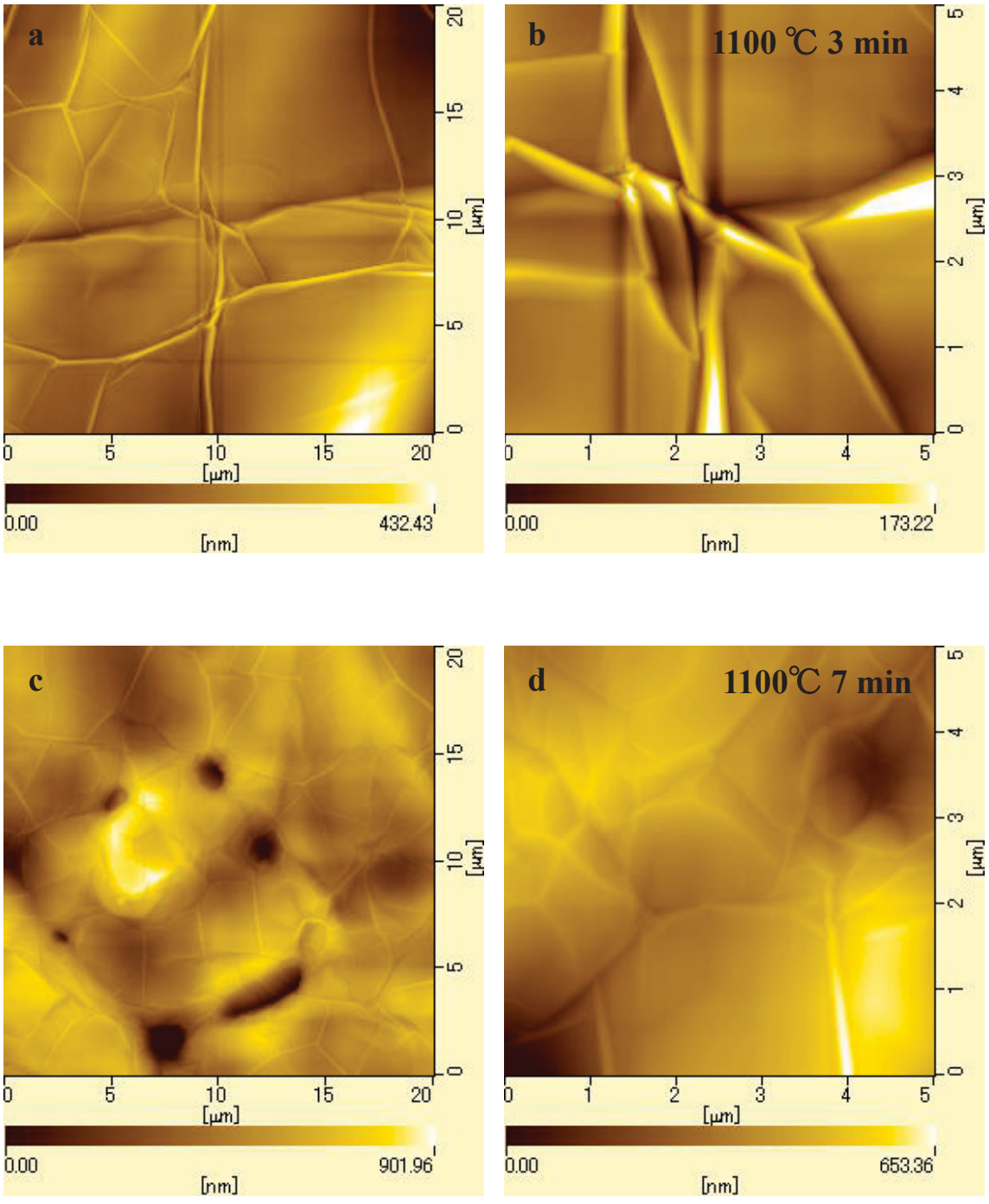
a
b
1100 ℃ 3 min
c
d
1100℃ 7 min
0.00
432.43
173.22
901.96
653.36
[nm]
[μm]

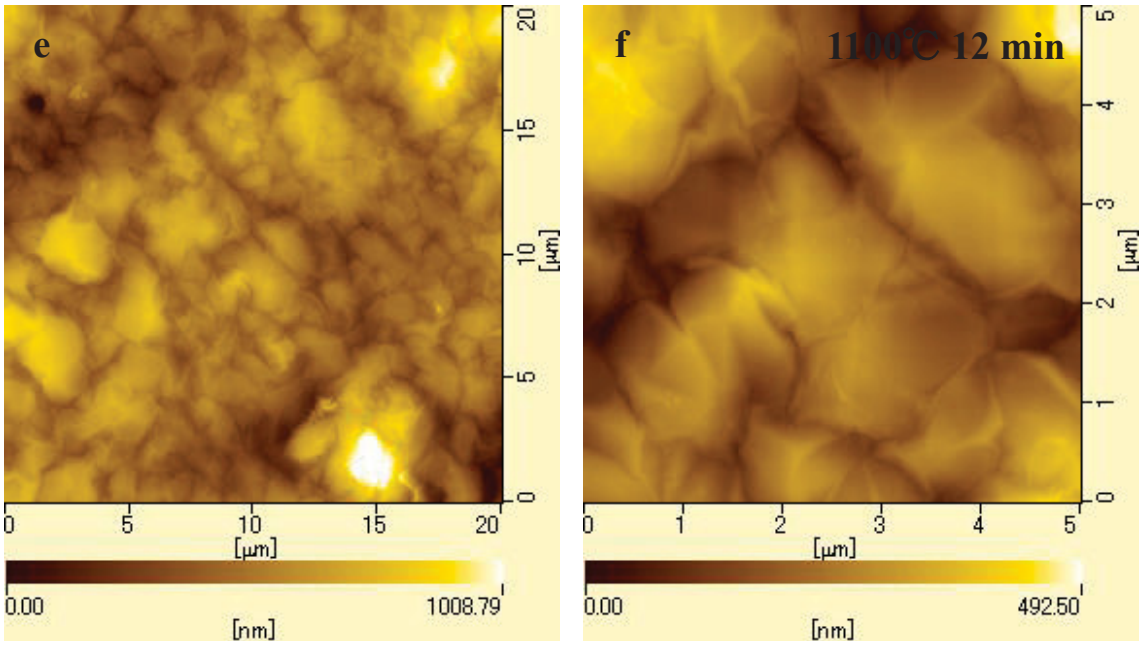

Figure 4.8 (a-f) show AFM images of as-grown samples synthesized at 1100 °C for 3 min, 7 min, and 12 min on polycrystalline Ni substrates.

To confirm the nitrogen-doped graphene sheets morphology and numbers of layers TEM characterization were carried out. The sample synthesized on polycrystalline Ni substrates with 7 min at 1100 °C were dispersed in ethanol and drying a few drops to holey carbon TEM grids. TEM were operated at 200 kV. As shown in Figure 4.9 (a), the graphene planar sheets are clearly observed, indicating that the features of high surface/volume ratio and the two-dimensional structure. The edges of the suspended film partially fold back, allowing for a cross-sectional view of the film. The observation of these edges by HRTEM provides an accurate way to measure the number of layers (shown in Figure 4.9 (b)). Typically, sections of monolayer - >10 layers (shown in figure 4.9 (c-h)) are observed in close agreement with Raman mapping results.

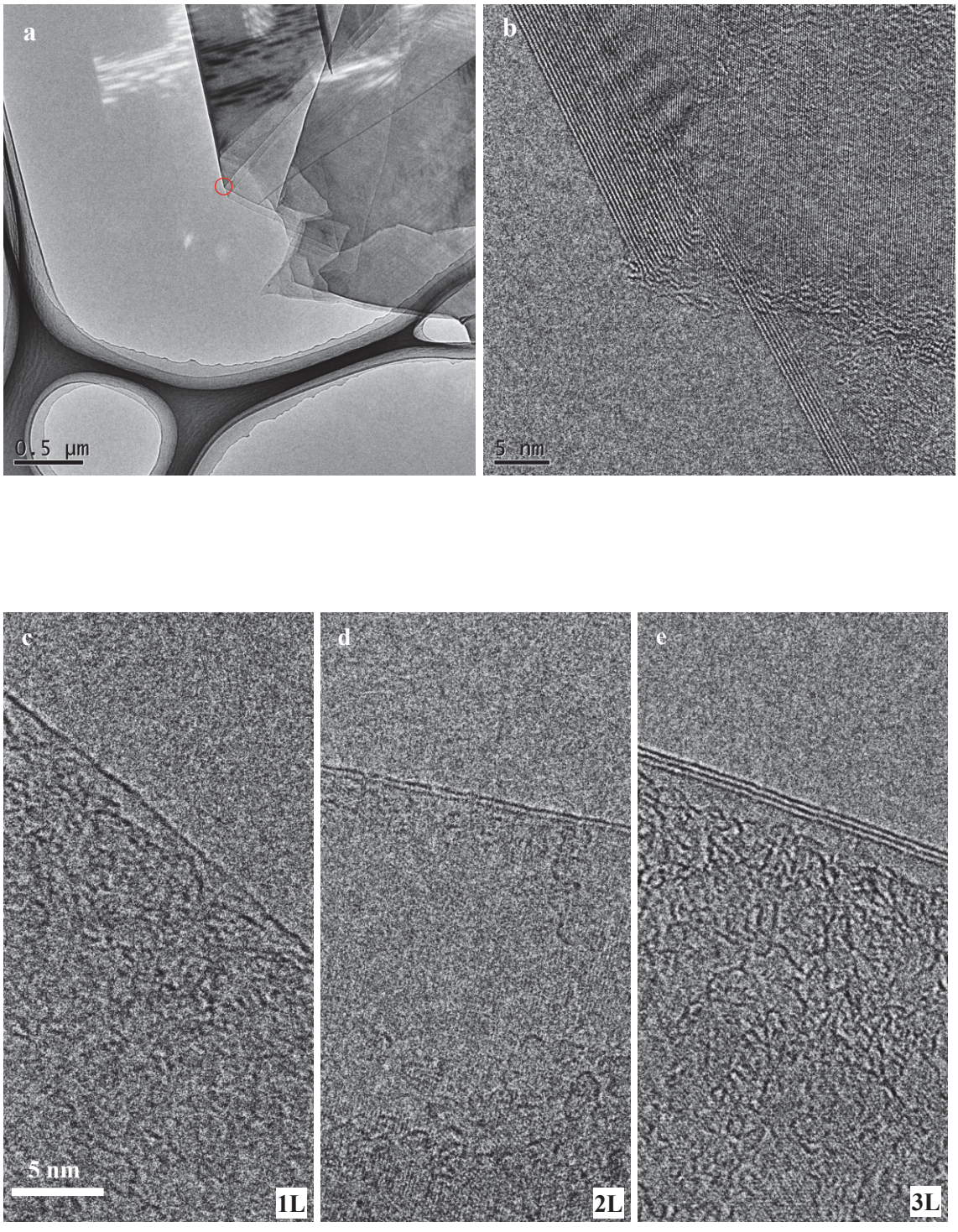
a
0.5 μm
b
5 nm
c
5 nm
1L
d
2L
e
3L

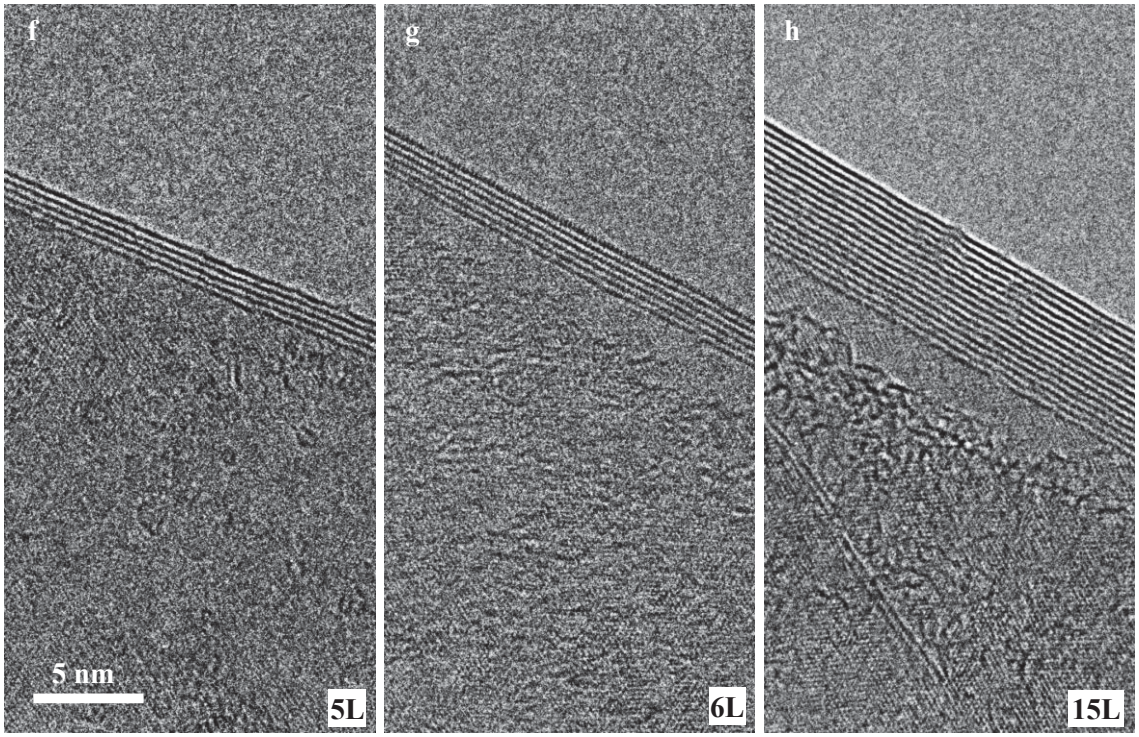

Figure 4.9 (a) low-magnification TEM image of nitrogen-doped graphene synthesized on polycrystalline Ni substrates at 1100 °C for 7 min, (b) high-resolution TEM images of circle A marked in (a), (c-h) high-resolution TEM images of (c) one-, (d) two-, (e) three-, (f) five-, (g) six-, and (h) fifteen-layers nitrogen-doped graphene.

On the basis of the results and discussion above, the possible mechanism of nitrogen-doped graphene is proposed that; with increasing the growth time, grain boundary were increased, allows more carbon and nitrogen atoms diffused and segregated to surface of polycrystalline Ni substrates to formed thicker layers nitrogen-doped graphene and increase the nitrogen concentration [4.20].

4.4. Summary

In this chapter, synthesis of nitrogen-doped graphene by ambient pressure

thermal CVD technique using monoethanolamin as a precursor that combines carbon and nitrogen on polycrystalline Ni substrates were presented. As the growth temperature increased from 1000 °C to 1100 °C, the intensity of the Raman D-band peak decreased. This indicated that increasing the growth temperature improved the nitrogen-doped graphene quality. XPS results show that nitrogen doping levels were increased from 0 at % to 2.9 at % with increasing the deposition time. High-resolution XPS spectrum of C 1s signal show that the relative proportion of sp^2 bonded carbon atoms decreased as the nitrogen doping level increased. Spatially resolved Raman spectroscopy results show that longer deposition times increased the number of nitrogen-doped graphene layers. Low magnification TEM characterization show nitrogen-doped graphene have a planar sheet morphology, and HRTEM confirm that nitrogen-doped graphene layers formed with thickness between a monolayer and >10 layers. I believe that these results will play an important role in the development of facile synthetic routes to pristine graphene and nitrogen-doped graphene materials using liquid precursor.

References

[4.1] K S Novoselov, A K Geim, S V Morozov, D Jiang, Y Zhang, S V Dubonos, I V Grigorieva and A A Firsov. Science 306, (2004) 666.

[4.2] Novoselov K S, Geim A K, Morozov S V, Jiang D, Katsnelson M I, Grigorieva I V, Dubonos S V and Firsov A A. Nature 438, (2005) 197.

[4.3] Zhang Y, Tan Y W, Stormer H L and Kim P. Nature 438, (2005) 201.

[4.4] Keun S K, Yue Zhao, Houk J, Sang Y L, Jong M K, Kwang S K, Jong H A, Philip K, Jae Y C and Byung H H. Nature 457, (2009) 706.

[4.5] A Yu, I Roes, A Davies, Z Chen. Applied physics letters 96, (2010) 253105.

[4.6] Zhen H S, Hong L G, Wen J B, Feng B W and Xing H X. J. Mater. Chem. 22, (2012) 390.

[4.7] Hwee L P, Petr S, Zdenek S and Martin P. ACS Nano 7, (2013) 5262.

[4.8] Arava L M R, Anchal S, Sanketh R G, Hemtej G, Madan D and Pulickel M A. ACS Nano 4, (2010) 6337.

[4.9] Lijie C, Li S, Chuanhong J, Deep J, Dangxin W, Yongjie L and Anchal S. Nature Mater 9, (2010) 430.

[4.10] Ying W, Yuyan S, Dean W M, Jinghong L and Yuehe L. ACS Nano 4, (2010) 1790.

[4.11] Liangti Q, Yong L, JongBeom B and Liming D. ACS Nano 4, (2010) 1321.

[4.12] R Imran J, N Rajalakshmib and S Ramaprabhu. J. Mater. Chem. 20, (2010) 7114.

[4.13] Haibo W, Chuanjian Z, Zhihong L, Li W, Pengxian H, Hongxia X, Kejun Z, Shanmu D, Jianhua Y and Guanglei C. J. Mater. Chem. 21, (2011) 5430.

[4.14] Yuanjian Z, Keisuke F, Toshiyuki M, Li N and Jinhua Y. J. Mater. Chem. 22, (2012) 6575.

[4.15] Zhengzong S, Zheng Y, Jun Y, Elvira B, Yu Z and James M T. Nature 468, (2010) 549.

[4.16] Zhong J, Jun Y, Carter K and James M T. ACS Nano 5, (2011) 4112.

[4.17] Ferrari AC, Meyer JC, Scardaci V, Casiraghi C, Lazzeri M, Mauri F, et al. Phys. Rev. Lett. 97, (2006) 187401.

[4.18] Mildred S. D, Ado J, Mario H, Gene D and Riichiro S. Nano Lett. 10, (2010) 751.

[4.19] Pimenta MA, Dresselhaus G, Dresselhaus MS, Cancado LG, Jorio A and Saito R. Phys. Chem. Chem. Phys. 9, (2007) 1276.

[4.20] Yi. Z, Lewis. G, et al. J. Phys. Chem. Lett. 1, (2010) 3101.

Chapter 5

Summary and Future Works

5.1 Summary

Synthesis of carbon nanomaterials with low cost and high quality is a one of the fundamental research to understand growth mechanism and intrinsic properties. In this thesis, carbon nanomaterials (CNFs, N-doping CNTs, and N-doping graphene) were synthesized by simple thermal CVD of single liquid precursors and the basic experimental parameter dependence were investigated. The main achievements of the thesis are as follow:

1. CNFs were synthesized on silicon and quartz substrates by ultrasonic spray pyrolysis of alcohol (methanol, ethanol, and 2-propanol) without using additional catalyst. The Substrates, growth temperature, and alcohol type (carbon precursor) dependence were investigated. When methanol was used as carbon precursor, the CNFs with an amorphous structure were formed at the center of furnace, whereas similar results were in both ethanol and 2-propanol that some hollow structure thin diameter of CNFs were formed at the downstream of the furnace. This is concluded that the presence of the alkyl groups in the alcohols played important role in the CNFs morphology. The mechanisms of catalyst-free synthesis of CNFs by ultrasonic spray pyrolysis of alcohol is proposed that: first, alcohol mist were decomposed on the surface of the substrates then formed carbon nanoparticles, second, these carbon nanoparticles played to nucleation site and grow to CNFs.
2. In general, syntheses of N-doping CNTs have a multi process and/or multi feedstock.

In this thesis N-doping CNTs were synthesized on the metal (Ni and Fe) substrates by thermal CVD method of monoethanolamine only without using additional catalyst and process at temperature range of 850 °C – 1000 °C. All of the prepared N-doping CNTs were exhibit bamboo-like and corrugated structures. The concentration of nitrogen in the N-doped CNTs did not depend on synthesis temperature. However the ratio of pyridine-like to graphite-like nitrogen increased with increasing the growth temperature. The crystallinity of the N-doping CNTs were improved with increasing the growth temperature, whereas have a same nitrogen doping levels. The average diameters of the N-doped CNTs were increased with increasing the growth temperature; this is concluded that with increasing the growth temperature the large curvature Ni islands were formed on the surface of the Ni substrates.

3. Nitrogen content controllable graphene were synthesized by thermal CVD of monoethanolamine on polycrystalline Ni substrates at ambient pressure. The growth temperature and growth time dependence were investigated. The N-doping graphene qualities were improved with increasing the growth temperature whereas the layers of N-doping graphene were decreased. Moreover, with increasing the growth time large Ni grain covered with graphene sheets were formed. The nitrogen content was controlled by the growth time at 1100 °C. However with increasing the nitrogen content the numbers of N-doping graphene layers were increased. Based on our experimental results, the possible mechanism of nitrogen-doped graphene is proposed that; with increasing the growth time the grain boundary were increased and allows more carbon and nitrogen atoms diffused and segregated to surface of polycrystalline Ni substrates to formed thicker layers nitrogen-doped graphene and

increase the nitrogen concentration.

5.2 Future Works

For the future work I would like to improve the experimental apparatus explore the growth mechanism of CNFs synthesized by ultrasonic spray pyrolysis of alcohol and optimize the experimental parameters to fabrication CNFs films then to characterize the optical and electronic properties.

Improve the experimental apparatus and optimize the experimental parameters to synthesize the large area uniform N-doping graphene and transferred to insulation substrates to characterize the transparent and sheet resistance moreover to compare the nitrogen doping and pristine graphene for the further understanding the nitrogen doping effects.

Acknowledgement

I would like to express my sincere gratitude to my supervisor, Professor Tetsuo Soga, for his invaluable guidance and continued encouragements throughout this research. I would like to express my deep appreciation to assistant professor Naoki Kishi, for teaching me a scientific research style, for his expertise in writing, for his encouragements. I appreciate his timely pointing out of my mistake on research direction.

I would like to express my sincere gratitude to Professor Masaki Tanemura and Professor Makoto Miyoshi, for their thorough evaluation and invaluable comments.

The financial support provided by the NGK scholarship is gratefully acknowledged. I would also like to express my sincere appreciation to the Nagoya Institute of Technology for the resources provided.

I am grateful to all members at Soga laboratory for their experimental supports on my research. Lastly I would like to show my deep thanks to my respectable parents for the emotional support and encouragement.

List of publications

1. "Catalyst-free Synthesis of Carbon Nanofibers by Ultrasonic Spray Pyrolysis of Ethanol"

   Jianfeng Bao, Naoki Kishi, Ishwor Khatri, Tetsuo Soga, Takashi Jimb

   Materials Letters 68, (2012) 240.

2. "Similar device architectures for inverted organic solar cell and laminated solid-state dye-sensitized solar cells"

   Ishwor Khatri, Jianfeng Bao, Naoki Kishi, Tetsuo Soga.

   ISRN Electronics 2012, (2012)180787.

3. "Carbon Precursor Dependence of Carbon Nanofibers Synthesized by Catalyst-Free Ultrasonic Spray-Pyrolysis of Alcohol"

   Jianfeng Bao, Naoki Kishi, Tetsuo Soga

   Modern Physics Letters B 27, (2013) 1350213.

4. "Nitrogen-Doped Carbon Nanotubes Synthesized on Metal Substrates From a Single Precursor"

   Jianfeng Bao, Naoki Kishi, Ishwor Khatri, Tetsuo Soga

   Materials Letters 113, (2013) 114.

5. "Synthesis of Nitrogen-Doped Graphene by Thermal Chemical Vapor Deposition Method from a Single Liquid Precursor"

   Jianfeng Bao, Naoki Kishi, Tetsuo Soga

   Materials Letters (in press).

Conference

1. Synthesis of carbon nanofibers using ultrasonic spray pyrolysis of alcohol (poster)

Jianfeng Bao, Ishwor Khatri, Naoki Kishi , Tetsuo Soga

NANO SciTech2011 International Conference on Nanoscience and Nanotechnology

Shah Alam, Malaysia, March 2011

2. Synthesis of high purity Carbon nanofibers by ultrasonic spray pyrolysis of ethanol and methanol (oral)

   Jianfeng Bao, Naoki Kishi, Tetsuo Soga

   Nanomaterials Technology Specialized Conference 2012

   Shah Alam, Malaysia, March 2012